

University of Arkansas, Fayetteville

ScholarWorks@UARK

---

Civil Engineering Undergraduate Honors Theses

Civil Engineering

---

5-2008

## A Comparison of Nondestructive Testing Backcalculation Techniques for Rigid and Flexible Pavements

Trenton Ellis

*University of Arkansas, Fayetteville*

Follow this and additional works at: <https://scholarworks.uark.edu/cveguht>



Part of the [Civil Engineering Commons](#), and the [Structural Engineering Commons](#)

---

### Citation

Ellis, T. (2008). A Comparison of Nondestructive Testing Backcalculation Techniques for Rigid and Flexible Pavements. *Civil Engineering Undergraduate Honors Theses* Retrieved from <https://scholarworks.uark.edu/cveguht/1>

This Thesis is brought to you for free and open access by the Civil Engineering at ScholarWorks@UARK. It has been accepted for inclusion in Civil Engineering Undergraduate Honors Theses by an authorized administrator of ScholarWorks@UARK. For more information, please contact [scholar@uark.edu](mailto:scholar@uark.edu), [uarepos@uark.edu](mailto:uarepos@uark.edu).



A COMPARISON OF NONDESTRUCTIVE TESTING BACKCALCULATION  
TECHNIQUES FOR RIGID AND FLEXIBLE PAVEMENTS

A COMPARISON OF NONDESTRUCTIVE TESTING BACKCALCULATION  
TECHNIQUES FOR RIGID AND FLEXIBLE PAVEMENTS

A thesis submitted in partial fulfillment  
of the requirements for Honors Studies in Civil Engineering

By

Trenton Blake Ellis

May 2008  
University of Arkansas

# A COMPARISON OF NONDESTRUCTIVE TESTING TECHNIQUES FOR RIGID AND FLEXIBLE PAVEMENTS

Trenton B. Ellis

## **ABSTRACT**

In designing new pavements, engineers rely on many different measures to characterize the average traffic, climate and soil conditions of the region. Of those, soil conditions are the most elusive, but are also the most crucial for designing a pavement of proper thickness and stiffness. This problem is compounded when the design is for an overlay instead of a new pavement. For overlay designs, engineers require a quantitative characterization of the strength of the existing pavement as well as the underlying soil. Especially for new Mechanistic-Empirical design procedures, direct measures and/or estimates of pavement stiffness are essential inputs. A variety of methods exist for measuring the appropriate strength properties for soil, concrete and asphalt. The most traditional method – regardless of the material – is to retrieve a sample of the material from the field and use laboratory tests to determine the strength of the material, which is then considered representative for other materials near the location from which the sample was taken. The problem with this approach is that, in the field, construction materials experience a confining pressure from the other materials that surround them; even when carefully removed, the strength properties measured in the laboratory are not truly representative of the strength of the materials in the field. Nondestructive testing (NDT) refers to a collection of methods that are used to estimate material properties without removing or otherwise damaging the material. Generally, NDT is faster, cheaper and less intrusive to the traveling public. Two NDT methods, the falling weight deflectometer (FWD) and the spectral analysis of surface waves (SASW), have both become popular for their ability to estimate in-situ (in-place) stiffness properties of pavement materials. Each method measures a different local response (i.e. deflection or wave propagation) caused by a specific load. The measurement of the local response is then used to “backcalculate” the strength property that is desired. The appropriate backcalculation technique is different for each test, and for each test the appropriate technique varies according to the type of material on which the test is being performed and for which stiffness is sought. This study proposes to assess the validity of several backcalculation procedures associated with these two NDT methods and to compare their relative appropriateness in backcalculating pavement stiffness.

This thesis is approved for  
recommendation to the  
Undergraduate Council

Thesis Director:

---

Kevin D. Hall, PhD.

Thesis Committee:

---

Norman D. Dennis, PhD.

---

Robert P. Elliott, PhD.

## **THESIS DUPLICATION RELEASE**

I hereby authorize the University of Arkansas Libraries to duplicate this thesis when needed for research and/or scholarship.

**Agreed** \_\_\_\_\_

**Refused** \_\_\_\_\_

## **ACKNOWLEDGEMENTS**

I would like to thank my thesis director Dr. Kevin D. Hall for his support and guidance throughout this project. Thanks are also extended to the remaining members of my thesis committee, Dr. Robert P. Elliott and Dr. Norman D. Dennis. Their reviews and advice throughout the writing process have been extremely helpful. In addition, I could not have completed this project without the help that I have received from Dr. Brady Cox, Dr. Nam Tran, Meagan Berlau, Sarah Tamayo, and Sutapa Hazra. Finally, I would like to thank Dr. Anastasios Ioannides for making backcalculation software available to this project.

## TABLE OF CONTENTS

Section	Page
1. INTRODUCTION .....	1
1.1. Background .....	1
1.2. Problem Statement .....	2
1.3. Objectives.....	3
1.4. Experimental Plan .....	3
1.4.1. Task 1: Literature Review.....	3
1.4.2. Task 2: Data Analysis .....	4
1.4.2.1. Software Acquisition.....	4
1.4.2.2. Collection of Field Data .....	5
1.4.2.3. Perform Backcalculations.....	5
1.4.2.4. Document Results from Backcalculations.....	6
1.4.3. Task 3: Report Findings.....	6
2. LITERATURE REVIEW .....	7
2.1. Nondestructive Testing Background.....	7
2.2. Falling Weight Deflectometer.....	9
2.2.1. Theoretical Background.....	9
2.2.2. Field Procedures.....	12
2.2.3. Backcalculation Methods.....	17
2.2.3.1. 1993 AASHTO Method for Estimating $M_r$ from Deflection Tests.....	19
2.2.3.2. ILLI-BACK .....	23
2.2.3.3. NUS-BACK for Rigid Pavements.....	25
2.2.3.4. AREA Method for Rigid Pavements.....	33

2.2.3.5.	Best-Fit Procedure .....	38
2.2.3.6.	LTPP Forward Calculation .....	40
2.2.3.7.	MODULUS .....	45
2.2.3.8.	ELMOD 5 .....	50
2.2.3.9.	BAKFAA .....	52
2.2.3.10.	DIPLO-DEF .....	52
2.3.	Spectral Analysis of Surface Waves .....	56
2.3.1.	Theoretical Background .....	56
2.3.2.	Field Procedures .....	59
2.3.3.	Backcalculation Procedure .....	68
2.4.	Case Studies: Comparisons of Backcalculation Procedures .....	76
2.4.1.	Oregon: FWD vs. Laboratory for HMA and Base Course Materials .....	77
2.4.2.	LTPP Database: Comparison of FWD Backcalculation Methods .....	81
3.	DATA ANALYSIS .....	86
4.	RESULTS .....	92
4.1.	SASW Results .....	92
4.2.	NUS-BACK Results .....	92
4.3.	AREA <sub>72</sub> Results .....	95
4.4.	LTPP Forward Calculation Results .....	96
4.5.	BAKFAA Results .....	96
4.6.	ELMOD Results .....	98
4.7.	Comparisons .....	98
5.	DISCUSSION .....	109

5.1.	SASW Results .....	109
5.2.	NUS-BACK .....	109
5.3.	AREA <sub>72</sub> .....	110
5.4.	LTPP Forward Calculation.....	111
5.5.	BAKFAA .....	111
5.6.	ELMOD.....	112
5.7.	NUS-BACK Variations.....	113
5.8.	NUS-BACK vs. AREA <sub>72</sub> .....	114
5.9.	ELMOD Variations .....	115
5.10.	Other Comparisons for Estimating Subgrade Stiffness .....	116
5.11.	Other Comparisons for Estimating PCC Stiffness .....	117
6.	CLOSING .....	118
	REFERENCES .....	121
APPENDIX A	Raw Data from SASW Testing .....	125
APPENDIX B	Raw Data from FWD Testing.....	134
APPENDIX C	Example SASW Inversion.....	139

### LIST OF FIGURES

FIGURE 1	Dynatest FWD (11).....	13
FIGURE 2	KUAB FWD (11).....	14
FIGURE 3	Effect of Existing Distresses On FWD Testing (12) .....	16
FIGURE 4	Sensor Location Effect On Sampling Depth (13).....	16
FIGURE 5	Graphical NUS-BACK Dense Liquid Solution for $\ell$ .....	31
FIGURE 6	Graphical NUS-BACK Elastic Solid Solution for $\ell$ .....	31

FIGURE 7	Graphical NUS-BACK Solutions for $F_k$ and $F_E$ .....	32
FIGURE 8	AREA <sub>36</sub> Deflection Sensor Layout.....	34
FIGURE 9	AREA <sub>S60</sub> Deflection Sensor Layout .....	34
FIGURE 10	AREA <sub>72</sub> Deflection Sensor Layout.....	35
FIGURE 11	Curves Relating AREA <sub>X</sub> to General AREA Parameter (12).....	36
FIGURE 12	AREA <sub>12</sub> Deflection Sensor Layout .....	43
FIGURE 13	WESDEF Relationship Between Deflection and Modulus (19).....	54
FIGURE 14	Idealized Layered Half Space .....	58
FIGURE 15	SASW Configuration .....	60
FIGURE 16	HP 35670A Digital Signal Analyzer (37) .....	61
FIGURE 17	Common Receivers Midpoint Geometry for SASW (38).....	63
FIGURE 18	Common Source Geometry for SASW (38) .....	64
FIGURE 19	Typical Coherence Function (35).....	66
FIGURE 20	Typical Wrapped Cross-Power Spectrum (35) .....	67
FIGURE 21	Strains Under Repeated Loads (19) .....	71
FIGURE 22	Normalized Shear Modulus Reduction Curve (19).....	73
FIGURE 23	HMA Moduli for Rufus Project (47).....	79
FIGURE 24	HMA Moduli for Centennial Project (47).....	79
FIGURE 25	Base Course Moduli for Rufus Project (47).....	80
FIGURE 26	Base Course Moduli for Centennial Project (47) .....	80
FIGURE 27	Comparison of Backcalculated and Measured $k$ Values (22) .....	82
FIGURE 28	Comparison of Backcalculated and Measured $E_{PCC}$ Values for JPC (22).....	83

FIGURE 29	Comparison of Backcalculated and Measured $E_{PCC}$ Values for CRCP (22)	83
FIGURE 30	Errors of Backcalculated $k$ Values (22).....	84
FIGURE 31	Errors of Backcalculated $E_{PCC}$ Values for JPC (22).....	84
FIGURE 32	Errors of Backcalculated $E_{PCC}$ Values for CRCP (22).....	85
FIGURE 33	Spatial Distribution of Soil Types in Nashville, AR (48).....	87
FIGURE 34	Backcalculated $E_{PCC}$ from NUS-BACK.....	93
FIGURE 35	Backcalculated Soil Stiffness from NUS-BACK.....	94
FIGURE 36	Backcalculated $E_{PCC}$ from $AREA_{72}$ .....	95
FIGURE 37	Backcalculated $k$ from $AREA_{72}$ .....	95
FIGURE 38	$M_r$ and $E_{Comp}$ from LTPP Forward Calculation.....	96
FIGURE 39	$E_s$ and $E_{PCC}$ from BAKFAA.....	97
FIGURE 40	$E_s$ and $E_{PCC}$ from ELMOD.....	98
FIGURE 41	NUS-BACK: $D_3-D_1$ vs. $D_7-D_4$ for $E_{PCC}$ .....	99
FIGURE 42	NUS-BACK: $D_3-D_1$ vs. $D_7-D_4$ for $k, E_s$ .....	99
FIGURE 43	NUS-BACK: Dense Liquid vs. Elastic Solid for $E_{PCC}$ .....	100
FIGURE 44	NUS-BACK: Dense Liquid vs. Elastic Solid for $k$ & $E_s$ .....	100
FIGURE 45	NUS-BACK (Elastic Solid) vs. $AREA_{72}$ for $E_{PCC}$ .....	101
FIGURE 46	NUS-BACK Average (Elastic Solid) vs. $AREA_{72}$ for $E_{PCC}$ .....	101
FIGURE 47	NUS-BACK $D_7-D_4$ (Dense Liquid) vs. $AREA_{72}$ for $k$ .....	102
FIGURE 48	ELMOD: Radius of Curvature vs. Basin-Matching.....	102
FIGURE 49	NUS-BACK $D_7-D_4$ (DL) $k$ vs. BAKFAA $E_s$ .....	103
FIGURE 50	NUS-BACK $D_7-D_4$ (DL) $k$ vs. LTPP $M_r$ .....	103

FIGURE 51	NUS-BACK D <sub>7</sub> -D <sub>4</sub> (DL) $k$ vs. ELMOD $E_S$ .....	103
FIGURE 52	AREA <sub>72</sub> $k$ vs. BAKFAA $E_S$ .....	104
FIGURE 53	AREA <sub>72</sub> $k$ vs. LTPP $M_f$ .....	104
FIGURE 54	AREA <sub>72</sub> $k$ vs. ELMOD $E_S$ .....	104
FIGURE 55	BAKFAA $E_S$ vs. LTPP $M_f$ .....	105
FIGURE 56	BAKFAA $E_S$ vs. ELMOD $E_S$ .....	105
FIGURE 57	LTPP $M_f$ vs. ELMOD $E_S$ .....	106
FIGURE 58	AREA <sub>72</sub> $E_{PCC}$ vs. BAKFAA $E_{PCC}$ .....	106
FIGURE 59	AREA <sub>72</sub> $E_{PCC}$ vs. LTPP $E_{Comp}$ .....	107
FIGURE 60	AREA <sub>72</sub> $E_{PCC}$ vs. ELMOD $E_{PCC}$ .....	107
FIGURE 61	BAKFAA $E_{PCC}$ vs. LTPP $E_{Comp}$ .....	107
FIGURE 62	BAKFAA $E_{PCC}$ vs. ELMOD $E_{PCC}$ .....	108
FIGURE 63	LTPP $E_{Comp}$ vs. ELMOD $E_{PCC}$ .....	108

# 1. INTRODUCTION

## 1.1. Background

Maintaining structurally and functionally sound roads is an expensive endeavor in the United States and around the world. Much of the current transportation infrastructure in the United States was built in the 1960s and 1970s, and is reaching the end of its design life. There is a need for roadway rehabilitation on a large scale, and maintenance measures are most effective when pavement distresses are detected early on and treated properly before more costly damage occurs.

Laboratory tests can be used for detecting structural deficiencies in subgrade soil and pavement layers. For these tests, a sample of the material in question is excavated from the roadway and taken to the laboratory for examination. Care must be taken when collecting samples in the field because the stresses applied to the specimen during excavation can alter the material properties under investigation. Indeed, removing the specimen from the field will inevitably result in measured material properties that stray from those that exist in the field.

A more favorable method is to conduct tests in the field without removing materials from the roadway. Methods collectively known as nondestructive tests (NDT) have become increasingly popular in recent years because of their speed, low cost, and reliability (*1*). By testing the materials in-situ (in-place), field conditions can be maintained and represented in the results. The falling weight deflectometer (FWD) and the spectral analysis of surface waves (SASW) are two types of NDT commonly used for pavement analysis.

## **1.2. Problem Statement**

Nondestructive testing techniques such as FWD and SASW have gained popularity because of their ease of use as well as the potential accuracy of their results. As these tools have increased in use, a number of different techniques for reducing their field data have been proposed. The process of reducing field data from an NDT into more pertinent information about the roadway is commonly referred to as backcalculation.

A growing number of backcalculation methods exist to accommodate variables such as the type of test being used, the underlying theory used to model the pavement structure, and the amount of computing power that is available. These accommodations, while appropriate, have resulted in a large collection of backcalculation methods that do not lend themselves to a simple comparison. One straight-forward manner of comparison is to perform field tests on a single section of pavement and use several different techniques to reduce the common data set. Then, the ability and/or accuracy of each method to backcalculate the engineering properties of the pavement can be gauged by comparing the backcalculation results to known parameters of the pavement structure on which the field tests were conducted.

If the number and variety of backcalculation procedures that are compared is large enough, then the results of the comparison could be used to gauge the effect of factors such as type of test being used, underlying theory used to model the pavement structure, and/or available computing power upon the accuracy of the final results. This study is limited to backcalculation procedures for FWD and SASW tests, but methods for reducing data from both rigid and flexible pavements will be considered for each type of test. Backcalculation procedures to be considered include closed form solutions via

spreadsheet, database software, and iterative software. The set of data reduction methods that is used for this study will be chosen so that it is large enough for a worthwhile comparison between the types of tests being used (FWD and SASW) and between the different types of backcalculation software inherent to each method.

### **1.3. Objectives**

The objective of this research is to compare various backcalculation techniques for both FWD and SASW testing of rigid and flexible pavements. This has been accomplished by completing the following related objectives:

- Identify commonly used backcalculation procedures for data from FWD and SASW field tests.
- Assess the ability and/or accuracy of several different procedures for evaluating structural properties of pavement layers (both individually and as a single effective layer) and underlying subgrade by using several different methods to reduce the data from a common set of field tests.
- Compare the results from the backcalculations to known properties of the pavement on which the field tests were run. Report the relative ease and accuracy of each of the techniques considered at reducing field test data.

### **1.4. Experimental Plan**

The objectives of this study will be achieved by completing the following tasks:

#### *1.4.1. Task 1: Literature Review*

A comprehensive literature review of FWD and SASW tests will be undertaken to gain an understanding of the backing theories, field procedures, and common backcalculation techniques for each test. It is not the goal of this research to provide a detailed explanation for the backing theory of each test. Instead, this report will describe the theories in sufficient detail so that the reader may gain a working knowledge of how and/or why the corresponding backcalculation procedures work.

Similarly, this report will describe the manner in which field tests are performed for FWD and SASW testing. This section of the literature review is included so that readers who are unfamiliar with the equipment and/or procedures involved with each test may become sufficiently aware of each so that references to these things later on the report will not be a source of confusion.

Finally, for FWD and SASW, a number of backcalculation procedures will be described in detail. The two goals of this portion of the literature review are to introduce the reader to the most common types of backcalculation procedures that are currently in use for FWD and SASW tests and to provide an explanation of how these procedures work.

#### *1.4.2. Task 2: Data Analysis*

##### *1.4.2.1. Software Acquisition*

Based upon results from the literature review, a number of different types of software will be sought for use in the comparison of this study. Software for the study will be limited by what is available for use at either no cost or a modest price. In addition, some procedures employing database software may not lend themselves to this study for the

reason that the software is available, but the database that the software uses is not.

Computer processing speed has been an issue to consider with some procedures in the past, but initial thoughts are that modern computers possess such high processing speeds that this will not be a limiting issue for the present study.

It is anticipated that some closed-form solution backcalculation techniques will be most efficiently utilized via spreadsheet applications such as Microsoft Excel. For this reason, a number of spreadsheets will likely be programmed with applicable closed-form solutions for the comparison of this study. These spreadsheets, along with the software that is obtained according to the preceding paragraph, will comprise the backcalculation techniques studied during the comparison.

#### ***1.4.2.2. Collection of Field Data***

Field data from actual FWD and SASW tests will be obtained in order to compare the backcalculation methods of the study. Raw data will be collected from past and ongoing research at the University of Arkansas as well as records from the Arkansas State Highway and Transportation Department (AHTD).

#### ***1.4.2.3. Perform Backcalculations***

After a sufficient number of spreadsheets and other software have been collected for backcalculation, the raw data from the FWD and SASW tests will be used to test the ability and/or accuracy of each applicable backcalculation method to determine various properties of the pavement structure. This process will be repeated as many times as is necessary to ensure that the backcalculation techniques are being used correctly.

#### ***1.4.2.4. Document Results from Backcalculations***

Once the backcalculations have been performed using all of the techniques under investigation, the calculated pavement properties will be organized in a manner conducive to comparison. The results obtained using each technique will be accompanied by notes that outline the general instructions for using the method as well as potential difficulties specific to that method. The end result of this step will be a table of raw output data and user notes for each of the backcalculation techniques investigated in this study.

#### ***1.4.3. Task 3: Report Findings***

The final phase involves the actual comparison of the results from the backcalculations. This comparison may range from broad observations such as user friendliness and outlying results to more advanced observations from statistical analysis. After all comparisons have been drawn, a concise summary of the findings will be presented that identifies the most pertinent findings from this study as well as unanswered questions that may be relevant for future studies.

## **2. LITERATURE REVIEW**

### **2.1. Nondestructive Testing Background**

Nondestructive testing (NDT) refers to a collection of field testing methods that facilitate the in-situ (in-place) testing of materials instead of conventional laboratory testing. NDT is attractive to highway engineers for several reasons. Testing subgrade and pavement materials in-situ preserves the confining stresses that are present in the field, whereas laboratory testing requires the removal of a sample and consequently introduces a change in confining stress. In addition, NDT requires significantly less time and money to estimate the same material properties that would otherwise be measured in the laboratory. Thus, NDT may provide a relatively fast, inexpensive and accurate alternative to laboratory testing.

A great deal of the current highway system in the United States was constructed in the 1960s and the 1970s, and much of that system is beginning to reach the end of its design life. In order to maintain a functional transportation infrastructure, maintenance is and will be required on a large scale. The cost of this maintenance effort can be minimized if highway engineers are able to obtain a more detailed knowledge of the structural condition of the aging highway system. Laboratory tests are the conventional method for measuring the structural properties and stiffness of pavements, but the time and expense associated with laboratory testing allows only a minimal amount of locations to be assessed. NDT, on the other hand, can estimate the same material properties as laboratory tests, but at a much larger number of locations and at a fraction of the cost. Integrating NDT into standard highway evaluation techniques has and will continue to

improve the extent to which the structural capacity of existing highways can be measured.

NDT has been practiced in several different forms for a number of decades, but two types of NDT have emerged as the front-runners in recent years: the falling weight deflectometer (FWD) and the spectral analysis of surface waves (SASW). Currently, the FWD is the type of NDT that is preferred by most agencies. The FWD involves dropping a weight on the ground and “backcalculating” the stiffness of the pavement and/or subgrade from the measured pavement surface deflections. If the pavement system consists of multiple layers, a rough idea of the thickness of each layer must be known prior to backcalculation so that iterative bounds may be set.

SASW is also emerging as a valuable tool for highway engineers. This method is also used to determine the stiffness of pavement and/or subgrade from an impulse load. The main differences are that SASW can also determine the thickness of multiple layers, and that SASW estimates these properties from measurements of wave propagation. The techniques for measuring the necessary characteristics of wave propagation and for converting those measurements to a usable output (inversion) have been advanced greatly in the past two decades. Advancements in technique and computing power have and will continue to make SASW a considerable alternative and/or compliment to the FWD.

Both FWD and SASW testing are promising candidates for providing estimates of pavement and subgrade stiffnesses, which are the most important input parameters used by engineers to plan maintenance of existing roadways. These tests will become increasingly valuable with time as mechanistic-empirical (M-E) design becomes more popular in the United States. M-E design software requires extensive inputs such as

subgrade stiffness that will need to be closely approximated for each location that uses the software. NDT will facilitate the development of much less expensive and more representative catalogs of local subgrade properties for M-E design of new pavements.

## **2.2. Falling Weight Deflectometer**

The falling weight deflectometer (FWD) is an “impulse load” variety of NDT, and it is currently the most popular type of NDT that is practiced by highway officials in the United States. The FWD operates much in the way that its name implies. Some amount of mass is dropped from a specific height in order to impart a particular magnitude of impulse load onto a strategic location on the pavement surface. That stress causes a strain through the pavement and subgrade, and several sensors are positioned on the pavement surface at precise horizontal distances from the location of the impulse load to measure the vertical deflection at each point. The vertical deflections measured by each sensor define a single deflection basin that is caused by the falling mass. The stiffness of the pavement and/or subgrade is then backcalculated from the magnitude of the imparted load and the size of the measured deflection basin.

### *2.2.1. Theoretical Background*

The type of backcalculation that is used to estimate pavement and/or subgrade stiffness depends upon the assumptions that are made and also upon the type of theoretical model that is used to idealize the pavement structure.

The most significant assumption that is commonly made for FWD backcalculation is that despite the dynamic nature of the load, the pavement materials

react as though the load is purely static. That is, the loading rate is assumed to be low enough so that pavement materials experience no dynamic effects such as damping. This assumption is often made in order to simplify the mechanics that are utilized for backcalculation. If, however, a significant time lapse occurs between the peak stress and the peak deflection, the assumption of static loading is not appropriate. Generally, static behavior is a more realistic assumption for pavements with stiff concrete or thick asphalt layers than for pavements comprised of a thin asphalt layer (2).

The mechanical behavior of soil is affected by a variety of factors, including (i) the shape, size and mechanical properties of the individual soil particles, (ii) the configuration of the soil structure, (iii) the intergranular stresses and stress history, and (iv) the presence of soil moisture, the degree of saturation and the soil permeability. Considering the myriad factors that influence the mechanical behavior of soil, it is no surprise that naturally occurring soils exhibit non-linear, irreversible and time-dependent stress-strain behavior. Furthermore, naturally occurring soil masses almost always exhibit anisotropic and non-homogeneous material properties. Any analysis that accounts for all of these factors - if possible - would be far too rigorous and time-consuming to be practical. Therefore, several simplifying assumptions other than static behavior are also commonplace for FWD backcalculation (3).

As the science of theoretical soil mechanics has advanced in recent decades, a number of prudent assumptions for idealizing in-situ soil behavior have emerged. In general, a prudent assumption is one that simplifies analytical computations while introducing a minimal amount of error in the corresponding results. While the models and assumptions used for different backcalculation methods may vary slightly, the most

common and important assumptions for any idealization of naturally occurring soils are as follows (4):

1. The soil is assumed to be an elastic, homogeneous, isotropic medium.
2. The soil is assumed to act as an ideal half-space, bound by a horizontal ground surface.
3. The material obeys Hooke's law of proportionality between stress and strain.
4. The deformations of the soil medium are so small that they can be neglected in setting up equilibrium conditions.

The previous assumptions idealize the soil structure on a micro-level, but there is also a need to model the soil structure on a macro-level. This can be accomplished by employing one of two common models. The simpler of the two methods was introduced by Winkler, and it is commonly known as the dense liquid model. For this model, the subgrade is assumed to act as a field of springs that do not interact with each other. That is, each spring's movement is only affected by the load directly above it, and springs do not share any of their load with neighboring springs. The spring constant,  $k$ , is called the coefficient of subgrade reaction. Winkler's method is the most commonly used model because of its computational simplicity. More information on the development of this model is provided elsewhere (5).

Most backcalculation procedures are derived not from Winkler's original model, but instead from amendments to that model that were proposed by Westergaard (6). Westergaard accepted the soil behavior that was proposed by Winkler, but advanced the model by including a rigid plate at the top of the half-space to represent a rigid pavement. Westergaard's studies provide a simplified means to find the maximum tensile stress in a

concrete slab (plate) under point loads at mid-slab, slab edge, and slab corner. The methods used by Westergaard are not well documented, but a detailed review of his results and their applicability is available (7).

The dense liquid idealization proposed by Winkler does have its shortcomings. For instance, soils with any degree of cohesion do not obey the assumptions of a Winkler foundation. That is, the soil directly underneath a point load is not the only soil that experiences a vertical deflection. Instead, a somewhat continuous deflection basin forms around the point load. This type of deflection basin was originally described by Boussinesq (8), and it leads to the second type of model for macro-level behavior of soils: the elastic continuum model. This model, in contrast to the Winkler model, assumes continuous behavior throughout the soil half-space. Both two- and three-dimensional analyses may be performed using the Boussinesq distribution and plate theory to model pavement-soil systems. The elastic continuum (also called elastic solid or ES) model provides a more accurate representation of in-situ behavior, but the accompanying analysis involves mathematics that are often too complex to be practical (3). Backcalculation procedures that do employ the ES model are mostly based off the works of Panc (9) and Losberg (10), which model an infinitely long slab on an elastic foundation.

### *2.2.2. Field Procedures*

FWD apparatus are usually trailer-mounted and carried by a vehicle with onboard computer processors. Two commonly used commercial FWDs, the Dynatest and KUAB FWDs, are shown in Figures 1 and 2, respectively (11). During field testing, the FWD is

driven to the testing location and positioned so that the load plate is above the location to be tested. For the purposes of determining pavement layer moduli, rigid (or asphalt-overlaid rigid) pavements are tested at slab interiors and flexible pavements are tested in the outer wheel path of the outer lane. When flexible (or asphalt-overlaid) pavements are tested, it is important to record the temperature of the asphalt pavement at least 3 times during a full day of testing. The temperature measurements can be used to calibrate the measurements for a more accurate backcalculation. In every case, tests are conducted every 100 to 500 ft. In general, longer intervals are more appropriate for newer pavements and vice versa (11).



**FIGURE 1** Dynatest FWD (11)



**FIGURE 2 KUAB FWD (11)**

Once the FWD is in place, the loading begins. After the load plate and deflection sensors are hydraulically lowered to the pavement, a seating load is applied to ensure proper placement of the load plate. The magnitude of the pre-load varies for different equipment, but is usually between 8 to 18% of the maximum impulse load. Once the pre-load is performed, a series of impulse loads are performed that mimic the design load of the roadway being tested. In other words, a larger peak load is applied for roads with predominantly truck traffic than for roads with relatively light traffic loads. The magnitude of the load that is delivered by the FWD is altered by changing the amount of mass that is dropped and by changing the height from which it is dropped. A load cell at the load plate reports the delivered load. Peak loads and deflections are stored in the

onboard computer for backcalculation, the equipment is hydraulically lifted back to the trailer, and the entire apparatus is moved to the next testing location (12).

At least three different loadings are usually performed at each testing location. This manner of testing allows highway officials to identify any non-linear response of the foundation, and it also helps to ensure that at least one of the deflection basins is satisfactory for backcalculation. Typical target loads for FWD testing on highway pavements are 6000, 9000, and 12000 pounds (11).

At least two drops should be performed at each target load to check for any permanent deformation under the loading plate. If the difference in the deflections caused by two loads of the same magnitude at the same location is greater than 3% for any sensor, the apparatus should be moved and the applied force should be reduced (1).

It is worth noting that existing pavement distresses can and do affect the deflections that are measured during FWD testing. Figure 3 shows an example in which alligator cracking causes higher deflection readings. An effort should be made to avoid FWD testing in the vicinity of existing distresses insofar as possible.

It is well known that deflections measured closer to the point load are more indicative of pavement stiffness, whereas deflections measured further horizontally outward from the point load are more indicative of subgrade stiffness. Consider Figure 4 (13). The dotted line represents the boundary of the zone of stress, and beyond a radial distance from the load of  $a_{3e}$  all deflections at the surface are due to stress that occurs only in the subgrade layer. This simplistic explanation assumes Winkler behavior, but it is sufficient to explain why the outer sensors are indicative of subgrade behavior.

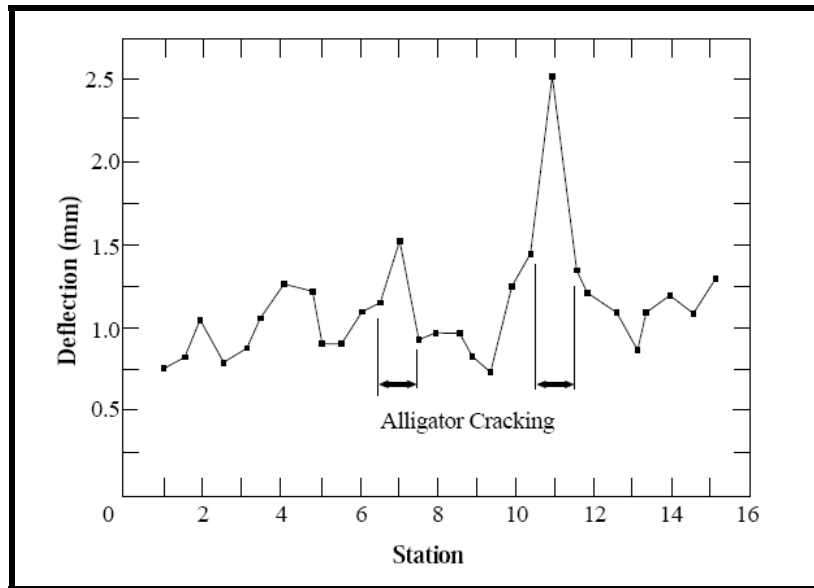


**FIGURE 3** Effect of Existing Distresses On FWD Testing (12)

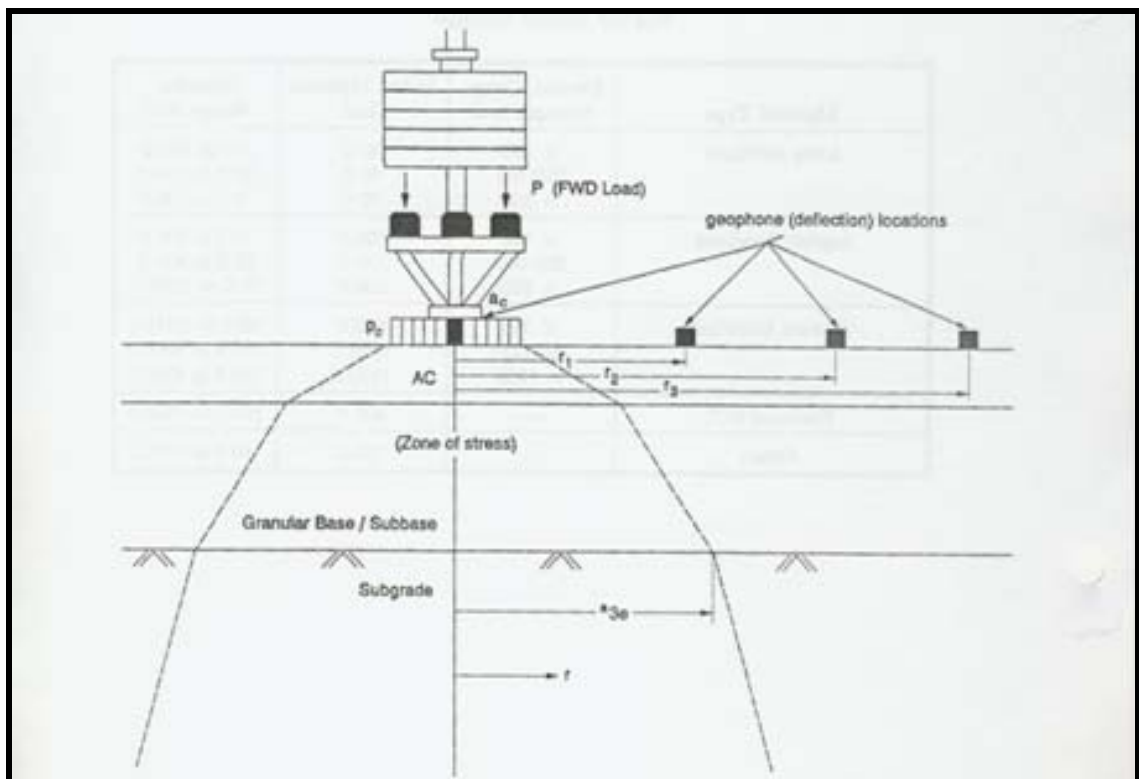


**FIGURE 4** Sensor Location Effect On Sampling Depth (13)

It is desirable to place at least one sensor far enough away from the load plate so that its measured deflection can be used to estimate subgrade stiffness. Seven deflection sensors are commonly used, including one sensor at the middle of the load plate. The most common configuring for the seven-sensor system on highway pavements is 0, 8, 12, 18, 24, 36, and 60 inches from the center of the load plate. Whatever configuration is used, it is important to place one sensor further than 36 inches from the center of the load plate to account for subgrade stiffness [\(11\)](#).

### *2.2.3. Backcalculation Methods*

Backcalculation methods vary according to a number of factors such as the theory that was used to develop the method and the type of pavement system that is under investigation. Rigid pavements are typically the simplest types of pavement structures to analyze with NDT. Portland cement concrete (PCC) layer(s) are typically assumed to act as rigid plates, which can allow for a closed-form solution.

A more common pavement structure is a 3-layered system consisting of a PCC and a base layer that are underlain by subgrade soil. The addition of the base layer adds complexity to the backcalculation procedure, but closed-form solutions are still possible. In fact, two classes of closed-form solutions are available for 3-layer rigid pavement systems, depending on the type of interface that exists between the PCC and base layers [\(14\)](#). If the two layers are completely bonded, the parallel axis theorem is used to combine layer thicknesses and stiffnesses for backcalculation. Otherwise, if the two layers are not bonded together, the composite layer of PCC and base is simply defined by the PCC thickness and the sum of the layer stiffnesses.

Most backcalculation procedures are too sensitive to adhere to general rules or procedures, but research has shown a general trend for 3-layer rigid pavement systems (15). First, neglecting the presence of a base layer tends to overestimate the stiffness of the overlying PCC layer. Second, assuming a full bond between the PCC and base layers usually underestimates the stiffness of the base material. Slab curling and moisture warping can cause a rigid slab to maintain a full bond at mid-slab, where deflection testing occurs, while exhibiting no bond at the edges. From these observations, a decision could be made to model the PCC-base interface as unbonded unless field conditions clearly indicate a full bond.

Flexible pavements involve a higher degree of complexity for backcalculations than rigid pavements. This is because flexible pavements are viscoelastic materials, meaning that they act both as an elastic solid and as a viscous liquid. The viscous behavior causes a variation in HMA stiffness with changes in temperature. Thus, the effects of temperature gradients cause more computational complications with flexible pavements (13). In addition, flexible pavement deflections occur not only because of movement of the underlying subgrade, but also because of deflections within the hot-mix asphalt (HMA) layer(s).

Typical backcalculation procedures for flexible pavements are not closed-form and require some form of computer software to carry out the iterative, finite element, and/or database-search type of computations. Some of the more common types of software will be discussed in terms of their computational approach, appropriateness for various pavement types, and general availability.

The ultimate goal of deflection testing is to provide material characterizations that can be used as inputs for the design of new pavements or for overlays of existing pavements. The primary material characterization parameters have not changed drastically from 1993 AASHTO Pavement Design Guide to the Mechanistic-Empirical Pavement Design Guide (MEPDG). Subgrade soils for flexible pavements are characterized by Resilient Modulus ( $M_r$ ), and those for rigid pavements by the Coefficient of Subgrade Reaction ( $k$ ). Both of these quantities can be estimated from FWD testing (16).

The characterization of pavement stiffness has changed in the new mechanistic-empirical procedures. The structural number (SN) was used to indicate material stiffness in the 1993 guide, but it has been eliminated in the MEPDG software. If pavement designers choose to use the 1993 guidelines to obtain baseline designs, FWD results can be used to estimate the effective structural number ( $SN_{eff}$ ) or effective depth ( $D_{eff}$ ).  $SN_{eff}$  is used to characterize the structural capacity of a flexible pavement as a whole, and  $D_{eff}$  does the same for rigid pavements. MEPDG software, on the other hand, uses the material thicknesses and stiffnesses that are obtained from FWD backcalculation directly.

#### **2.2.3.1. 1993 AASHTO Method for Estimating $M_r$ from Deflection Tests**

The 1993 AASHTO specifications for pavement design offers the most straight-forward method for estimating the resilient modulus ( $M_r$ ) of subgrade soils (16). To use this method, however, it is necessary to iterate the subgrade resilient modulus and total pavement thickness. The benefit is that  $M_r$  can be estimated using a single deflection measurement.

To begin, it is necessary to identify the radial distance from the load plate at which deflections will be outside the influence of the pavement layers. Equation 1 is used to estimate this value, which is termed  $a_{3e}$  in Figure 4. Note that Equation 1 requires an estimate of the subgrade resilient modulus ( $M_r$ ) as well as the effective modulus of all pavement layers ( $E_p$ ) above the subgrade. Table 1 provides a list of reasonable guesses and ranges that can be used in this equation or any other application that requires an estimate of material moduli (13). Equation 2 is used to find a value for  $E_p$  to be used in Equation 1. Finally, after  $a_e$  has been calculated,  $M_r$  is found via Equation 3. If the pavement is comprised of a single PCC layer that rests directly on the subgrade, Equation 4 can also be used to calculate a  $k$ -value from the previously estimated  $M_r$  value. Note, however, that Equation 4 has been shown to consistently underestimate  $k$  values (17, 18).

The obtained value for  $M_r$  must also be multiplied by a reduction factor not less than 0.33 for fine-grained, stress-dependent soils. While FWD loads do emulate the loads that are considered for AASHTO design standards, the amount of soil that exists between the load impact and the deflection sensor tends to absorb some of the stress before it reaches the deflection sensor. For fine-grained, stress-dependent soils,  $M_r$  decreases as the magnitude of strain increases. Thus, the reduction factor is in place to correct the falsely inflated estimate of  $M_r$  that occurs because of some amount of stress that is absorbed by soil that lies between the load plate and the deflection sensor (16).

$$a_e = \sqrt{a^2 + \left( D \cdot \sqrt[3]{\frac{E_p}{M_r}} \right)^2} \dots\dots\dots \text{Eq. 1}$$

$$d_0 = 1.5pa \cdot \left\{ \frac{1}{M_R \sqrt{1 + \left( \frac{D}{a} \cdot \sqrt[3]{\frac{E_p}{M_r}} \right)^2}} + \frac{\left[ 1 - \frac{1}{\sqrt{1 + \left( \frac{D}{a} \right)^2}} \right]}{E_p} \right\} \dots \text{Eq. 2}$$

$$M_r = \frac{0.24P}{d_x \cdot r} \dots \text{Eq. 3}$$

$$k = \frac{M_r}{19.4} \dots \text{Eq. 4}$$

Where:

$a_e$  = Radius of stress bulb at the subgrade-pavement interface (in.)

$a$  = FWD load plate radius (in.)

$D$  = Total thickness of pavement layers above the subgrade (in.)

$E_p$  = Effective modulus of all pavement layers (psi)

$d_0$  = Deflection measured at the center of the load plate (in.)

$p$  = FWD load plate pressure (psi)

$a$  = FWD load plate radius (in.)

$M_R$  = Subgrade resilient modulus (psi)

$P$  = Applied load (lb)

$d_x$  = Deflection at a distance X from the center of the load (in.)

$r$  = Distance from center of load (in.)

$k$  = Composite modulus of subgrade reaction (psi/in.)

**Table 1 Reasonable Estimates and Ranges for Material Moduli (13)**

<b>Material Type</b>	<b>Estimate of Moduli (ksi)</b>	<b>Range of Moduli (ksi)</b>
Crushed Stone, Gravel or Slag Bases	50.0	10.0 to 150.0
Subbases	30.0	10.0 to 100.0
Gravel or Soil-Agg. Mix, Coarse Bases	30.0	10.0 to 100.0
Subbases	20.0	5.0 to 80.0
Sand Bases	20.0	5.0 to 80.0
Subbases	15.0	5.0 to 60.0
Gravel or Soil-Agg. Mix, Fine Bases	20.0	5.0 to 80.0
Subbases	15.0	5.0 to 60.0
Lime-Treated Base/Subbase $f_c' < 250$ psi	30.0	5.0 to 100.0
250 - 500 psi	50.0	10.0 to 150.0
> 500 psi	70.0	15.0 to 200.0
Asphalt-Treated Base/Subbase $f_c' < 300$ psi	100.0	10.0 to 300.0
300 - 800 psi	150.0	25.0 to 800.0
> 800 psi	200.0	50.0 to 1500.0
Cement-Treated Base/Subbase $f_c' < 750$ psi	400.0	50.0 to 1500.0
750 - 1250 psi	1000.0	100.0 to 3000.0
> 1250 psi	1500.0	150.0 to 4000.0
Fractured PCC	500.0	100.0 to 3000.0
PCC	3500	3000.0 to 8000.0
HMA	400	250 to 500

### 2.2.3.2. *ILLI-BACK*

ILLI-BACK was the first closed-form backcalculation method to be developed for rigid pavements (19). Very similar to the AREA method (see Section 2.2.3.3), ILLI-BACK relies on the unique relationship between radius of relative stiffness to a ratio of deflection measurements. To better explain this relationship, consider Westergaard's equations for normalized deflections both under a load ( $d_0$ ) and at some distance from the load ( $d_i$ ), presented below as Equations 5 and 6, respectively. If the radius of the load plate ( $a$ ) is known and the deflection ( $w$ ) is measured, then an important observation can be drawn. The normalized deflection, whether it be directly underneath the load or at some distance from the load, is a function of only one unknown: the radius of relative stiffness ( $\ell$ ).

$$d_0 = \frac{w_0 k \ell^2}{P} = f\left(\frac{a}{\ell}\right) \dots \dots \dots \text{Eq. 5}$$

$$d_i = \frac{w_i k \ell^2}{P} = f_i(\ell) \dots \dots \dots \text{Eq. 6}$$

ILLI-BACK works by the relationship that is found by taking the ratio of the two above equations. The result, given below as Equation 7, indicates that the ratio of any two measured deflections may be defined as a function of  $\ell$ . This means that a theoretically sound relationship can be developed to calculate  $\ell$  that is representative of how much one location deflects relative to another from the same load. Thus, for an FWD setup, the relative deflections between the different sensors are representative of a unique value of  $\ell$  for the pavement system. Furthermore, instead of limiting the relationship to the ratio of two deflections, the AREA parameter can be used to provide an even more reliable development of  $\ell$ .

$$\frac{d_1}{d_2} = \frac{w_1}{w_2} = \frac{f_1}{f_0} = f(\ell) \dots \text{Eq. 7}$$

Though this derivation was presented in terms of a dense liquid foundation, the relationship between relative deflections and radius of relative stiffness also exists for elastic solid foundation models. ILLI-BACK can use either of the two models to analyze a pavement structure. After  $\ell$  is determined, and depending on the subgrade model that is specified, the  $k$  value or  $E_s$  is calculated using Equation 8 or 9, respectively. Finally, the stiffness of the PCC layer is calculated using Equation 10 or 11.

$$k = \frac{Pd_i}{\ell^2 w_i} \dots \text{Eq. 8}$$

$$E_s = \frac{2(1 - \nu_s^2)Pd_i}{\ell w_i} \dots \text{Eq. 9}$$

$$E_{PCC} = \frac{12(1 - \nu_{PCC}^2)k\ell^4}{h^3} \dots \text{Eq. 10}$$

$$E_{PCC} = \frac{6(1 - \nu_{PCC}^2)E_s\ell^3}{(1 - \nu_s^2)h^3} \dots \text{Eq. 11}$$

- Where:
- $k$  = Coefficient of subgrade reaction
  - $P$  = Impact load
  - $d_0, d_i$  = Normalized loading under the center of loading and at some distance from the load, respectively
  - $\ell$  = Radius of relative stiffness
  - $w_0, w_i$  = Measured vertical deflections under the center of loading and at some distance from the load, respectively
  - $E_s$  = Young's modulus of the subgrade

$\nu_s$  = Poisson's ratio of the subgrade

$\nu_{PCC}$  = Poisson's ratio of the PCC

ILLI-BACK is available as a DOS based computer program, and it has been developed for both 4-sensor arrangements (AREA<sub>36</sub>) and 7-sensor arrangements (both AREA<sub>72</sub> and AREA<sub>S60</sub>) (20). If necessary, Table 2 can be used to find reasonable estimates of Poisson's Ratio to use during manual backcalculation (13).

**Table 2** Typical Poisson's Ratio Values for Pavement Materials (13)

Material Type	Poisson's Ratio
HMA	
E > 500 ksi	0.30
E < 500 ksi	0.35
PCC	0.15
Stabilized Base/Subbase	
Lime	0.20
Cement	0.20
Asphalt	0.35
Other (stabilized subgrade)	0.35
Other (fractured PCC)	0.30
Granular Base/Subbase	0.35
Cohesive Subgrade	0.45
Cohesionless Subgrade	0.35

### 2.2.3.3. NUS-BACK for Rigid Pavements

The simplest type of pavement system for backcalculation is a PCC layer resting on a homogeneous subgrade. In this case, a closed-form solution may be developed using either the dense liquid or elastic solid subgrade models (21). This simple method requires only two measured deflections to estimate the stiffness of the rigid pavement and

the subgrade. Since FWD tests provide more than two deflections, NUS-BACK can be used for certain types of quality control in addition to just stiffness estimation. Since the deflections from any two sensors may be used as input data, faulty sensors can be easily spotted and their data discarded. The variance in estimated stiffnesses from different sensor combinations can also be used to test the robustness of the backcalculation theory. At least one study has shown that using the fourth and seventh sensors is most accurate for estimating subgrade stiffness, and using the first and third sensors is most accurate for estimating pavement stiffness (22).

Simplifying assumptions for NUS-BACK include the ignoring of effects from load transfer across joints and dynamic loading as well as slab curling. These assumptions allow deflections in the two-layer system (PCC and subgrade) to be defined solely in terms of the elastic modulus of the slab ( $E_{PCC}$ ) and a measure of stiffness for the subgrade. For the dense liquid model this would be the coefficient of subgrade reaction ( $k$ ) and for the elastic solid model this would be the elastic modulus of the subgrade ( $E_S$ ).

The situation is described in terms of two equations that may be simultaneously solved to provide unique values for radius of relative stiffness ( $\ell$ ) and either  $k$  or  $E_S$  for two measured values of deflection ( $D_{m1}$  and  $D_{m2}$ ). Equations 12 and 13 describe this setup for a dense liquid model, and Equations 15 and 16 do the same for an elastic solid model.

After unique solutions have been found for radius of relative stiffness and subgrade stiffness, the stiffness of the PCC pavement is solved directly from the definition of the radius of relative stiffness. Equation 14 or 17 is used to calculate  $E_{PCC}$  for the dense liquid or elastic solid model, respectively.

For dense liquid-modeled subgrades:

$$D_{m1} = \frac{P}{k\pi a^2} F_K(\ell_K, r_1) \dots \text{Eq. 12}$$

$$D_{m2} = \frac{P}{k\pi a^2} F_K(\ell_K, r_2) \dots \text{Eq. 13}$$

$$\ell_K = \left( \frac{E_{PCC} h_{PCC}}{12(1 - \mu_{PCC}^2) K} \right)^{1/4} \dots \text{Eq. 14}$$

For elastic solid-modeled subgrades:

$$D_{m1} = \frac{P(1 - \mu_S^2)}{E_S \ell_E} F_E(\ell_E, r_1) \dots \text{Eq. 15}$$

$$D_{m2} = \frac{P(1 - \mu_S^2)}{E_S \ell_E} F_E(\ell_E, r_2) \dots \text{Eq. 16}$$

$$\ell_E = \left( \frac{E_{PCC} h_{PCC}^3 (1 - \mu_S^2)}{6(1 - \mu_{PCC}^2) E_S} \right)^{1/3} \dots \text{Eq. 17}$$

Where:

$D_{m1,2}$  = Measured deflections

P = Applied load

K = Modulus of subgrade reaction

a = Radius of loaded area

$E_S$  = Subgrade elastic modulus

$\mu_S$  = Poisson's ratio of the subgrade

$E_{PCC}$  = Elastic modulus of the pavement slab

$h_{PCC}$  = Slab thickness

$r_{1,2}$  = Horizontal distances of points 1 and 2 from the center of loaded area

$\ell_{1,2}$  = Radii of relative stiffness

NUS-BACK exists in the form of a computer program, but it is also possible to go through the same process graphically. For the graphical procedure the two deflections are labeled  $D_{mi}$  and  $D_{mj}$  so that  $D_{mi}$  is greater than or equal to  $D_{mj}$ . The first step is to compute the ratio of the two deflections,  $D_{mj}/D_{mi}$ . Depending on the preferred analysis (dense liquid or elastic solid) the appropriate radius of relative stiffness ( $\ell_k$  or  $\ell_E$ ) is taken from the chart in Figure 5 or 6. Then, instead of solving for  $F_k$  or  $F_E$  analytically, it is taken from a chart (Figure 7) using the previously determined value of  $\ell_k$  or  $\ell_E$ . This is done for  $r_i$  and  $r_j$ , and the rest of the procedure is performed in the previously described manner using Equations 12 – 17. Regardless of whether the software- or graphical-based method is used, stiffness values can be estimated using many different combinations deflection readings to check the accuracy of the sensors and the model itself.

It is common practice to include a granular base layer between PCC slabs and the subgrade to facilitate drainage. Accordingly, there are also two NUS-BACK procedures for analyzing a two-layer rigid pavement. A computer program called NUS-BACK3 may be used, or the two upper pavement layers may be combined into a single equivalent layer so that the three-layer pavement can be analyzed as a two-layer pavement. If the interface between PCC and base material is considered bonded, Equations 18 and 19 are used to define an equivalent pavement layer; otherwise, if the interface is completely unbonded, Equation 20 is used. For these analyses, there are three unknowns: modulus of the concrete slab ( $E_{PCC}$ ), modulus of the base layer ( $E_b$ ), and stiffness of the subgrade ( $E_S$  or  $k$ ). In order to find unique solutions for all three parameters, an initial input must be provided. The most convenient additional parameter is the modular ratio ( $\beta$ ) of  $E_B$  to  $E_{PCC}$ . Typical values are provided in Table 3 (13).

$$E_{eq} = \frac{4E_{PCC}}{h_{eq}^3} [h_0^3 - (h_0 - h_{PCC})^3] + \frac{4E_b}{h_{eq}^3} [(h_{PCC} + h_b - h_0)^3 - (h_0 - h_{PCC})^3] \dots \text{Eq. 18}$$

$$h_0 = \frac{E_{PCC}h_{PCC}^2 + 2E_b h_b h_{PCC} + E_b h_b^2}{2(E_{PCC}h_{PCC} + E_b h_b)} \dots \text{Eq. 19}$$

$$E_{eq} = E_{PCC} \left( \frac{h_{PCC}}{h_{eq}} \right)^3 + E_b \left( \frac{h_b}{h_{eq}} \right)^3 \dots \text{Eq. 20}$$

Where:

$E_{eq}$ ,  $E_{PCC}$ ,  $E_b$  = Young's modulus of equivalent pavement layer, top PCC layer, and base layer, respectively

$h_{eq}$ ,  $h_{PCC}$ ,  $h_b$  = Thickness of equivalent pavement layer, top PCC layer, and base layer, respectively

$h_0$  = Depth to neutral axis of equivalent pavement layer

The method of solution for NUS-BACK3 is similar to the two-layer solution that was previously discussed, except that it only uses the elastic solid subgrade model and it utilizes the work of Burmister (23) as well as Panc (9). The three-layer system is analyzed by simultaneously solving Equations 21, 22, and 23 for unique values of  $\ell$ ,  $c$  and  $E_b$ . It is noted that the 3-layer system requires three deflection measurements instead of just two in order to find a unique solution.

**Table 3 Typical Modular Ratios ( $\beta$ ) for  $E_{Base} / E_{PCC}$  (13)**

Base Type	$\beta$	Base Type	$\beta$
Hot-mixed, hot-laid asphalt concrete (AC), dense graded	10	Sand asphalt	50
Hot-mixed, hot-laid AC, open graded	15	PCC, prestressed	1
Jointed plain concrete pavement	1	PCC, fiber reinforced	1
Jointed reinforced concrete pavement	1	Recycled JPCP	100
Continuously reinforced concrete pavement	1	Recycled JRCP	100
Plant mix (emulsified asphalt) material, cold-laid	20	Recycled CRCP	100
Plant mix (cutback asphalt) material, cold-laid	20	Crushed Rock	150
Recycled AC, hot-laid, central plant mix	10	Gravel, uncrushed	200
Recycled AC, cold-laid, central plant mix	15	Crushed stone	150
Recycled AC, cold-laid, mixed-in-place	15	Crushed gravel	175
Recycled AC, heater scarification/recompaction	15	Crushed slag	175
Fine-grained soils: lime-treated soil	100	Sand	250
Fine-grained soils: cement-treated soil	50	Hot-mixed AC	15
Bituminous treated subgrade soil	100	Asphalt-treated mix	50
Soil-aggregate mixture (predominantly fine-grained)	400	Econcrete	4
Soil-aggregate mixture (predominantly coarse-grained)	250	Cement-treated soil	50
Dense-graded, hot-laid, central plant mix AC	10	Lean concrete	2
Dense-graded, cold-laid, central plant mix AC	15	Cracked/sealed PCC	25
Dense-graded, cold-laid, mixed-in-place AC	15	Treatment: lime	100
Open-graded, hot-laid, central plant mix AC	15	Treatment: lime, fly ash	150
Open-graded, cold-laid, central plant mix AC	15	Treatment: bitumen	100
Open-graded, cold-laid, mixed-in-place AC	15	Pozzolanic-aggregate mixture	100

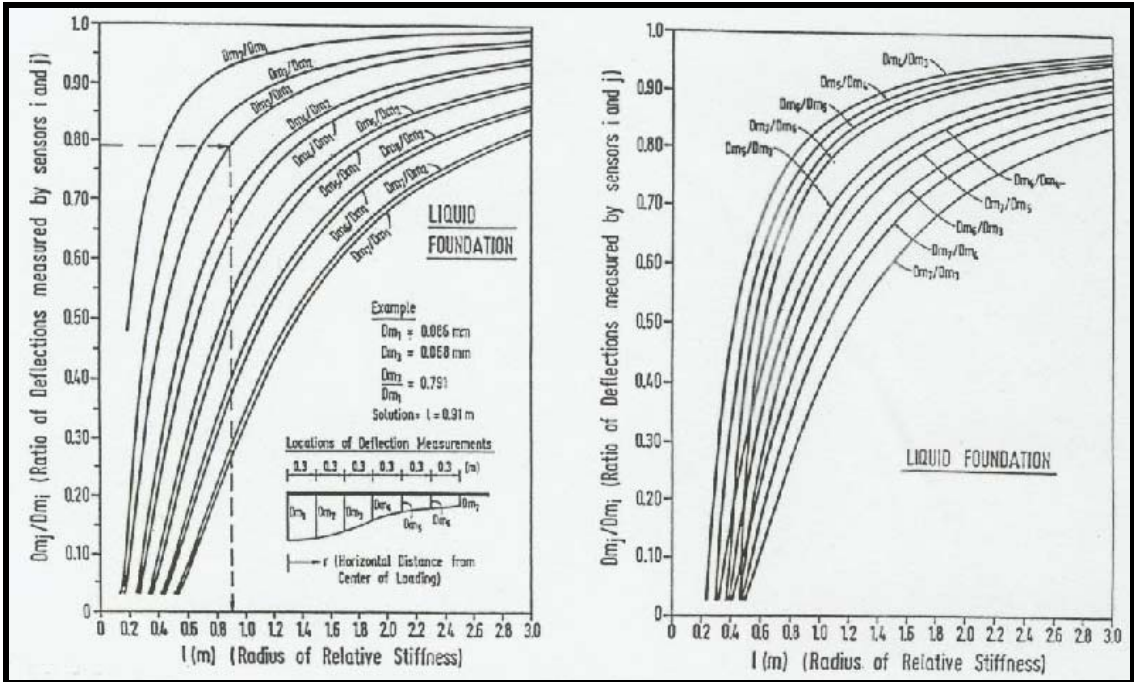


FIGURE 5 Graphical NUS-BACK Dense Liquid Solution for  $l$

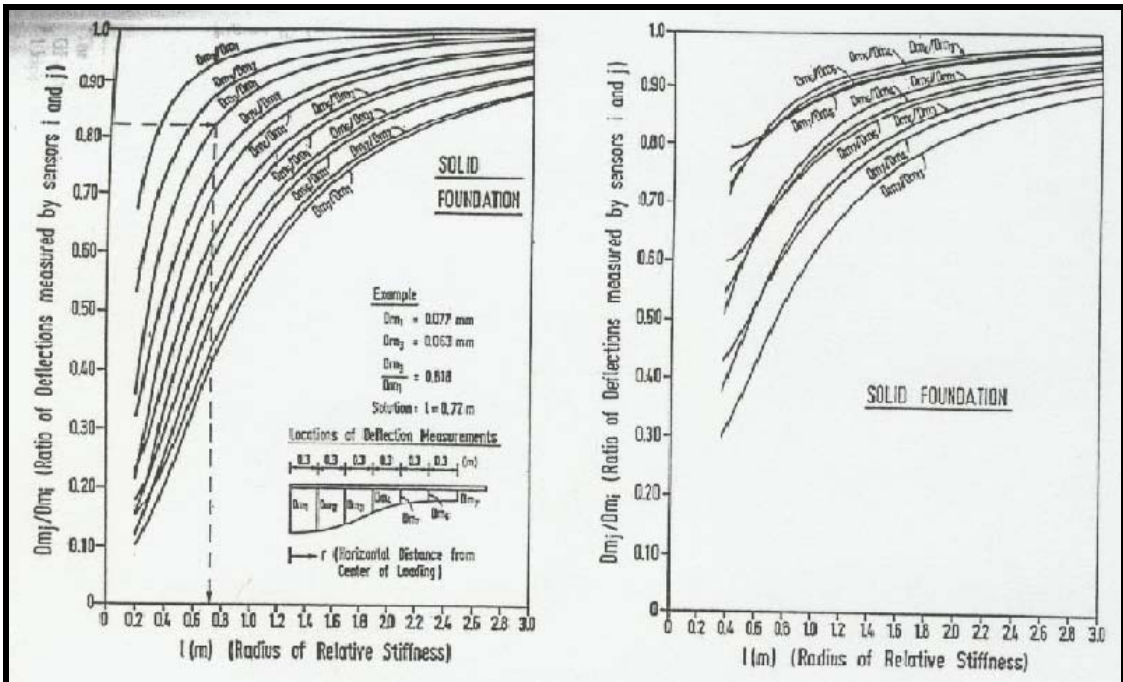
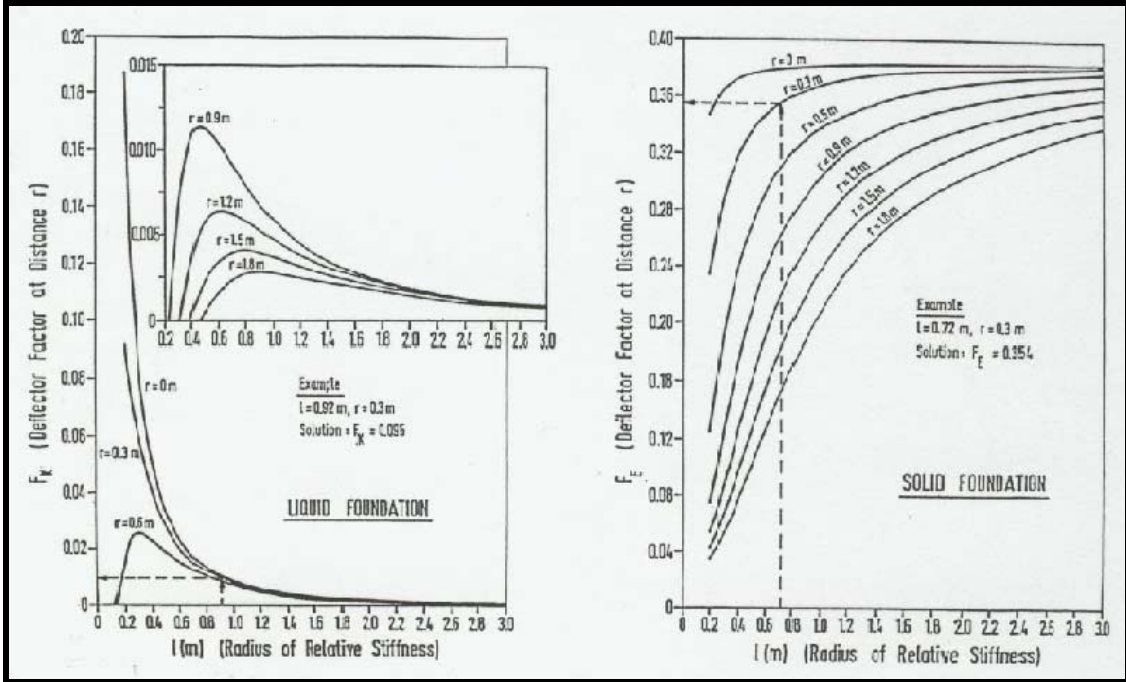


FIGURE 6 Graphical NUS-BACK Elastic Solid Solution for  $l$



**FIGURE 7 Graphical NUS-BACK Solutions for  $F_k$  and  $F_E$**

$$d_{m1} = \frac{2(1 - \mu_b^2)P}{\pi a E_b} F(\ell, c, r_1) \dots \dots \dots \text{Eq. 21}$$

$$d_{m2} = \frac{2(1 - \mu_b^2)P}{\pi a E_b} F(\ell, c, r_2) \dots \dots \dots \text{Eq. 22}$$

$$d_{m3} = \frac{2(1 - \mu_b^2)P}{\pi a E_b} F(\ell, c, r_3) \dots \dots \dots \text{Eq. 23}$$

$$c = \frac{(1 + \mu_b)E_s}{(1 + \mu_s)E_b} \dots \dots \dots \text{Eq. 24}$$

$$\ell = \left( \frac{E_c h_c^3 (1 - \mu_b^2)}{6(1 - \mu_c^2)E_b} \right)^{1/3} \dots \dots \dots \text{Eq. 25}$$

In the above equations,  $\mu_b$  is the Poisson ratio of the base;  $c$  and  $\ell$  are given by Equations 24 and 25, respectively. The definition of all other variables is consistent with the definitions given for two-layer NUS-BACK equations. Unfortunately, a graphical solution for NUS-BACK3 is not available.

**2.2.3.4. AREA Method for Rigid Pavements**

Another graphical backcalculation process has been developed to account for preferential FWD sensor spacings in which the radius of the load plate is 5.9 inches (12). The first step for this graphical procedure is to calculate the AREA of the deflection basin. The AREA parameter is the area of the deflection basin normalized to some height to negate the effect of load magnitude. Figures 8, 9, and 10 illustrate three common layouts for arranging sensors during FWD testing,  $AREA_{36}$ ,  $AREA_{S60}$ , and  $AREA_{72}$ . Equations 26, 27, and 28 are used to calculate the AREA parameter for the  $AREA_{36}$ ,  $AREA_{S60}$ , and  $AREA_{72}$  layouts, respectively. In each of the figures below, the term “ $d_x$ ” refers to the vertical deflection that is measured at a horizontal distance “ $x$ ” from the center of the load plate.

The  $AREA_{S60}$  layout is generally considered to provide the best measure of curvature in the basin, but the following graphical procedure may be used for  $AREA_{36}$ ,  $AREA_{S60}$ , or  $AREA_{72}$ . After the  $AREA_x$  parameter is calculated using the appropriate equation, the next step is to calculate the radius of relative stiffness. This may be done empirically using Equation 29 and the coefficients from Table 4.

$$AREA_{36} = 6 \cdot \left( 1 + 2 \cdot \frac{d_{12}}{d_0} + 2 \cdot \frac{d_{24}}{d_0} + \frac{d_{36}}{d_0} \right) \dots\dots\dots Eq. 26$$

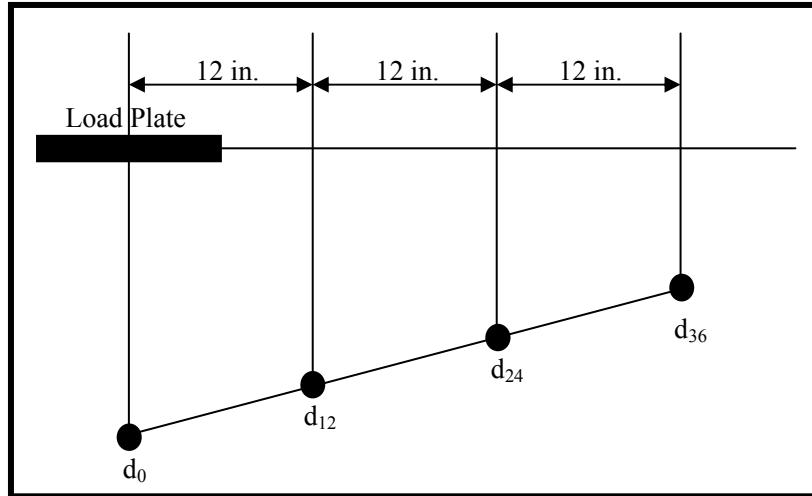


**FIGURE 8** AREA<sub>36</sub> Deflection Sensor Layout

$$AREA_{S60} = 4 + 6 \cdot \frac{d_8}{d_0} + 5 \cdot \frac{d_{12}}{d_0} + 6 \cdot \frac{d_{18}}{d_0} + 9 \cdot \frac{d_{24}}{d_0} + 18 \cdot \frac{d_{48}}{d_0} + 12 \cdot \frac{d_{60}}{d_0} \dots \dots \dots \text{Eq. 27}$$

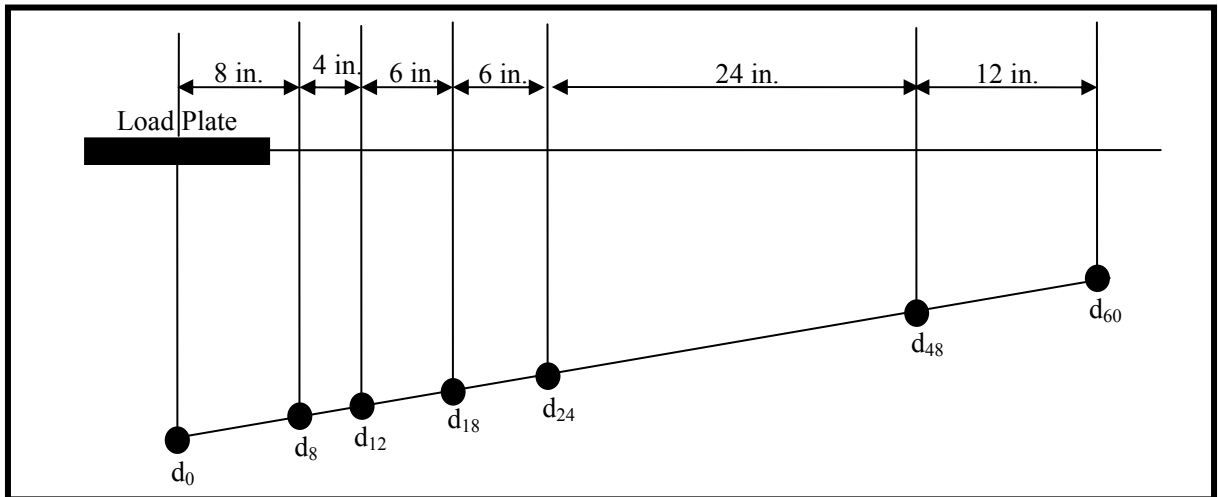


**FIGURE 9** AREA<sub>S60</sub> Deflection Sensor Layout

$$AREA_{72} = 6 \cdot \left( 1 + 2 \cdot \frac{d_{12}}{d_0} + 2 \cdot \frac{d_{24}}{d_0} + 2 \cdot \frac{d_{36}}{d_0} + 2 \cdot \frac{d_{48}}{d_0} + 2 \cdot \frac{d_{60}}{d_0} + \frac{d_{72}}{d_0} \right) \dots \dots \dots \text{Eq. 28}$$

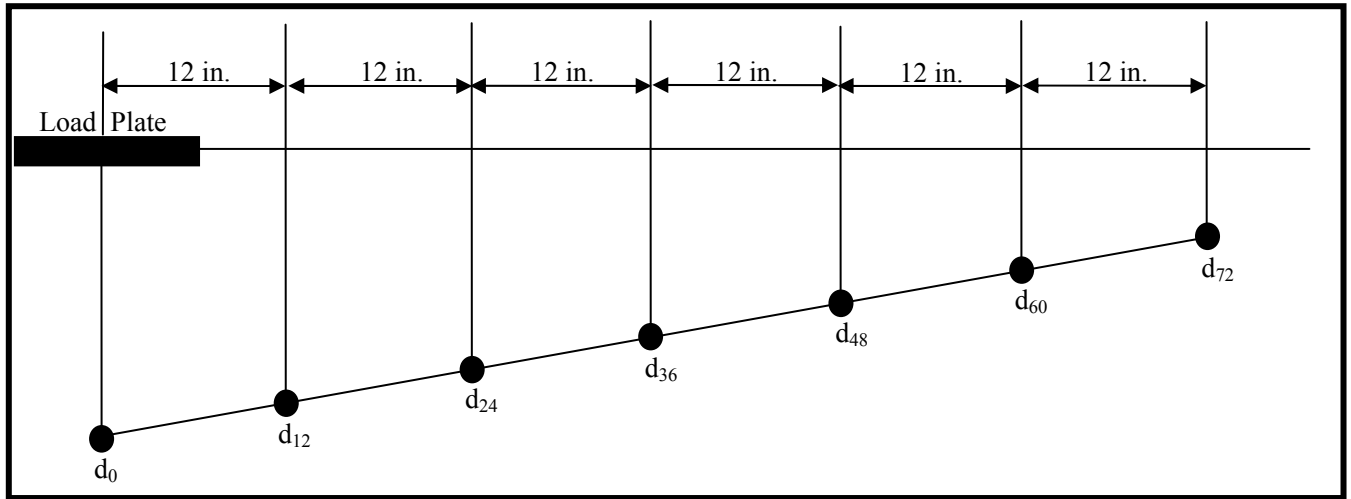


**FIGURE 10** AREA<sub>72</sub> Deflection Sensor Layout

$$\ell = \left[ \frac{\ln\left(\frac{k_1 - AREA}{k_2}\right)}{-k_3} \right]^{1/k_4} \dots\dots\dots \text{Eq. 29}$$

**Table 4** Empirical Coefficients for Calculating Radius of Relative Stiffness (12)

	<b>k<sub>1</sub></b>	<b>k<sub>2</sub></b>	<b>k<sub>3</sub></b>	<b>1/k<sub>4</sub></b>
AREA <sub>36</sub>	36	1812.597	2.559	4.387
AREA <sub>S60</sub>	60	289.708	0.698	2.566
AREA <sub>72</sub>	72	242.385	0.442	2.205

The radius of relative stiffness is then used to match the AREA<sub>X</sub> parameter with the general AREA parameter using an appropriate curve from Figure 11 that corresponds to the appropriate sensor layout.

One last empirical quantity, a nondimensional deflection coefficient ( $d_r^*$ ), has to be calculated before the pavement and subgrade stiffness can be estimated. The deflection coefficient is calculated using Equation 30 and the empirical coefficients from Table 5. After  $d_r^*$  is found, the stiffness of the subgrade and pavement are estimated for each individual deflection measurement using Equations 31 and 32, respectively. The arithmetic average of those values is taken to be representative of the entire basin.

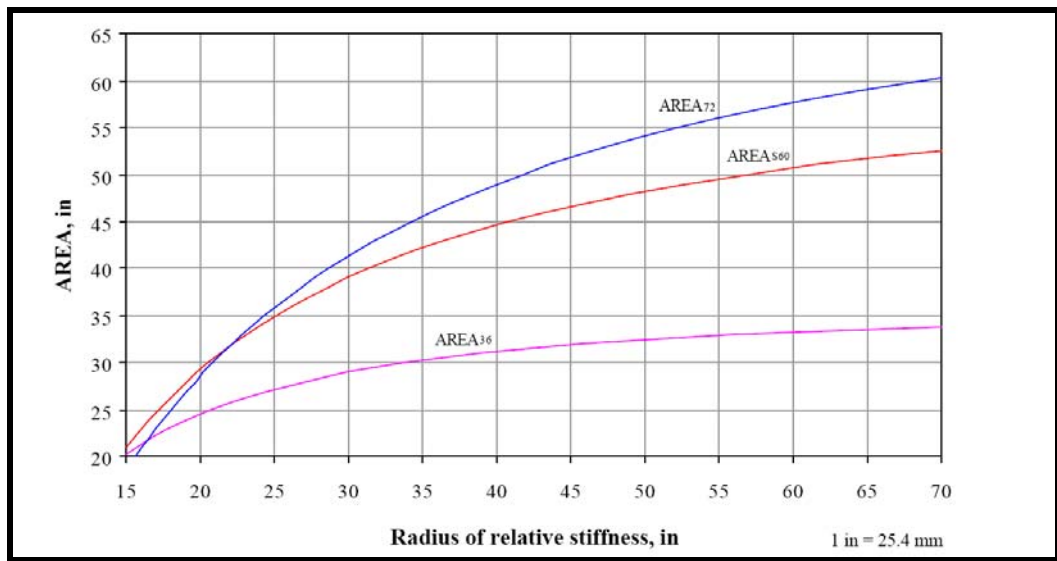


**FIGURE 11 Curves Relating AREA<sub>X</sub> to General AREA Parameter (12)**

$$d_r^* = a \cdot e^{-b \cdot e^{-c \cdot \ell}} \dots \dots \dots \text{Eq. 30}$$

Where:  $d_r^*$  = Nondimensional deflection coefficient for the deflection at a radial distance  $r$  from the load plate

$a, b, c$  = Coefficients from Table 2

$\ell$  = Radius of relative stiffness

**Table 5 Empirical Coefficients for Calculating Deflection Coefficient (12)**

<b>d<sub>x</sub>*</b>	<b>a</b>	<b>b</b>	<b>c</b>
d <sub>0</sub> *	0.12450	0.14707	0.07565
d <sub>8</sub> *	0.12323	0.46911	0.07209
d <sub>12</sub> *	0.12188	0.79432	0.07074
d <sub>18</sub> *	0.11933	1.38363	0.06909
d <sub>24</sub> *	0.11634	2.06115	0.06775
d <sub>36</sub> *	0.10960	3.62187	0.06568
d <sub>48</sub> *	0.10241	5.41549	0.06402
d <sub>60</sub> *	0.09521	7.41241	0.06255
d <sub>72</sub> *	0.08822	9.59399	0.06118

The *k* value obtained from the AREA method is representative of dynamic loading conditions (*k<sub>d</sub>*), but the 1993 AASHTO Pavement Design Guide uses the static *k* value (*k<sub>s</sub>*). Therefore, the obtained value must be converted to a static *k* value. Robust methods for converting between the two measurements are available, but AASHTO recommends that Equation 33 be used for a simplified conversion (16, 24).

$$k = \frac{P \cdot d_x^*}{d_x \cdot \ell^2} \dots\dots\dots \text{Eq. 31}$$

$$E_{PCC} = \frac{12 \cdot \ell^4 \cdot (1 - \mu^2) \cdot k}{h^3} \dots\dots\dots \text{Eq. 32}$$

$$k_s = k_d \div 2 \dots\dots\dots \text{Eq. 33}$$

Where: *k* = Modulus of subgrade reaction (psi/in.)

*P* = Applied load (lb)

$d_X^*$  = Nondimensional deflection coefficient for deflection at  
radial distance  $r$  from load

$d_X$  = Measured deflection at radial distance  $r$  from the load (in.)

$\ell$  = Radius of relative stiffness (in.)

$E_{PCC}$  = PCC elastic modulus (psi)

$\mu$  = Poisson's ratio of PCC

$h$  = Slab thickness (in.)

#### **2.2.3.5. Best-Fit Procedure**

The preceding graphical AREA approach is one of two common AREA backcalculation methods that utilize Westergaard's solution for the interior loading of a horizontally infinite plate on a dense liquid foundation. The other main method is called the Best Fit procedure (15). The graphical AREA method matched a theoretical deflection basin to the measured deflection basin. That is, layer properties were found that provided the best match between the deflection basins, as a whole. The Best-Fit Procedure, however, matches deflections point-by-point. The point-by-point criteria is less stringent than fitting an entire deflection basin, and the Best-Fit Method actually provides a better match between measured and calculated deflection basins.

Consider Equation 34, which describes the distribution of deflections ( $w$ ) at a distance ( $r$ ) from the center of a vertical load evenly distributed across a circular area with radius  $a$ . The Best Fit method finds the combination of  $k$  and  $\ell_k$  that causes Equation 34 to predict a deflection basin closest to the actual measured basin. Then, an algorithm uses those two values to find the combination of  $k$  and  $E_{PCC}$  that again causes

the best match between calculated and measured deflection basins. The mechanics of the algorithm involve minimizing an error function, the mathematics of which are described elsewhere (15).

$$w(r) = \frac{P}{k} \cdot f(r, \ell_k) \dots \dots \dots \text{Eq. 34}$$

- Where:
- w = Vertical deflection
  - r = Radial distance from center of load
  - p = Applied pressure
  - k = Coefficient of subgrade reaction
  - $\ell_k$  = radius of relative stiffness

The Best-Fit Method can also be used to analyze two-layered rigid pavements such as a PCC slab that is underlain by a granular base (21, 25). The analyzing of such a pavement is facilitated by the same method that was described for NUS-BACK in Section 2.2.3.3.

The main advantage to using the Best Fit method is that the theoretically derived deflection basin is made to be as close as possible to the measured deflection basin. The biggest problem with this approach is that there exist too many combinations of parameters ( $\ell_k$ , k, and  $E_{PCC}$ ) that will make the Best Fit procedure appear to work even if the results are incorrect and/or unreasonable. Best Fit procedures are performed by software, and most of the time the computer program will request “seed” values and acceptable ranges of necessary parameters to ensure that the values chosen for the “best fit” are at least reasonable. There is no guarantee, however, that the values will be correct.

### 2.2.3.6. *LTPP Forward Calculation*

The Long-Term Pavement Performance (LTPP) program has documented a closed-form procedure termed “forward calculation” for estimating the stiffness of subgrade soils as well as rigid and flexible pavements on a closed-form basis (14). Forward calculation spreadsheets are available in both English and Metric format, free of charge, from LTPP. Note, however, that forward calculation is only intended to be used for generating approximate estimations of pavement and subgrade stiffnesses. Those estimates can then be used to check the reasonableness of other estimates from more complex backcalculations.

Forward Calculation uses two deflection values to approximate the upper subgrade stiffness. The deflection under the center of the FWD load plate ( $d_0$ ) and the deflection at an offset where the deflection is approximately one-half of  $d_0$  are used as inputs into a model based on the Hogg model, which idealizes the pavement structure as a thin plate on an elastic foundation (26, 27). The model used for Forward Calculation can be altered to reflect 3 distinct cases: (1) infinite elastic foundation and  $\mu = 0.5$ ; (2) and (3) finite elastic foundation with thickness assumed equal to 10 times the characteristic length of the deflection basin and  $\mu = 0.4$  and  $0.5$ , respectively. Case 2 is strongly recommended.

The upper subgrade stiffness ( $E_0$ ) is approximated from the sequence of Equations 35 - 38 in conjunction with Table 6.

$$E_0 = I \cdot \frac{(1 + \mu_0)(3 - 4\mu_0)}{2(1 - \mu_0)} \left( \frac{S_0}{S} \right) \left( \frac{P}{\Delta_0 I} \right) \dots \dots \dots \text{Eq. 35}$$

$$r_{50} = r \frac{\left(\frac{1}{\alpha}\right)^{1/\beta} - B}{\left[\frac{1}{\alpha} \left(\frac{\Delta_0}{\Delta_r} - 1\right)\right]^{1/\beta} - B} \dots\dots\dots \text{Eq. 36}$$

$$l = y_0 \frac{r_{50}}{2} + \left[ (y_0 r_{50})^2 - 4mar_{50} \right]^{1/2} \dots\dots\dots \text{Eq. 37}$$

if  $\frac{a}{l} < 0.2$ , then  $l = (y_0 - 0.2m)r_{50}$

$$\left(\frac{S_0}{S}\right) = 1 - \bar{m} \left(\frac{a}{l} - 0.2\right) \dots\dots\dots \text{Eq. 38}$$

if  $\frac{a}{l} < 0.2$ , then  $\frac{S_0}{S} = 1.0$

- Where:
- $E_0$  = Upper subgrade modulus
  - $\mu_0$  = Poisson's ratio for subgrade
  - $S_0$  = Theoretical point load stiffness
  - $S$  = Pavement stiffness =  $p/\Delta_0$  (area loading)
  - $p$  = Applied load
  - $\Delta_0$  = Deflection at center of load plate
  - $\Delta_r$  = Deflection at offset distance  $r$
  - $r$  = Distance from center of load plate
  - $r_{50}$  = Offset distance where  $\Delta_r/\Delta_0 = 0.5$
  - $l$  = Characteristic length
  - $h$  = Thickness of subgrade
  - $I$  = Influence factor
  - $\alpha, \beta, B$  = Curve fitting coefficients
  - $y_0, m$  = Characteristic length coefficients
  - $m(\text{bar})$  = Stiffness ratio coefficient

**Table 6 Forward Calculation Subgrade Stiffness Coefficients (14)**

Case		1	2	3
I		0.1925	0.1689	0.1614
Range $\Delta r/\Delta_0$		All Values	> 0.43	> 0.70
$R_{50} = f(\Delta r/\Delta_0)$	A	0.3210	0.3804	0.4065
	$\beta$	1.7117	1.8246	1.6890
	B	0	0	0
Range $\Delta r/\Delta_0$			< 0.43	< 0.70
$R_{50} = f(\Delta r/\Delta_0)$	A		4.3795E-4	2.6947E-3
	$\beta$		4.9903	4.5663
	B		3	2
$l = f(r_{50}, a)$	$y_0$	0.527	0.603	0.642
	m	0.098	0.108	0.125
$(S/S_0) = f(a/l)$	m(bar)	0.185	0.208	0.219

The LTP Forward Calculation procedure applies the previously described 4-sensor AREA<sub>36</sub> method for rigid pavements as well as a revised AREA<sub>12</sub> method for flexible pavements to estimate the stiffness of bound surface course. AREA<sub>12</sub> is defined by Equation 39 and the setup shown in Figure 12.

$$A_{12} = 2 \cdot \left[ 2 + 3 \left( \frac{d_8}{d_0} \right) + \left( \frac{d_{12}}{d_0} \right) \right] \dots \dots \dots \text{Eq. 39}$$

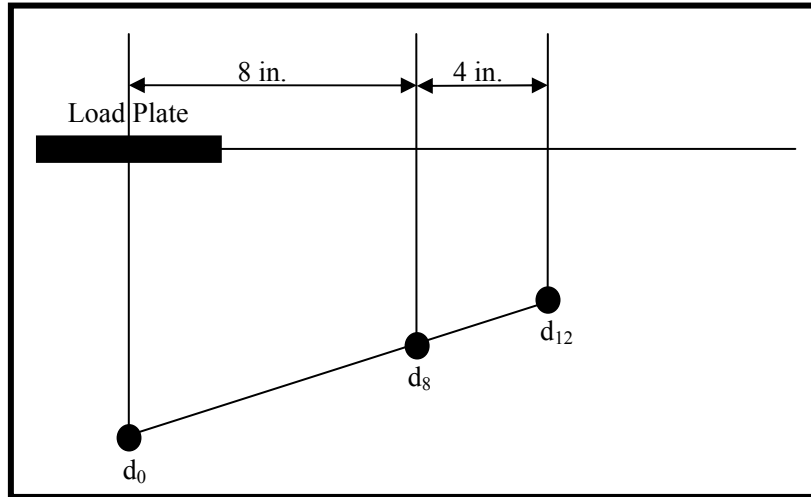


**FIGURE 12 AREA<sub>12</sub> Deflection Sensor Layout**

The Forward Calculation procedure is based on the AREA of a given pavement system relative to that of an idealized system whose layers all have identical values for stiffness and Poisson's ratio. If continuity is assumed between layers of the ideal pavement system, AREA<sub>36</sub> and AREA<sub>12</sub> will reach minimum values of 11.04 and 6.85, respectively. This holds for any value of stiffness and/or Poisson's ratio so long as it is held constant through the different layers. A more realistic pavement structure consists of a surface course that is stiffer than the underlying pavement and/or subgrade layers. The larger the difference between the stiffness of the wearing course and underlying layers, the larger the AREA will be. Equations 40 and 41 are used to calculate the AREA factors for rigid and flexible pavements, respectively. These area factors essentially give a measure of how much a given pavement increases the AREA from its theoretical minimum value. Finally, Equations 42 and 43 are used to estimate the stiffness of the upper PCC or HMA layers, respectively.

$$AF_{PCC} = \left[ \frac{k_2 - 1}{k_2 - \left( \frac{AREA_{36}}{k_1} \right)} \right]^{1.79} \dots\dots\dots Eq. 40$$

Where:  $AF_{PCC}$  = AREA factor for PCC  
 $k_1 = 11.04$  (theoretical minimum  $AREA_{36}$ )  
 $k_2 = 3.262$  (theoretical maximum  $AREA_{36} = 36/11.04$ )

$$AF_{HMA} = \left[ \frac{k_2 - 1}{k_2 - \left( \frac{AREA_{12}}{k_1} \right)} \right]^{1.35} \dots\dots\dots Eq. 41$$

Where:  $AF_{HMA}$  = AREA factor for HMA  
 $k_1 = 6.85$  (theoretical minimum  $AREA_{12}$ )  
 $k_2 = 1.752$  (theoretical maximum  $AREA_{36} = 12/6.85$ )

$$E_{PCC} = \frac{E_0 \cdot AF_{PCC} \cdot k_3 \left( \sqrt[3]{AF_{PCC}} \right)}{k_3^{2.38}} \dots\dots\dots Eq. 42$$

$$E_{HMA} = \frac{E_0 \cdot AF_{HMA} \cdot k_3 \left( \sqrt[3]{AF_{HMA}} \right)}{k_3^2} \dots\dots\dots Eq. 43$$

Where:  $E_{PCC}$  = Elastic modulus of upper PCC layer(s)  
 $E_{HMA}$  = Elastic modulus of upper HMA layer(s)  
 $AF_{PCC}, AF_{HMA}$  = AREA factors  
 $k_3$  = Thickness ratio of upper layer thickness to load plate diameter  
 $a$  = Load plate radius  
 $E_0$  = Composite modulus of the entire pavement system beneath the load plate

And, 
$$E_0 = \frac{1.5 \cdot a \sigma_0}{d_0}$$

$\sigma_0$  = Peak pressure of FWD impact load under the load  
plate

#### **2.2.3.7. MODULUS**

MODULUS is a program that utilizes the database-search technique to backcalculate the moduli of pavement layers (19). Such a program is developed by using a linear elastic computer program to simulate the deflection basins that would result from an FWD-type load on thousands of combinations of hypothetical layer thicknesses and stiffnesses. All of the fictitious deflection basins are then stored in a permanent database. The program works by searching and interpolating between these previously calculated deflection basins to find the combination of layer thicknesses and stiffnesses that would theoretically exhibit a deflection basin closest to what was measured in the field. Until recently, MODULUS has been a DOS based program. The newest version, MODULUS 6.0, has been built on a Windows platform and appears to be much more user friendly than previous versions of the program.

The manner in which MODULUS calculates a deflection is depicted by Equation 44. Ultimately, an error function in the form of Equation 45 is minimized to find the best solution from the database. In order for this process to work, the user must input known layer thicknesses, plus seed values and acceptable ranges for the moduli of those layers. Equation 44 shows that MODULUS works in terms of modular ratios instead of independent moduli. For this reason, an estimate of the subgrade modulus ( $E_n$ ) must be provided so that the program can report actual moduli instead of ratios.

$$w_i^c = \frac{qa}{E_n} f_i \left( \frac{E_1}{E_n}, \frac{E_2}{E_n}, \dots, \frac{E_{n-1}}{E_n} \right) \dots \text{Eq. 44}$$

$$\varepsilon^2 = \sum_{i=1}^s \left( \frac{w_i^m - w_i^c}{w_i^m} \right)^2 = \sum_{i=1}^s \left( 1 - \frac{w_i^c}{w_i^m} \right)^2 \dots \text{Eq. 45}$$

- Where:
- $w^c$  = Computed deflection
  - $w^m$  = Measured deflection
  - $i$  = sensor number from 1 to S
  - $E_x$  = Elastic modulus for layer number x
  - $q$  = Contact pressure
  - $a$  = Contact radius
  - $\varepsilon^2$  = Squared error
  - $f_i$  = Value from layer system program and used as a data base

The Strategic Highway Research Program (SHRP) found in 1993 that MODULUS showed superior performance to other programs (MODCOMP3 and WESDEF) for analyzing the roughly 800 test sections that comprised the SHRP deflections database at the time (13). SHRP published a set of recommendations for performing backcalculations with MODULUS that focused on three major areas: definition of layer moduli ranges, modeling of the pavement structure, and evaluation of the analysis results. A summary of those recommendations is now presented.

When deciding a seed value for HMA layers, Equation 46 should be used whenever the necessary inputs are available. Equation 47 should be used in lieu of Equation 46 for cases in which little is known about the HMA mixture. Table 7 can be used to supply some of the variables for Equation 47 if they are unknown.

$$\log_{10}[E^*] = 2.2250053 - 0.091756V_{be} - 0.027949V_a - 0.096881P_{200} + \dots \text{Eq. 46}$$

$$0.250094P_{abs} - 0.006447t_p + 0.060612f - 0.00007404t_p^2 +$$

$$0.00191539V_{be}^2 + 0.0082813P_{200}^2 - 0.0010225P_{3/4}^2 +$$

$$0.0001909P_{3/8}^2 - 0.0801155P_{abs}^2 + 0.0148592\eta_{70,10^6}^2 - 0.0024159f^2$$

$$+ 0.00094015P_{3/8}V_{be} + 0.00084534P_{3/4}V_{be} + 0.0004965P_{3/4}P_4 -$$

$$0.00034328P_{3/8}P_{abs}$$

$$\log_{10}[E^*] = 0.553833 + 0.028829P_{200}f^{0.17033} - 0.03476V_a + 0.070377\eta_{70,10^6} + \dots \text{Eq. 47}$$

$$0.000005[t_p^{(1.3 + 0.49825\log(f))}P_{HMA}^{0.5}] - 0.00189[t_p^{(1.3 + 0.49825\log(f))}P_{HMA}^{0.5}f^{1.1}]$$

- Where:
- $E^*$  = HMA modulus, in  $10^5$  psi
  - $V_{be}$  = Effective binder content, by volume percentage
  - $G_{mb}$  = Maximum specific gravity of the mix
  - $G_b$  = Specific gravity of bitumen (assume 1.010 if unknown)
  - $V_a$  = Percent air voids in mix
  - $P_{200}$  = Percentage aggregate weight passing the No. 200 sieve
  - $P_{abs}$  = Percent asphalt absorption, by weight of aggregate

$$P_{abs} = \frac{G_{se} - G_{sb}}{G_{sb} - G_{se}} \times G_b \cdot 100\%$$

- $P_{HMA}$  = Percent asphalt content by weight of mix
- $f$  = Test frequency of load wave, assume 16 Hz in all cases
- $t_p$  = Mid-depth HMA temperature, degrees Fahrenheit
- $P_4, P_{3/8}, P_{3/4}$  = Percent aggregate weight retained in No. 4, 3/8", and 3/4" sieves, respectively
- $\eta_{70,10^6}$  = Asphalt viscosity at 70°F, in  $10^6$  Poises

**Table 7 Default Values for Determining HMA stiffness (19)**

	V <sub>a</sub>	P <sub>HMA</sub>	P <sub>200</sub>
Surface Courses	4%	6%	6%
Binder Courses	5%	5%	5%
Base Courses	7%	4%	4%
Sand Asphalt Mixtures	-	8%	6%

All HMA layers that have the same construction age are combined into a single composite asphalt layer with thickness  $h_{comp}$  and stiffness  $E_{comp}$  as defined by Equations 48 and 49, respectively. The range of moduli that is reported to MODULUS should be determined according to Equation 50.

$$h_{comp} = \sum_{i=1}^n h_i \dots\dots\dots \text{Eq. 48}$$

$$E_{comp} = \sum \left[ \left( \frac{h_i}{h_{comp}} \right) \cdot \sqrt[3]{E_i} \right]^3 \dots\dots\dots \text{Eq. 49}$$

$$\text{Range} = 0.25 \cdot E_{(\text{initial or composite})} \text{ to } [3.00 \cdot E_{(\text{initial or composite})} < 3,000,000 \text{ psi}] \dots\dots \text{Eq. 50}$$

MODULUS also requires seed and range values for PCC layers in the pavement structure. A seed value for  $E_{PCC}$  is determined according to the methods in Table 8, which are listed in order of highest to lowest accuracy. The most accurate method for which input parameters are known should be used. The range of moduli that is reported to MODULUS is determined using Equation 51.

MODULUS is capable of modeling 4 layers, and if a given pavement system contains more than 4 layers, SHRP recommends 7 prioritized steps (available elsewhere)

for combining the layers so that all composite layers will maintain an accurate representation of field conditions.

**Table 8 Methods for Estimating Seed Value for  $E_{PCC}$  (19)**

Required Inputs	Methodology
Static modulus (E) test results	Report E directly
Compressive strength ( $f_c'$ ) in psi	$E = 57,000 \cdot (f_c')^{0.5}$
Splitting tensile strength in psi	$f_c' = [12.53 \cdot \text{Splitting tensile strength}] - 1275$ $E = 57,000 \cdot (f_c')^{0.5}$
No data	Assume $E = 4,000,000$ psi

$$\text{Range} = 0.25 \cdot E_{\text{initial}} \text{ to } [3.00 \cdot E_{\text{initial}} < 9,000,000 \text{ psi}] \dots \text{Eq. 51}$$

Unbound granular base and subbase materials may be estimated using values Table 1 unless the reported lower modulus bounds are lower than the seed value for subgrade modulus. In such a case, the seed value for subgrade modulus should be used as the lower bound for the unbound granular base or subbase material.

The seed value for subgrade modulus is calculated in two steps. First, Equations 52 and 53 are used to calculate the composite modulus of the pavement structure for each deflection that is measured at a radius beyond that of the load plate. The seed value is then taken as the minimum of the calculated composite moduli values.

$$E_{\text{comp}} = \frac{P_c \cdot a_c^2 \cdot (1 - \mu^2) \cdot C}{d_r \cdot r} \dots \text{Eq. 52}$$

$$C = 1.1 \log\left(\frac{r}{a_c}\right) + 1.15 \dots \text{Eq. 53}$$

Where:  $E_{\text{comp}}$  = Composite modulus of the pavement  
 $P_c$  = Contact pressure applied by FWD  
 $a_c$  = Load plate radius, in.  
 $\mu$  = Poisson's ratio (assume 0.4)  
 $d_r$  = Measured deflection at radial distance  $r$   
 $r$  = Radial distance from deflection  
 $C$  = deflection constant

When all of the preceding recommendations are followed, the backcalculated moduli have a good chance of being reasonable, but there is no guarantee. To ensure some degree of accuracy, SHRP also includes recommendations for evaluating the results of a MODULUS backcalculation. First, a limit of 2% average error is set for the matching of individual deflections. In addition, if the reported modulus for any layer is equal to either the upper or lower bound of acceptable moduli for that layer, the reported modulus is considered invalid. Finally, SHRP recommends that all backcalculation results be closely reviewed by a qualified engineer to check for reasonableness. If the results are considered unreasonable for any reason, the backcalculation process should be screened for obvious errors and/or the results should be discarded.

#### **2.2.3.8. *ELMOD 5***

ELMOD is a Windows based backcalculation program that is marketed by Dynatest<sup>®</sup> and usually sold with the Dynatest<sup>®</sup> Falling Weight Deflectometer (28). The name, ELMOD, is an acronym which stands for Evaluation of Layer Moduli and Overlay Design. LTPP

has noted that ELMOD is well suited for processing large batches of FWD readings without constant attention from the user (14).

ELMOD uses an iteration-based backcalculation procedure that can forward model the pavement response using a variety of techniques. ELMOD is also known for its ability to model the temperature-dependent behavior of HMA and the nonlinear response of subgrade and aggregate materials (29). Older versions of the software were limited to two different types of forward calculation. The first option was a common deflection basin matching routine. The other option was based on matching the radius of curvature of the deflection basin instead of trying to match the basin as a whole. The literature suggests that the radius of curvature option is more accurate, but still acknowledges the merit of the more typical deflection basin matching technique (14). The most current version, ELMOD 5, is equipped with a finite element module (FEM) can treat every layer as non-linear elastic.

ELMOD is used by the Arkansas State Highway and Transportation Department (AHTD), and is generally a good candidate for governmental agencies for several reasons. First of all, the software is available with the Dynatest® FWD, which is likely to be purchased by state DOTs even without the inclusion of software. Second, as noted by LTPP, ELMOD is capable of running large batches of FWD field data. This is a valuable feature when long stretches of highway or other roadways are being analyzed. In addition, ELMOD contains optional automated tools for determining the remaining life of a pavement and also for overlay design (28). The accuracy of these tools is beyond the scope of the current study, but their potential convenience is noted.

### **2.2.3.9.        *BAKF***

BAKF, as the name implies, was developed by the Federal Aviation Administration (FAA) specifically for the backcalculation of FWD data on airfield pavements (30).

BAKF used to be called FAABACKCAL, but the difference in names does not signify any significant difference in the software (31). BAKF is similar to ELMOD in that it is an iteration-based backcalculation that utilizes layered elastic theory (32).

BAKF is unique because it can model up to 10 pavement layers, and also because its code is written with a special emphasis on computational efficiency. It can be used for airfield or highway pavements for which a deflection basin (such as one created during FWD loading) is measured. A special feature of BAKF is its ability to calculate strains due to aircraft gear loads, which is accommodated by the FAA's linear elastic analyzing software, LEAF. The program is Windows based, and has a graphical user interface that is simple to use.

For the purposes of analyzing highway pavements, BAKF works by minimizing the error between LEAF-generated deflections and field-measured deflections. LEAF iteratively alters the moduli of user-defined layers and layer thicknesses until the generated and measured deflection measurements match within some tolerance.

### **2.2.3.10.      *DIPLO-DEF***

DIPLODEF is the newest and most versatile backcalculation software that is currently available (33). This program falls into the "iteration" class of backcalculation programs. The user must give DIPLO-DEF a seed and range moduli and thickness for each layer,

and then the program begins a process of forward-calculating theoretical deflections. DIPLO-DEF calculates theoretical deflections over and over again for different moduli until the theoretical, forward-calculated deflections match the measured deflections within some tolerance.

Even though DIPLO-DEF is theoretically superior to most existing backcalculation programs, it is relatively difficult to use. DIPLO-DEF is DOS based software that requires various sets of strings of alphanumeric characters to describe the deflection basin and the preferred method for backcalculation.

To better illustrate the features that set DIPLO-DEF apart from other programs, it is necessary to analyze the program in terms of each of its two main components: (1) the iterative search subprogram and (2) the methods by which forward calculations are conducted. DIPLO-DEF was created by combining two existing components. The computer optimization routine from a program called WESDEF is used as the iterative search subprogram, and a separate program called DIPLOMAT is used to perform forward calculations.

WESDEF works in the same manner as a stiffness matrix, and therefore will only work if it can generate enough equations to solve for the number of unknowns that are present. For backcalculation of pavement layer moduli, the number of layers for which moduli are to be determined represents the number of unknowns, and the number of deflection measurements represents the number of equations (19). For every deflection that is measured (j), a relationship in the form of Equation 54 is developed for each pavement and subgrade layer for which modulus is sought (i). Figure 13 illustrates the relationship that is developed between deflection and modulus. The system of equations

is solved to provide slopes ( $S_{ji}$ ) and intercepts ( $A_{ji}$ ) that can be used to predict a modulus to match the measured deflection. A reasonable solution is usually obtained within three iterations.

$$\log(\text{deflection}_j) = A_{ji} + S_{ji}(\log E_i) \dots\dots\dots \text{Eq. 54}$$

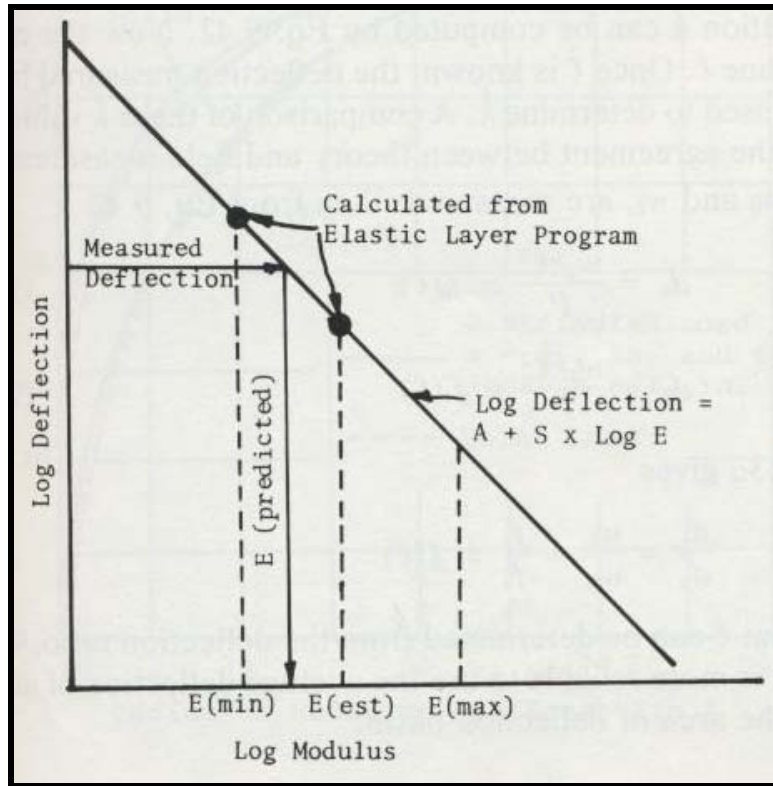


**FIGURE 13 WESDEF Relationship Between Deflection and Modulus (19)**

The second component of DIPLO-DEF, DIPLOMAT, is the part of the program that calculates new theoretical deflections after WESDEF performs an iteration.

DIPLOMAT is different from other forward calculation sub-programs because it can perform forward calculations using any combination of layered elastic theory and plate theory for pavement layers and either dense liquid or elastic solid modeling for the

subgrade. In addition, DIPLOMAT can handle any number of layers and model the layer interfaces as either fully bonded or unbonded.

In the grand scheme of pavement analysis, DIPLOMAT is most valuable because of its ability to analyze pavements with both HMA and PCC layers. The principles behind the software are not new, but DIPLOMAT is the first successful attempt to unify the various models that have been generally considered mutually exclusive since the onset of backcalculation in nondestructive testing. The development of DIPLOMAT is documented elsewhere (34).

The developers of DIPLO-DEF have recommended several guidelines for its use. First of all, care must be taken when choosing seed and range values for layer moduli. As with all iterative backcalculation procedures, the seed values do have an effect on the final backcalculated values. The user-input value for Poisson's Ratio of the subgrade should also be carefully considered. The developers found that using values above 0.45 seemed to cause DIPLO-DEF to abort early. Therefore, it is recommended that Poisson's Ratio values for the subgrade not be assumed above 0.45.

As a general note, the developers of DIPLO-DEF also stress the importance of patience when performing backcalculations. DIPLO-DEF offers many different options for modeling any given pavement structure, and the user should be prepared to exhaust all practical options and combinations in order to obtain reasonable results. In this effort, it is important to exercise engineering judgment and also to keep a careful record of all trials.

### **2.3. Spectral Analysis of Surface Waves**

A measure of seismic disturbances in pavement and subgrade layers can be used to estimate the stiffness and thickness of the different layers. More specifically, the elastic waves that are generated by a transient impulse load may be monitored by a recording device and then converted into a dispersion curve. The dispersion curve is then iteratively inverted to obtain a vertical profile of the shear wave velocity. Finally, discrepancies in the shear wave velocity profile are used to identify pavement and/or subgrade layer interfaces, and the average shear wave velocity within each layer is used to estimate the elastic modulus of the layer. This method of NDT is called the spectral analysis of surface waves (SASW) (35).

#### *2.3.1. Theoretical Background*

SASW is based on the theory of stress waves propagating in elastic media. For analysis, the pavement and subgrade layers are considered to comprise a layered elastic half space. This means that all of the various layers of pavement and subgrade are elastic, homogeneous, and isotropic, and that the entire elastic space ends at the ground surface. In contrast, an elastic whole space extends endlessly in all three dimensions. Two types of waves propagate radially outward from a disturbance in an elastic whole space: primary waves (also called P-waves or compression waves) and secondary waves (also called S-waves or shear waves). Primary waves cause particles in the elastic medium to deflect in the direction of wave propagation, and secondary waves cause particles in the elastic medium to deflect in the direction perpendicular to wave propagation. Primary waves always propagate at a higher velocity than secondary waves (35).

Half spaces accommodate two additional types of elastic waves: Rayleigh (R-waves) and Love (L-waves). Rayleigh waves are analogous to S-waves because they propagate perpendicular to the direction of wave propagation. The difference is that R-waves only exist near the boundary of a half space; the amplitude of an R-wave decays rapidly beyond a depth of 1.5 times the wavelength ( $\lambda$ ) of the R-wave. L-waves are similarly analogous to P-waves. The velocity at which these various types of waves travel is dependent upon the Poisson's ratio ( $\nu$ ) of the elastic medium. As  $\nu$  increases to its upper limit of 0.5, the ratio of P-wave velocity to S-wave velocity approaches infinity. This is due to the fact that a material with  $\nu = 0.5$  is theoretically incompressible, incapable of allowing the manifestation of S-waves. In contrast, the ratio of R-wave velocity to S-wave velocity remains within 0.86-0.95 for all values of  $\nu$  (35). This leads to a common practice of approximating shear wave velocity as 1.1 times the measured R-wave velocity.

A vertical disturbance on the surface of an idealized half space such as the one shown in Figure 14 results in the propagation of many different stress waves of myriad frequencies. Considering each different frequency of wave as a unique disturbance, it is convenient to define phase velocity ( $V_{ph}$ ) as the velocity at which a seismic disturbance travels. Low-amplitude, high-frequency waves will penetrate only shallow depths. Therefore, the phase velocity of such a wave is influenced mostly by the thin upper layers of the pavement system. Conversely, a high-amplitude, low-frequency wave penetrates through greater depths; its phase velocity is indicative of the properties of every layer through which it passes. Thus, the upper pavement layers do influence high-amplitude

waves, but with increasing amplitude, semi-infinite subgrade layers play a greater role in regulating the velocity of wave propagation.

For the purposes of SASW it is necessary to think of the phase velocity as a function of wave frequency instead of as a function of time. In the frequency domain, it is clear to see that a wave of particular frequency corresponds to a certain phase velocity, as a function of several elastic layer properties. Phase velocity depends upon the frequency of the wave ( $f$ ) and also the mass density ( $\rho$ ), Poisson's Ratio ( $\nu$ ), and

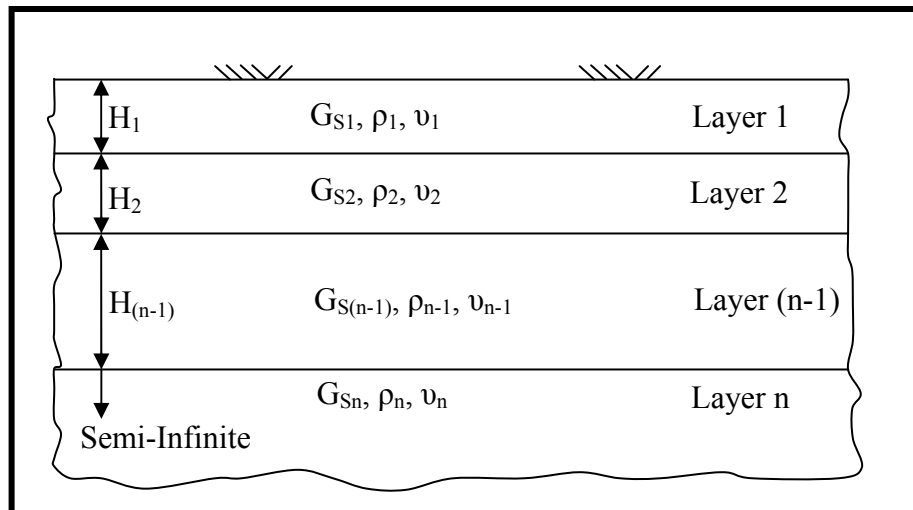


**FIGURE 14 Idealized Layered Half Space**

especially the Shear Modulus ( $G_S$ ) of the material in that layer. The height ( $H$ ) of each layer defines how much weight the elastic properties of that layer receive when averaging their impact with that from other layers through which a wave travels. Thus, by inputting known or assumed values for elastic layer properties, phase velocity can be solved directly in terms of an independent variable, wave frequency.

The relationship between wave frequency (or wavelength) and phase velocity over some frequency domain is called a dispersion function, the graph of which is called a dispersion curve. Plotting wavelength versus phase velocity is the more tactical choice because wavelength is used to estimate the sampling depth of the phase velocity. In practice the sampling depth is usually assumed to be between  $(\frac{1}{2})\lambda$  and  $(\frac{1}{3})\lambda$ ; a common assumption is to let the sampling depth equal  $(0.4)\lambda$ .

Dispersion curves that are created from hypothetical (not measured) elastic layer properties are referred to as theoretical dispersion curves. The ultimate goal of SASW testing is to identify pavement layer thicknesses and stiffnesses. This is done by creating a dispersion curve from measured R-wave phase velocities and then re-creating that shape with a theoretical dispersion curve that is defined by distinct layer thicknesses and properties. Though there is no unique solution of layer thicknesses and properties that will re-create a given dispersion curve, a solution can be found that adequately describes the layered pavement system under investigation through trial-and-error simulations (36).

### 2.3.2. *Field Procedures*

The basic idea behind SASW testing is to impart a transient vertical impact to the ground surface and measure the resulting particle motion from R-wave propagation at two or more known distances from the disturbance. The setup shown in Figure 15 will be used to illustrate the process of field data collection.

The transient impact that is used to generate seismic waves may be imparted by a hammer, falling weight, sinusoidal noise source, or a vehicle depending on the desired sampling depth. As was discussed in the previous section, high-frequency, low-

amplitude waves are used to sample shallow depths. Hand-held hammers are usually sufficient for creating such disturbances. Large vehicles and/or sinusoidal noise sources are more appropriate for generating the high-amplitude, low-frequency waves that are required for larger sampling depths.

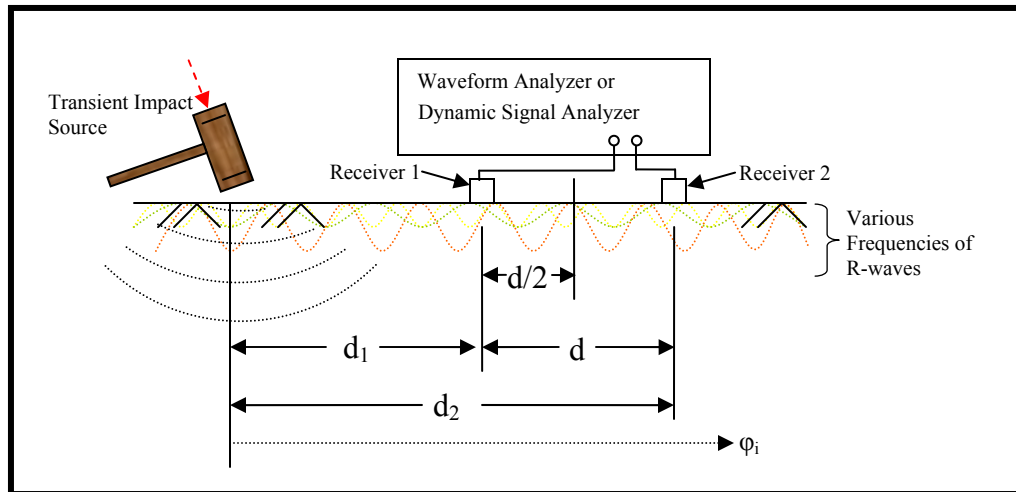


**FIGURE 15 SASW Configuration**

Sensor spacing ( $d$ ) is another setup issue that is chosen based upon desired sampling depth. For shallow sampling depths, small sensor spacings are both appropriate and convenient. As the sampling depth increases, however, so must the sensor spacing. The reason for this accommodation will be explained with the discussion of data reduction.

First, though, it is necessary to discuss how the raw field data is transformed into a format that can be used to create a dispersion curve. The first issue to consider is the switch from the time-domain to the frequency-domain. Fourier Transform is the mechanism by which the switch is made, and it is performed by an electronic machine

called a Wave Form Analyzer or a Digital Signal Analyzer. An example of one of these devices is shown in Figure 16 (37).

Depending on the type of analyzer that is being used, there are at least two - and sometimes many more - inputs for seismic disturbance readings. The device that is used to measure the particle motion from R-waves is chosen based on the depth and frequency of sampling. For large amplitudes and low frequencies, motion detectors (transducers) or velocity transducers (geophones) are sufficient to measure the particle motion for calculations of phase velocity. When performing SASW tests on a layered pavement system, however, it is more appropriate to use accelerometers. Accelerometers have a high frequency response that is better suited to the high-frequency waves that are used to analyze stiff pavement layers (38). The time domain can be used to convert the acceleration measurements to the desired value of vertical particle motion.



**FIGURE 16 HP 35670A Digital Signal Analyzer (37)**

One problem with using the Fourier Transform for transient impacts is the noise that is present from surrounding activities and from the reflection of waves between elastic layers. Noise can be thought of as vibrations in the elastic half space that are caused by a phenomenon other than direct propagation of individual R-waves. Examples of such phenomena could be nearby traffic, multi-modal R-waves, or even the reflection of just one R-wave.

SASW configurations in which only two measurements of vertical particle motion are taken are most susceptible to noise. The two most common and accepted ways to arrange a set of two receivers - common receivers midpoint (CRMP) geometry and common source (CS) geometry - are shown in Figures 17 and 18, respectively. It has been argued that CRMP geometry reduces scatter by maintaining equidistant spacing between receivers and impact, but others have not found the reduction in scatter to be significant enough to justify abandoning the convenience of CS geometry (38).

When using CRMP geometry the two receivers are positioned equal distances from an imaginary centerline and the transient impact is applied on either side of the receivers at a distance equal to the distance between the receivers. Next, the receivers and transient load are moved further away from the stationary imaginary centerline and the test is repeated, again from both sides. This process is usually repeated 5 or 6 times so that different ranges of R-wave wavelength may be measured. From Figure 17 it can be seen that for each repetition of the test both receivers and the transient impact must be moved. CS geometry is more convenient because the source of the transient impact can be left in one place for many different receiver spacings. The transient impact is still positioned at a distance equal to the distance between the two receivers, but instead of

rearranging the setup about a stationary imaginary centerline, the receivers are simply offset a further distance from the transient impact source (39).

Taking readings of seismic reactions for different sensor spacings provides a larger number of wavelength samples that can be averaged to reduce the error from noise.

Time-domain signals from all of the different spacings are averaged before being Fourier transformed (a process called stacking) to improve the quality of signal. It is particularly important to measure the seismic effect that the transient impact has from each side of the sensors. This serves to eliminate the error from phase shifts that occur within the

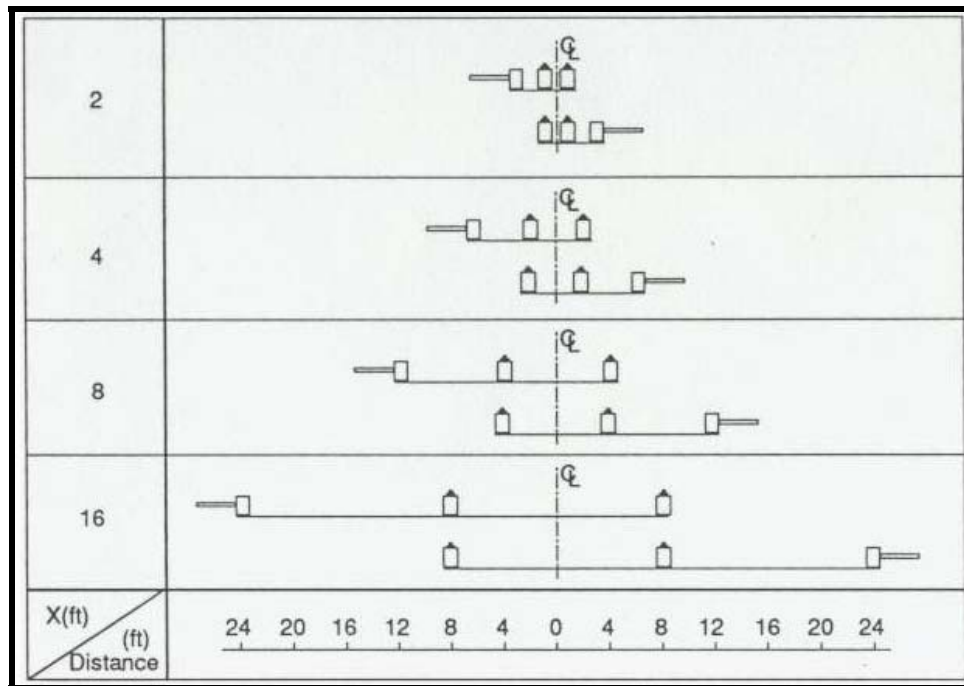


**FIGURE 17 Common Receivers Midpoint Geometry for SASW (38)**

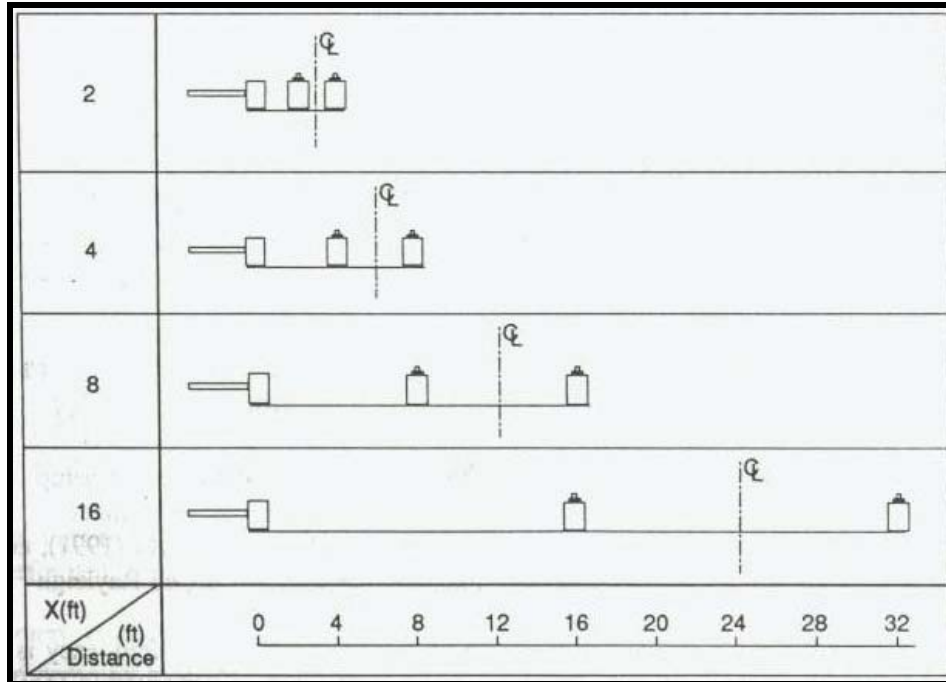


**FIGURE 18 Common Source Geometry for SASW (38)**

receivers and also to measure the homogeneity of the sublayers in the direction of the receivers (38, 39).

Another method of eliminating error is to increase the number of sensors (accelerometers) that are used during testing. When more than two receivers are used the process is sometimes referred to as the multi mode analysis of surface waves (MASW). Some wave analyzers may be limited to two input channels, but it is common for newer models to have inputs for several dozen sensors (38). A setup consisting of more than one receiver is called an array. The advantage of using an array is time efficiency. For just one transient impact, wavelengths can be sampled using any combination of two of the receivers from the array, whereas a setup of only two receivers can only measure a relatively limited amount of time-amplitude data. Thus, the more sensors that are included in the array, the more measurements can be obtained for averaging. Even for

MASW it is important to perform the test from both directions to eliminate any internal phase shifts from the receivers. The literature suggests, however, that testing at higher frequencies is more beneficial for pavement analysis than testing with more than two receivers (38, 40, 41).

For either SASW or MASW, the purpose of field testing is to measure particle motion that corresponds to the amplitude of R-wave motion in the time domain. After this data is collected for a given site, the measurements are averaged in an attempt to eliminate noise in the readings that will hinder contingent calculations. After the field measurements are averaged, the Waveform Analyzer or Dynamic Signal Analyzer is used to perform a Fourier transform so that the data can be analyzed in the frequency domain. The output from the Fourier transform includes two important pieces of information: the coherence function and the cross-power-spectrum.

The coherence function is essentially a measure of the signal-to-noise ratio that provides a quick way to evaluate the quality of recorded data. Coherence values range from zero to one, with values of one corresponding to signals absent of noise and values of zero corresponding to signals so noisy that no relationships can be found. Typically, data is considered to be clean enough to use for analysis when the coherence value is between 0.9 and 1.0. Figure 19 shows the plot of a typical coherence function (35). Along with the coherence function, the Waveform Analyzer or Digital Signal Analyzer gives the cross-power-spectrum. Consider the idealized R-wave motion represented in Figure 15. Each of the various R-waves travels a sinusoidal path, traversing a phase angle ( $\phi_i$ ) in the time domain that is dependant on the wave's frequency ( $f_i$ ). The cross-power-spectrum uses the Fourier transformed data to represent the particle motion in

terms of phase angle and frequency. Since, at any given point, a higher-frequency wave will have traversed a greater total phase angle than a lower-frequency wave, it is rational to expect a constant decreasing relationship between phase angle and frequency. As can be seen in Figure 20, the output of a cross-power-spectrum is not a constantly decreasing relationship. Instead, the relationship is asymptotic at regular frequency intervals. This is the result of plotting phase angle in terms of relative displacement (i.e. in terms of  $0 < |\varphi_i| < 180^\circ$ ) instead of total displacement (i.e.  $0 < |\varphi_i| < \infty$ ). When the phase angle is represented in terms of relative displacement it is called the wrapped phase. The phase can be unwrapped by adding  $360^\circ$  to the magnitude of  $\varphi_i$  every time the wrapped phase crosses the dotted line corresponding to  $\varphi_i = 0^\circ$  (35).

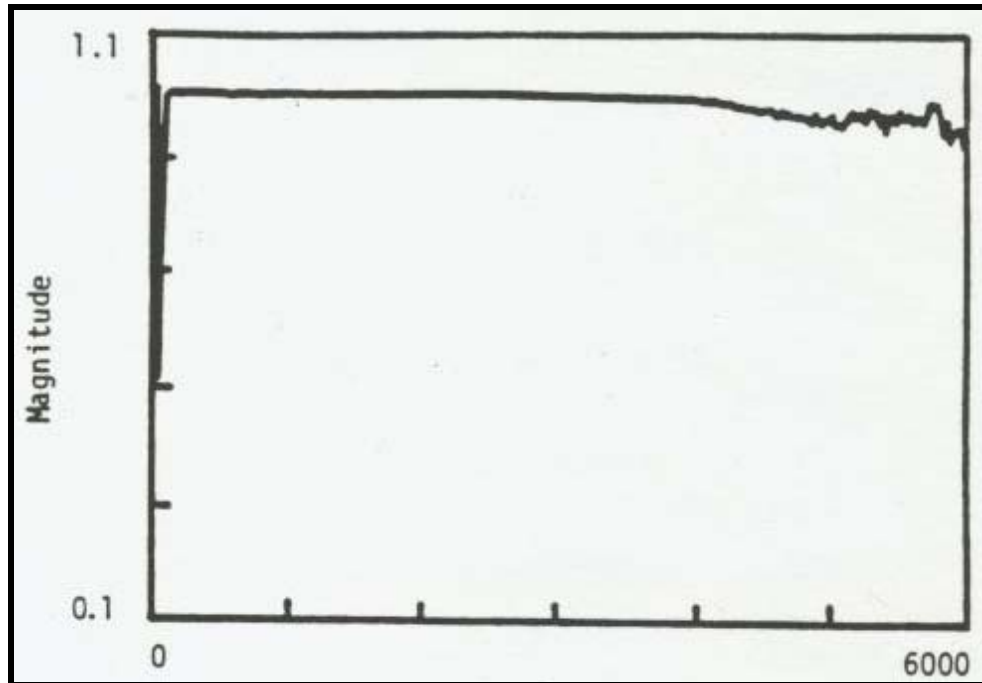


**FIGURE 19 Typical Coherence Function (35)**

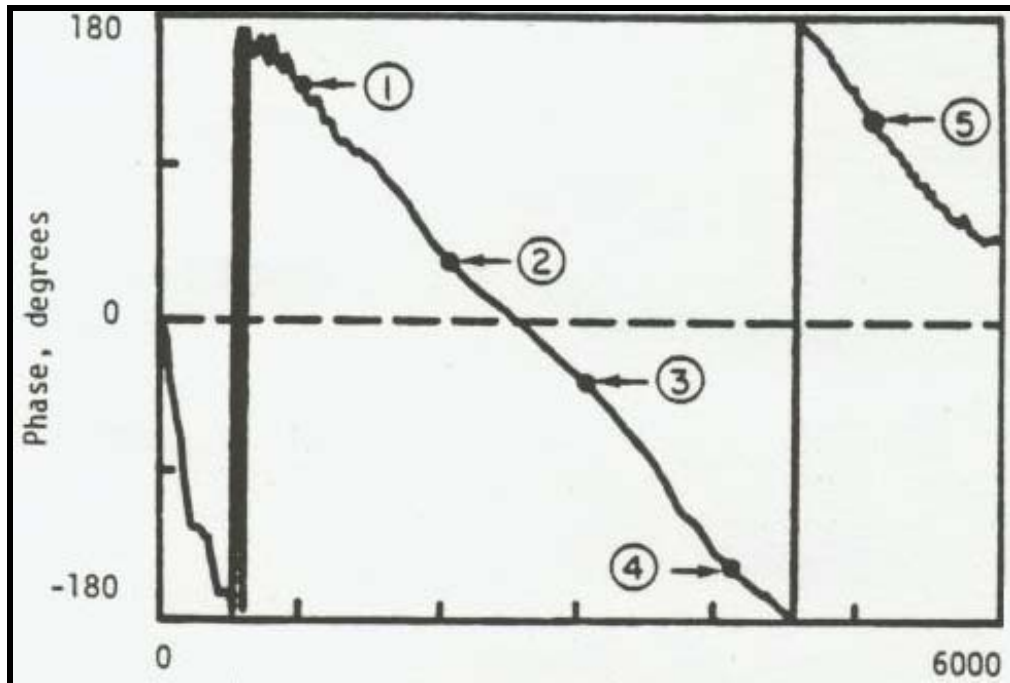


**FIGURE 20 Typical Wrapped Cross-Power Spectrum (35)**

The ultimate goal of the field test is to come up with a dispersion curve relating wavelength to phase velocity, and these quantities can be calculated using the cross-power-spectrum. The first step is to pick a point on the cross-power spectrum and identify its frequency and unwrapped phase angle. The time ( $t$ ) that it took the wave to travel to the unwrapped phase angle is calculated using Equation 55. Referring again to Figure 15, the phase velocity ( $V_{ph}$ ) is calculated by dividing the space between the 2 receivers ( $d$ ) by the previously calculated travel time ( $t$ ), Equation 56. The next step is to calculate the wavelength, which can be done using Equation 57. Finally, the process is repeated for a sufficient number of points to clearly define the experimental dispersion curve (35).

$$t = \frac{\varphi}{360 \cdot f} \dots\dots\dots \text{Eq. 55}$$

$$V_{ph} = \frac{d}{t} \dots\dots\dots \text{Eq. 56}$$

$$\lambda_{ph} = \frac{V_{ph}}{f} \dots\dots\dots \text{Eq. 57}$$

*2.3.3. Backcalculation Procedure*

Backcalculation for the SASW method consists of two major steps. First, the field dispersion curve is used to create a “true” profile of Shear wave velocity versus depth. The second and final step is forward modeling of pavement and subgrade properties to recreate the “true” shear wave velocity profile. The forward modeling process for SASW is called inversion. Inversion can be as simple as “eyeballing” dominant ranges of a dispersion curve for representative values, or considerably more exhaustive methods may also be undertaken.

Inversion can be a relatively complex task that requires a large amount of engineering judgment. Research is underway across the United States to develop automated inversion procedures so that SASW tests may be conducted with difficulty not significantly greater than other field tests. The University of Arkansas currently uses a computer program called SignalCapture2.0 that was written in LabVIEW to collect and store field data from SASW testing. SignalCapture collects data in the time domain, performs a Fourier analysis, and provides the necessary coherence function and cross-power spectrum. The program was first developed in 2003 by Kyle Bennett and later modified by Andrew Wilson and Sutapa Hazra. The cross-power spectra from SignalCapture are imported into a macro-enabled Excel spreadsheet to produce a field dispersion curve. The spreadsheet employs the approximations that are noted in

Equations 58 and 59 below. In addition, the user is allowed to mask any frequency ranges that appear to be inaccurate or scattered.

$$V_S = 1.1 \cdot V_R \dots\dots\dots \text{Eq. 58}$$

$$d_s = 0.4 \cdot \lambda \dots\dots\dots \text{Eq. 59}$$

- Where:
- $V_S$  = Shear wave velocity
  - $V_R$  = Rayleigh wave velocity
  - $d_s$  = Sampling depth
  - $\lambda$  = Wavelength

The inversion process is most robustly accomplished using the Haskell-Thompson transfer matrix, as discussed by Kausel and Roësset (42). The transfer matrix is used to describe the measured phenomenon in terms of all of the parameters that significantly affect the seismic behavior of the pavement system. The transfer matrix utilizes approximately 60 points from the field dispersion curve to estimate the shear wave velocity in roughly 15 discrete layers. Statistical methods are then used to minimize the error of the transfer matrix. The end result of this inversion is a profile of shear wave velocity versus depth, mechanistically based on measured field data (39). While this method is considerably more involving than the simplified procedure of “eyeballing” the field dispersion curve, it is the more robust method that will eventually allow the automation of SASW.

In either case, inversion involves a type of forward calculation to determine the actual thickness and stiffness of pavement and subgrade layers. First, either visual or

analytical inspection of the shear wave velocity profile is used to identify obvious discontinuities where layer interfaces are likely to exist. Then, some reasonable values for layer thickness, Poisson's ratio, density and shear modulus are assumed for each layer. For the simplified method,  $V_S$  may be directly read from the field dispersion curve and converted to the shear modulus using Equation 60.

$$G = V_s^2 \cdot \rho \dots\dots\dots\text{Eq. 60}$$

- Where:
- $G$  = Seismic shear modulus (lb/ft<sup>2</sup>)
  - $V_S$  = Shear wave velocity (ft/s)
  - $\rho$  = Mass density (lb\*s<sup>2</sup>/ft<sup>4</sup>)

For the transfer matrix method, these assumed values are used to create a theoretical dispersion curve which is then compared to the field dispersion curve. If the two curves do not agree within some tolerance, the assumed pavement parameters are changed and the theoretical dispersion curve is recreated. This process is continued by trial-and-error until the theoretical and field dispersion curves are sufficiently similar. The assumed pavement properties that result in the best-fitting theoretical dispersion curve are taken to be representative of field conditions (39).

Once the shear modulus is obtained for the pavement layers (either by the simplified method or the transfer matrix method), Equation 61 is used to convert the shear moduli to Young's moduli (E).

$$E = 2G(1 + \nu) \dots\dots\dots\text{Eq. 61}$$

Where:  $E$  = Young's modulus

$G$  = Shear modulus

$\nu$  = Poisson's ratio

The 1993 AASHTO Pavement Design Guide and the new Mechanistic-Empirical Pavement Design Guide (MEPDG) both use Resilient Modulus ( $M_r$ ) as the primary subgrade characterization criteria.  $M_r$  is defined as axial stress divided by recoverable strain, whereas Young's Modulus is the same axial stress divided by total strain. On a theoretical basis,  $M_r$  and  $E$  represent two different values. On a more realistic basis, however, the two quantities can be nearly equal.

As shown in Figure 21, as the number of load cycles increases, the recoverable strain begins to equal the total strain (19). This is especially true for loads well shy of a material's capacity and after 100 to 200 repetitions. Since seismic disturbances impart stresses that are well below the strength of all pavement materials, the characteristic  $E$  and  $M_r$  values should be nearly equal (43). Thus, a common assumption in SASW

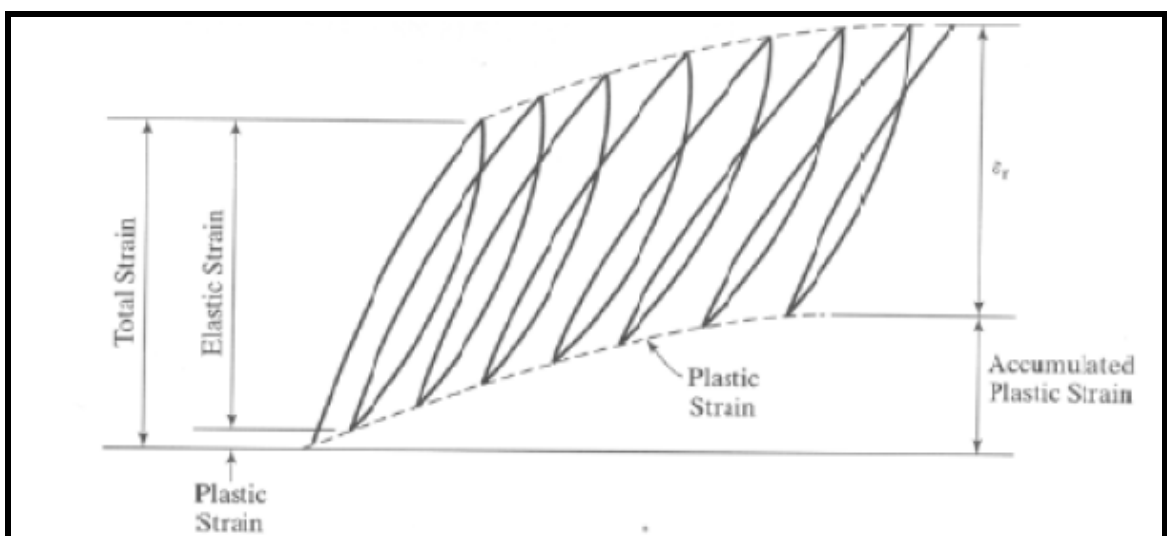


**FIGURE 21 Strains Under Repeated Loads (19)**

testing is to take the Resilient Modulus to be equal to Young's Modulus.

The last step of backcalculation is to adjust the seismically estimated modulus to a more appropriate strain level. Moduli that are measured at seismic strain levels ( $< 10^{-3}$  %) are essentially equal to the maximum modulus for the material (43). With increasing loads and corresponding strains, soils exhibit a non-linear decrease in modulus. This trend is shown graphically in terms of Shear Modulus (G) in Figure 22 (19).

Since traffic loads induce strains that are significantly greater than what is experienced during seismic testing, the modulus of a given soil is expected to be significantly less under traffic loading than for seismic loading. Accordingly, the moduli that are obtained from theoretical dispersion curves must be reduced by some amount to avoid reporting Resilient Modulus values far in excess of what is true or reasonable. An appropriate percent reduction can be estimated using a normalized modulus reduction curve, which relates  $G/G_{\max}$  to shear strain. Three methods for modeling  $G/G_{\max}$  and/or  $E/E_{\max}$  against corresponding strain are now presented.

The simplest method for adjusting seismic moduli is to use a two-parameter hyperbolic model (44). Equation 62 shows Darendeli's simplified hyperbolic model where the reference shear strain for normalization ( $\gamma_r$ ) represents  $0.5G_{\max}$ . . Equations 63 and 64 give the reference strain and curvature coefficient (a) for coarse and fine grained soils, respectively.

$$\frac{G}{G_{\max}} = \frac{1}{1 + \left(\frac{\gamma}{\gamma_r}\right)^a} \dots\dots\dots \text{Eq. 62}$$

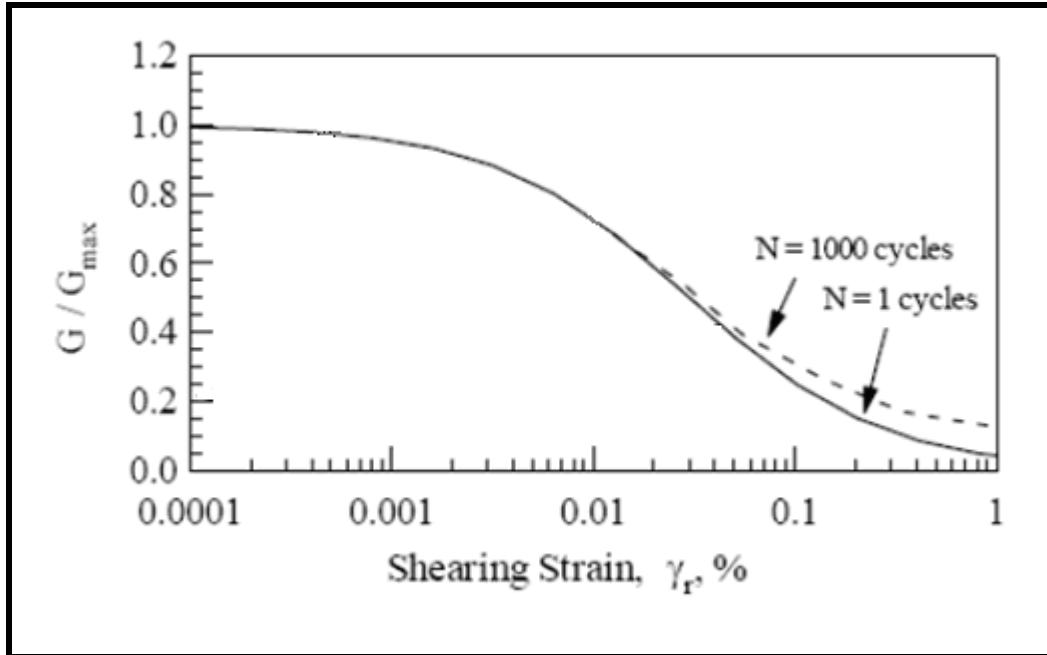


**FIGURE 22 Normalized Shear Modulus Reduction Curve (19)**

$$\gamma_r = 0.12 \times C_u^{-0.6} \times \left( \frac{\sigma_0'}{P_a} \right)^{0.5 \times C_u^{-0.15}} ; a = 0.86 + 0.1 \times \log \left( \frac{\sigma_0'}{P_a} \right) \dots \dots \dots \text{Eq. 63}$$

$$\gamma_r = (0.0352 + 0.0010 \times PI \times OCR^{0.3246}) \cdot \sigma_0'^{0.3483} ; a = 0.9190 \dots \dots \dots \text{Eq. 64}$$

- Where:
- G = Shear modulus at some arbitrary load/strain level
  - G<sub>max</sub> = Shear modulus at seismic strain level
  - γ = Shear strain corresponding to G
  - γ<sub>r</sub> = Reference shear strain corresponding to G = 0.5G<sub>max</sub>
  - a = Curvature coefficient
  - C<sub>u</sub> = Uniformity coefficient
  - σ<sub>0</sub>' = Effective confining pressure (atm)
  - P<sub>a</sub> = Atmospheric pressure (atm)

PI = Plasticity index

OCR = Overconsolidation ratio

Ke and Nazarian have developed another model that uses different parameters than the hyperbolic model (45). Their model is defined by Equation 65, which normalizes Young's modulus in terms of relative confining and deviatoric pressures. At very small or large deviatoric stresses, Equation 65 may report unrealistic values. As such, Nazarian recommends upper and lower limits of  $E_{seis}$  and  $0.05E_{seis}$ , respectively. The statically determined coefficients  $k_2$  and  $k_3$  for some pavement materials are listed in Table 9.

$$\frac{E}{E_{seis}} = \left( \frac{\sigma_{c-ult}}{\sigma_{c-init}} \right)^{k_2} \left( \frac{\sigma_{d-ult}}{\sigma_{d-init}} \right)^{k_3} \dots\dots\dots \text{Eq. 65}$$

- Where:
- E = Young's modulus at some arbitrary load/strain level
  - $E_{seis}$  = Young's modulus at seismic strain level
  - $\sigma_{c-ult}$ ,  $\sigma_{c-init}$  = Ultimate and initial confining pressures, respectively
  - $\sigma_{d-ult}$ ,  $\sigma_{d-init}$  = Ultimate and initial deviatoric stresses, respectively
  - $k_2$ ,  $k_3$  = Statically determined coefficients, Table 9

**Table 9      Statically Determined Coefficients  $k_2$  and  $k_3$  for Equation 65 (45)**

Material	Characterization	$k_2$	$k_3$
Base	High Quality	0.4	-0.2
	Average	0.2	-0.3
	Poor Quality	0.1	-0.4
Subgrade	Sandy	0.4	-0.2
	Low Plasticity Clay	0.1	-0.3
	High Plasticity Clay	0.0	-0.4

Two final constitutive models are now presented that provide separate, but similar models for sands and clays (46). The primary difference between the two models is that the model for clays includes an input for plasticity of the soil. Equations 66 - 68 are for the sand model, and Equations 69 - 72 are for modeling clays or other fines with plasticity.

$$\log \frac{G}{G_{\max}} = \log K(\gamma) + \{m(\gamma) - m_0\} \log \sigma'_0 \dots \text{Eq. 66}$$

$$k(\gamma) = 0.5 \left[ 1 + \tanh \left\{ \ln \left( \frac{0.000102}{\gamma} \right)^{0.492} \right\} \right] \dots \text{Eq. 67}$$

$$m(\gamma) - m_0 = 0.272 \left[ 1 - \tanh \left\{ \ln \left( \frac{0.000556}{\gamma} \right)^{0.4} \right\} \right] \dots \text{Eq. 68}$$

$$\frac{G}{G_{\text{seis}}} = K(\gamma, PI) (\sigma'_0)^{m(\gamma, PI) - m_0} \dots \text{Eq. 69}$$

$$K(\gamma, PI) = 0.5 \left\{ 1 + \tanh \left[ \ln \left( \frac{0.000102 + n(PI)}{\gamma} \right)^{0.492} \right] \right\} \dots \text{Eq. 70}$$

$$m(\gamma, PI) - m_0 = 0.272 \left\{ 1 - \tanh \left[ \ln \left( \frac{0.000556}{\gamma} \right)^{0.4} \right] \right\} e^{(-0.0145PI^{1.3})} \dots \text{Eq. 71}$$

$$n(PI) = \begin{cases} 0.0 & PI = 0 \\ 3.37 \times 10^{-6} PI^{1.404} & 0 < PI \leq 15 \\ 7.0 \times 10^{-7} PI^{1.976} & 15 < PI \leq 70 \\ 2.7 \times 10^{-5} PI^{1.115} & PI > 70 \end{cases} \dots \text{Eq. 72}$$

Where:  $G$  = Truck traffic load level modulus  
 $G_{\text{seis}}$  = Seismic modulus  
 $k_2, k_3$  = Statically determined coefficients  
 $\sigma_{\text{c-init}}$  and  $\sigma_{\text{c-ult}}$  = Initial and ultimate confining pressures  
 $\sigma_{\text{d-init}}$  and  $\sigma_{\text{d-ult}}$  = Initial and ultimate deviatoric pressures  
 $PI$  = Plasticity index of the base or subgrade material  
 $\gamma$  = Truck traffic load shear strain  
 $\sigma'_0$  = Mean effective confining pressure

This paper does not argue the relative accuracy of the three aforementioned methods, but instead suggests that is important to consider several different models and/or methods when attempting to estimate quantities that are not well understood or defined. For the case of adjusting seismic moduli, it is necessary to estimate properties such as effective confining stresses and/or shearing strains before the ultimate estimation of corrected modulus can ever be considered. Thus, in each step of the process, engineering judgment should be used and documented so that unreasonable results may be compared with their corresponding methods and assumptions.

#### **2.4. Case Studies: Comparisons of Backcalculation Procedures**

The literature includes a number of comparisons between pavement and subgrade moduli determined from different NDT and laboratory methods. Because of the relative popularity of FWD compared to SASW, most of the available comparisons either consider different FWD backcalculation procedures or a certain FWD procedure to

laboratory testing. For that reason, this section will only address two comparisons, and those will be limited to FWD and laboratory-determined stiffnesses. Sections 3 and 4 of this paper include a direct comparison of SASW and FWD-backcalculated moduli for a particular section of roadway.

#### *2.4.1. Oregon: FWD vs. Laboratory for HMA and Base Course Materials*

A KUAB FWD was used to estimate pavement layer moduli for two typical and similar flexible pavement sections in Oregon (47). The first section, the *Rufus Project*, consisted of a 173-mm (6.8-in.) thick HMA layer underlain by a 457-mm (18-in.) thick base layer. The HMA layer was moderately rutted and extensively cracked; the subgrade was non-plastic sandy gravel. The second section, the *Centennial Project*, consisted of a 102-mm (4-in.) thick HMA layer underlain by a 406-mm (16-in.) thick base layer. The HMA layer was moderately cracked; the subgrade was a well-graded sandy gravel.

A software called BOUSDEF was used to backcalculate layer moduli from FWD data. BOUSDEF is an iterative software that estimates moduli from user-input layer thicknesses and Poisson's ratios as well as measured deflection basin data. In addition, BOUSDEF determines a non-linear regression to model the stress-dependent nature of base course modulus if varying load levels are used during testing. ASTM D-4123 was used for laboratory resilient modulus testing.

Figures 23 and 24 show the backcalculated and laboratory-measured resilient moduli for the HMA layers of the Rufus and Centennial projects, respectively. It is clear from the figure that laboratory values are consistently higher than backcalculated values. This could be the result of removing cores at locations that are in relatively good

condition. If that is the case, the laboratory test would have no way to simulate the distresses that were encountered in the pavement that was tested via FWD.

Figures 25 and 26 show plots of the backcalculated regression for base course modulus versus laboratory-measured values for east-bound and west-bound lanes of the Rufus and Centennial projects, respectively. These values have exceptional agreement for the Rufus project and very close agreement for the Centennial project.

The Oregon report includes backcalculated values for subgrade resilient modulus, but states nothing of laboratory or otherwise determined values for comparison. This short comparison provides two pieces of information. First, iterative backcalculation software appears to be able to estimate the non-linear resilient modulus of base materials with a good deal of accuracy. While there is no clear reason why the backcalculated HMA moduli did not match up, it is likely that the field samples were taken at locations that were not representative of field conditions. This has dual consequence. First, it emphasizes the need to characterize pavements at many different locations. Also, it shows the importance of using engineering judgment throughout sampling and testing. If relatively few samples are taken from a material in the field, those samples need to err on the conservative side of the average. If an overlay were designed based on the laboratory testing of an unrepresentatively strong sample, the overlay may be too thin to serve its purpose.

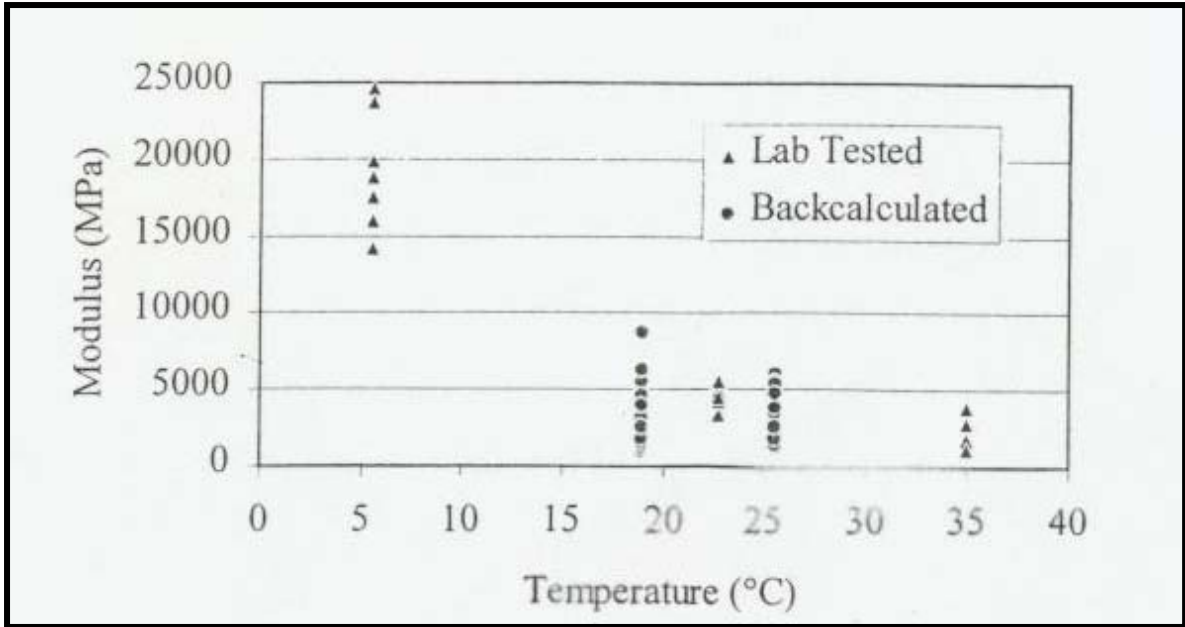


FIGURE 23 HMA Moduli for Rufus Project (47)

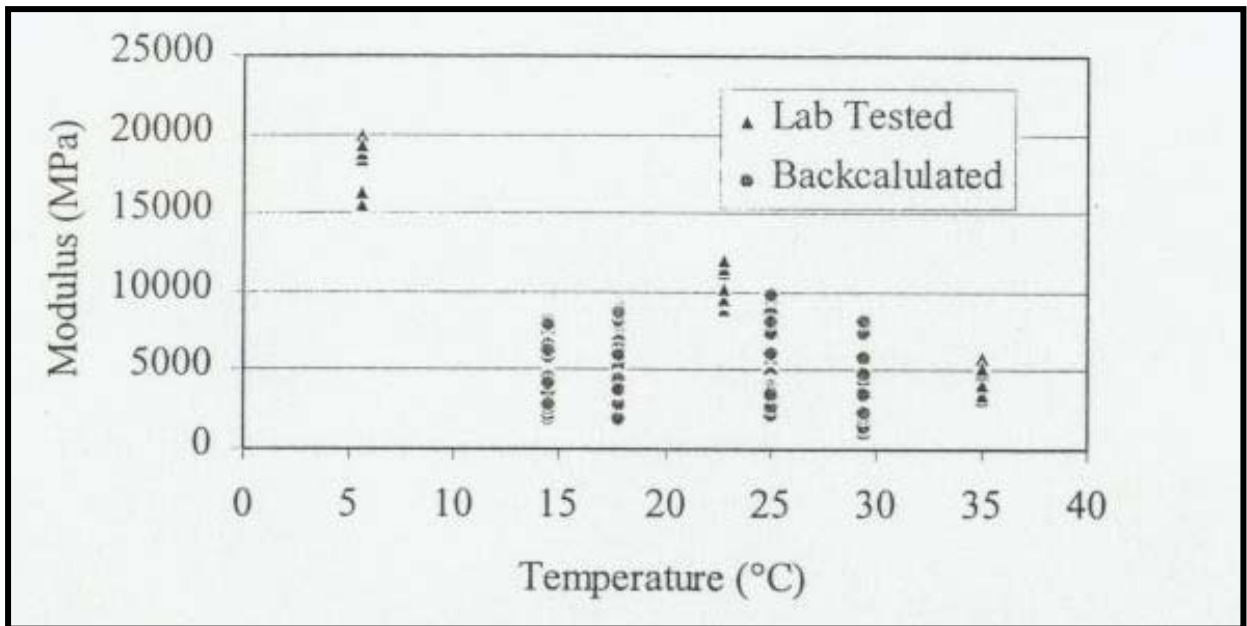


FIGURE 24 HMA Moduli for Centennial Project (47)

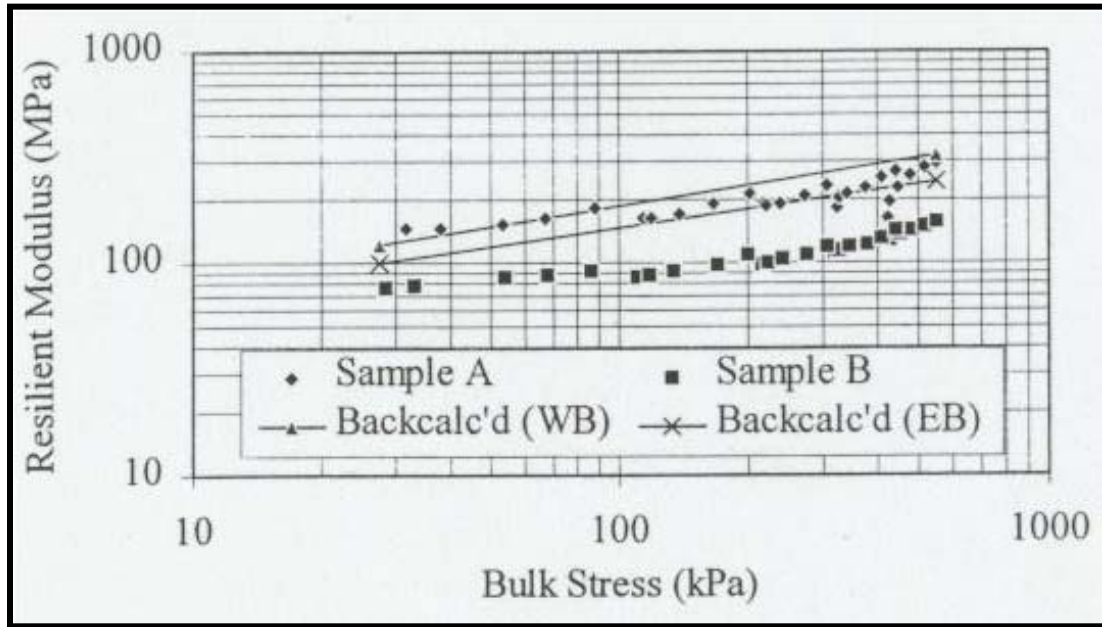


FIGURE 25 Base Course Moduli for Rufus Project (47)

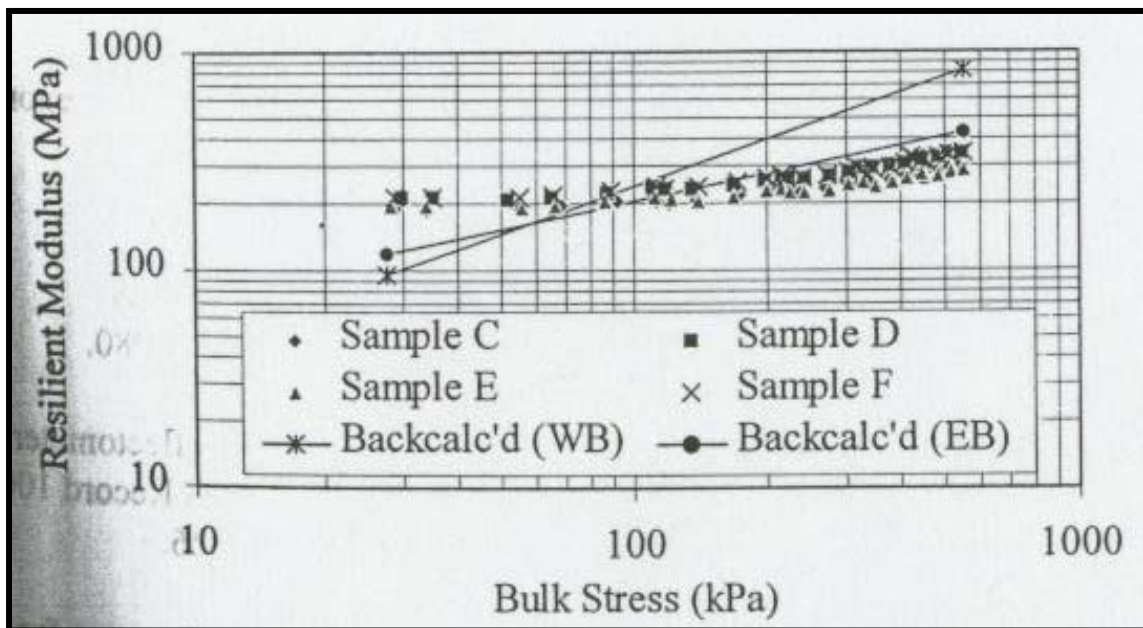


FIGURE 26 Base Course Moduli for Centennial Project (47)

#### 2.4.2. LTPP Database: Comparison of FWD Backcalculation Methods

The Long Term Pavement Performance (LTPP) Program has compiled a database of pavement sections for which FWD and/or laboratory testing has been performed, and one study used that database compare the effectiveness of different FWD backcalculation methods to estimate the measured stiffness of rigid pavements and subgrades (22).

Twenty-six jointed concrete pavement (JCP) sections were obtained that had deflection data and  $k$  values measured from plate-load tests, 50 JPC sections were chosen that had deflection data and measured  $E_{PCC}$  values, and 76 continuously reinforced concrete pavement (CRCP) sections were chosen that had deflection data and measured  $E_{PCC}$  values.

The deflection data was used as an input in ILLIBACK4, ILLIBACK7, NUSBACK, and the LTPP Best-Fit methods to determine the relative ability of each to estimate  $k$  and/or  $E_{PCC}$  for rigid pavements. Figures 27, 28, and 29 compare measured to backcalculated  $k$  values,  $E_{PCC}$  for JPC, and  $E_{PCC}$  for CRCP, respectively, (a) based on the average value for each pavement section and (b) based on each deflection basin. Similarly, Figures 30, 31, and 32 illustrate how many of the estimates contain varying levels of error.

The authors of the LTPP study offer some interpretation of the results. First, the relative inaccuracy of backcalculated  $k$  values is attributed to the likelihood that the plate load tests would have been conducted at different times and temperature than the FWD tests. The same is true for  $E_{PCC}$  measurements, but  $k$  is more dependent on environmental factors.

It is also noted that ILLIBACK4 and ILLIBACK7 have the most stringent deflection basin conformance requirement, and that this may be the cause of their relatively poor performance. The LTPP Best-Fit method attempts to match individual deflections instead of the entire deflection basin, and that is probably at least part of the reason why the forward calculation was more accurate. NUSBACK was clearly the most accurate backcalculation method, and the authors guess that this is because of NUSBACK's computational flexibility. NUSBACK can use any two deflection measurements, and this study used different strategic pairs for calculating  $k$  ( $d_4$  and  $d_7$ ) and  $E_{PCC}$  ( $d_1$  and  $d_3$ ). As a final note, the inclusion of tests on JCP seemed to prove that jointed pavements are sufficiently "infinite" to use layered elastic theory as long as the FWD test is conducted at an interior point on the slab.

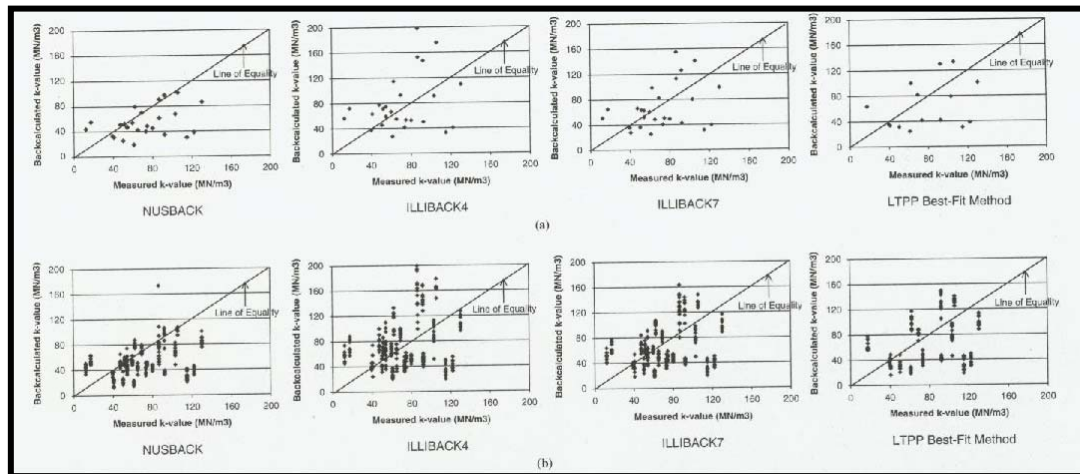


**FIGURE 27 Comparison of Backcalculated and Measured  $k$  Values (22)**

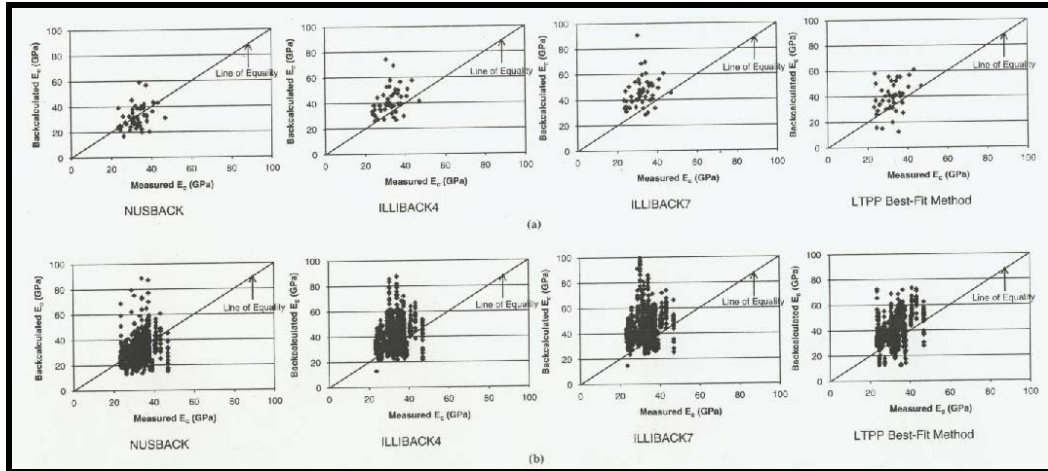


FIGURE 28 Comparison of Backcalculated and Measured  $E_{PCC}$  Values for JPC(22)

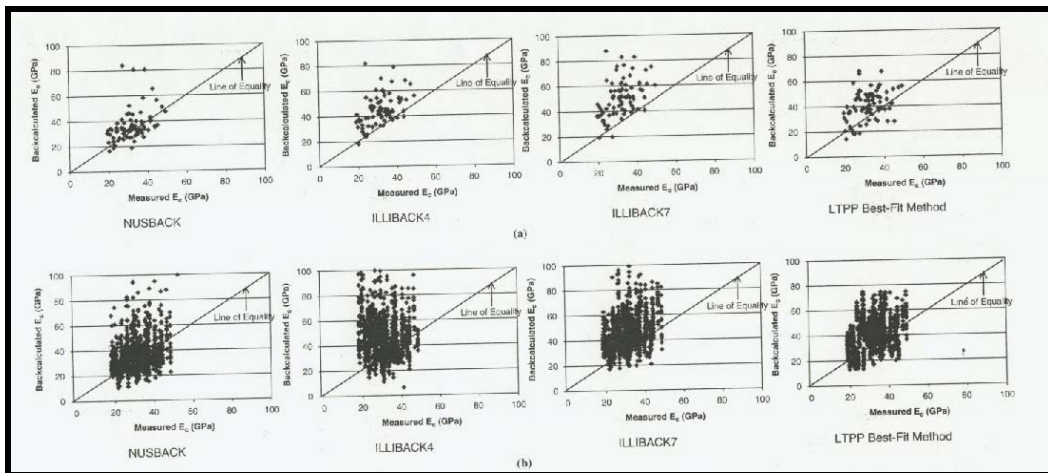
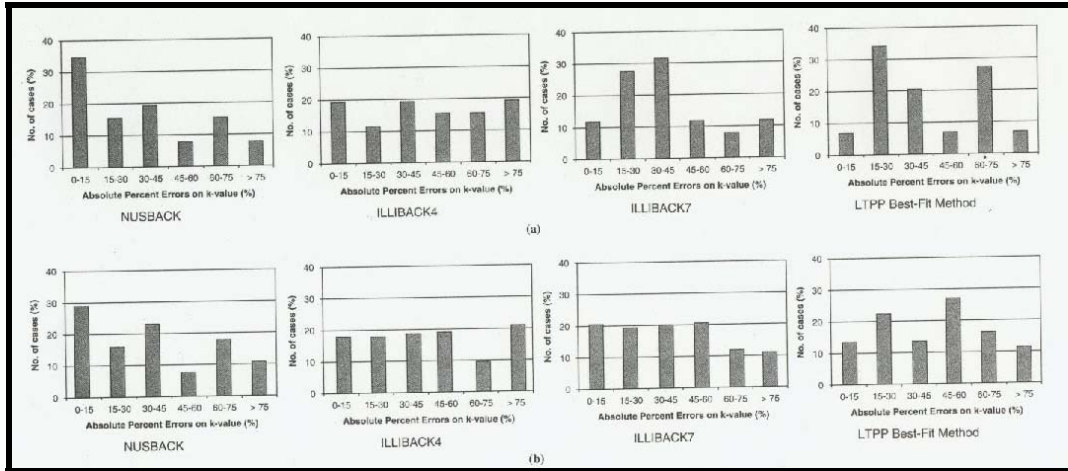
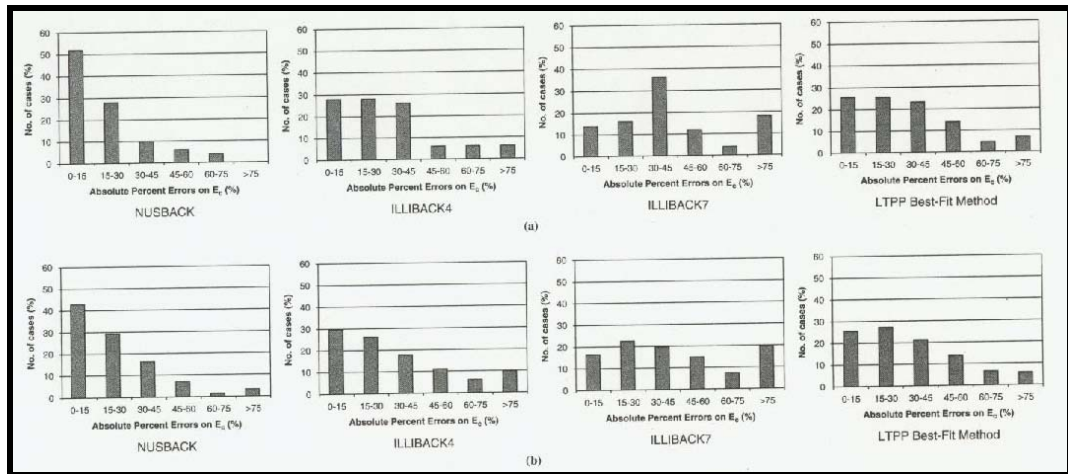


FIGURE 29 Comparison of Backcalculated and Measured  $E_{PCC}$  Values for CRCP

(22)



**FIGURE 30** Errors of Backcalculated  $k$  Values (22)



**FIGURE 31** Errors of Backcalculated  $E_{PCC}$  Values for JPC (22)

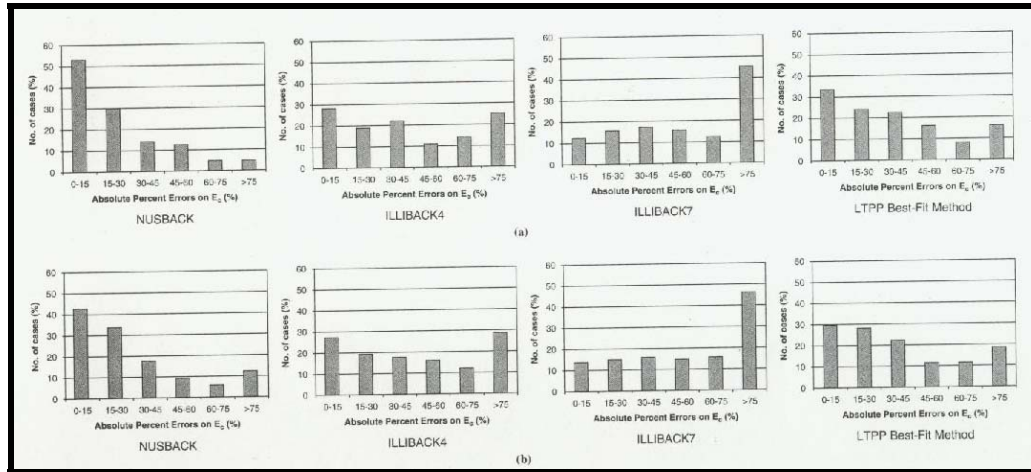


**FIGURE 32 Errors of Backcalculated  $E_{PCC}$  Values for CRCP (22)**

### 3. DATA ANALYSIS

Falling Weight Deflectometer (FWD) and (Spectral Analysis of Surface Wave) SASW tests were conducted for a FHWA project in Nashville, AR during the summer of 2007 by the Arkansas Highway and Transportation Department (AHTD) and the University of Arkansas, respectively. The current study is completely separate from the research that was being undertaken in Nashville, but the raw field data from those tests has been provided for this project at no expense. The data from Nashville were all taken from a single stretch of road comprised of approximately 76 adjacent 30-ft slabs, for a total length of just under half a mile. The road, AR-4/US-278/Main St, consisted of a roughly 6-inch thick, JRCP layer that is underlain by native soils. At the time of testing the road had never undergone major rehabilitation, and the primary distress was poor joint load transfer between slabs.

The Natural Resources Conservation's Web Soil Survey was used to classify Nashville's native soil (48). Figure 33 shows the spatial distribution of the three primary soil types that are found in the immediate vicinity of AR-4/US-278/Main St., which is drawn in yellow. Table 10 gives the engineering properties of the three types of soils that were available from the Web Soil Survey. The information from Table 10 was used to make educated assumptions about the remaining soil properties that were required for analysis. Table 11 documents the assumptions that were made for backcalculating moduli at the Nashville site.

SASW tests were also conducted at the Nashville site, but on a less frequent basis. For each SASW test, a plot of the field dispersion curve is presented in Appendix A. The estimated subgrade and pavement moduli are reported in Table 12 of Section 4. SASW



**FIGURE 33 Spatial Distribution of Soil Types in Nashville, AR (48)**

**Table 10 Description of Soil Types at Nashville Site (48)**

Symbol	Name	LL	PI	%Sand	%Clay	%Silt	AASHTO	USCS
RuB	Ruston Fine Sandy Loam	31	12	46.0	22.7	31.3	A-6	CL
SaC	Sacul Fine Sandy Loam	45	21	25.2	32.1	42.7	A-7-6	CL
SfB	Savannah Fine Sandy Loam	30	11	41.7	23.8	34.5	A-6	CL

**Table 11      General Assumptions for Materials at Nashville Site**

<b>Property</b>	<b>Assumed Quantity</b>
Poisson's Ratio of Subgrade Soil	0.40
Poisson's Ratio of JRCP	0.15
Unit Weight of Subgrade Soil	115 pcf
Unit Weight of JRCP	150 pcf
Thickness of JRCP	6 inches
Truck-load-level Strain for Subgrade	0.05%

tests were documented according to the slab at which they were conducted, but unfortunately there is not a similar record for the FWD tests. It is believed, however, that all of the nondestructive tests were performed in a close enough proximity to one another to facilitate a worthwhile comparison of backcalculated moduli. FWD tests were performed at mid-slab at two load levels for 65 adjacent slabs, both northbound and southbound, for a total of 260 measured deflection basins. The raw data from these measurements is presented in Appendix B.

In an effort to compare the relative performance of the various FWD backcalculation procedures, the raw data from Appendix B has been used to backcalculate moduli using all of the reviewed methods that were available and/or feasible for use. A spreadsheet was programmed to perform NUS-BACK and AREA<sub>72</sub> backcalculations for all 260 deflection basins. The LTPP spreadsheet for forward calculation of a rigid pavement was used to estimate the overall pavement stiffness and subgrade resilient modulus for 30 deflection basins. Twenty of the basins were taken straight from the raw data, and the other 10 were created by averaging the two sets of load and deflections from 10 different locations. All 30 basins were chosen from basins that produced reasonable results in both NUS-BACK and AREA<sub>72</sub>. BAKFAA software,

which is available to the public at no charge, was used to backcalculate the same 30 deflection basins. Lastly, ELMOD was used to evaluate the pavement structure using the data file that was output from the FWD. Tables 34 - 40 in Section 4 document the results of the various backcalculations that were performed.

The literature suggests that DIPLO-DEF and MODULUS are both valuable tools for estimating the stiffness of pavement layers, but they were not used for this study. Both programs were obtained, but the DOS environment proved too tedious and foreign to be practical. The largest single factor that hindered the feasibility of these programs was the process of identifying input and output files for computation. ILLI-BACK was also excluded from the analysis portion of this project for the same reason. A newer, Windows-based version of Modulus has been published, but it was not available for this study. The omission of these programs is justified by considering that any increase in accuracy from DIPLO-DEF or MODULUS would likely be offset by human error that could arise from attempting to implement such tedious programs for widespread use in state highway agencies.

SASW inversion was also conducted, but a significant additional assumption was required. Either the frequencies that were used or the sensors that were used to measure the surface waves generated field dispersion curves that are inconsistent and unreasonable for the PCC layer. The shear wave velocities were expected to be highest for the PCC layer, but the results on their own are not consistent enough to facilitate such a conclusion.

The readings from sensor spacings greater than 3 inches consistently report shear wave velocities similar to what is shown for the subgrade soil, and only the 3-inch

spacing gave results that showed the shear wave velocity to be highest in the PCC layer. There are two likely reasons for this problem. The simplified equation for estimating sampling depth could be inaccurate, causing the larger sensor spacings to report accurate readings at inaccurate depths. The other likely scenario is that the larger sensor spacings tend to mask the high-frequency signal that is required to analyze a stiff layer like PCC with lower-frequency background noise. For the purposes of this study, the modulus of the PCC layer was estimated by considering the most common shear wave velocity that was estimated from the 3-inch sensor spacing and ignoring all other readings.

Another issue with SASW is the correction of seismic subgrade moduli to account for the nonlinear stress-dependant variation. Since the soil at the Nashville site is a low plasticity silty soil, Darendeli's simplified hyperbolic relationship for fine grained soils was used. The process of modulus adjustment is discussed in further detail in Appendix C. A simplified example of the inversion process is also included in Appendix C.

One last technique of backcalculation is now discussed before the results are presented. The layered elastic models provide estimates for Young's modulus of the pavement and subgrade values, but rigid pavement design procedures necessitate a value for  $k$ , the coefficient of subgrade reaction. The two values are related, and Equation 73 is used to convert between the two throughout Sections 4 and 5. This is a modification of a relationship that is given in the ASTM specification for measuring soil stiffness by the electromechanical method, which gives stiffness in terms of force per depth penetration. In order to change that value into a pressure per depth penetration, the ASTM equation was simply divided by the area of the loading plate (49). For the purposes of this study, the load plate had a radius of 5.91 inches.

$$k = \frac{1.77RE}{(1-\nu^2)} \div \pi R^2 = \frac{0.563E}{R(1-\nu^2)} \dots\dots\dots \text{Eq. 73}$$

- Where:
- $k$  = Coefficient of subgrade reaction (psi/in.)
  - $R$  = Radius of load plate (in.)
  - $E$  = Young's modulus (psi)
  - $\nu$  = Poisson's ratio

The only laboratory measurement that is available for comparison with the nondestructive estimations is a single measurement of concrete compressive strength ( $f'_c$ ). This value was determined according to the specifications in AASHTO T 22. The single test reported a compressive strength of 9,441 psi. Equation 74 was used to estimate a value of 5,538,000 psi for  $E_{PCC}$ .

$$E_{PCC} = 57,000\sqrt{f'_c} \dots\dots\dots \text{Eq. 74}$$

- Where:
- $E_{PCC}$  = Young's Modulus of PCC (psi)
  - $f'_c$  = Concrete compressive strength (psi)

## 4. RESULTS

### 4.1. SASW Results

The dispersion curves for the Nashville SASW tests are presented in Appendix A. The reduced data from those curves is presented below in Table 12. A detailed explanation of the reduction procedure is presented in Appendix C.

**Table 12 Profile of Young's Modulus with Depth from SASW**

Depth (in.)	Young's modulus (psi) @ Slab (#)							
	3	17	25	34	42	52	66	76
0 – 6	-	2,478,000	6,999,000	11,624,000	3,142,000	189,000	214,000	297,000
6 – 12	68,000	321,000	564,000	-	-	645,000	191,000	222,000
12 – 18	134,000	321,000	564,000	618,000	-	645,000	191,000	333,000
18 – 24	134,000	321,000	564,000	618,000	395,000	645,000	191,000	333,000
24 – 30	134,000	321,000	564,000	-	395,000	161,000	191,000	333,000
30 – 36	134,000	321,000	-	-	175,000	161,000	-	333,000
36 - 42	134,000	-	-	-	175,000	161,000	-	333,000

### 4.2. NUS-BACK Results

Figure 34 provides a graphical illustration of the NUS-BACK estimates for  $E_{PCC}$  using different combinations of sensor spacing and subgrade modeling. Figure 35 provides the same illustration for estimates of  $k$  and  $E_S$ .

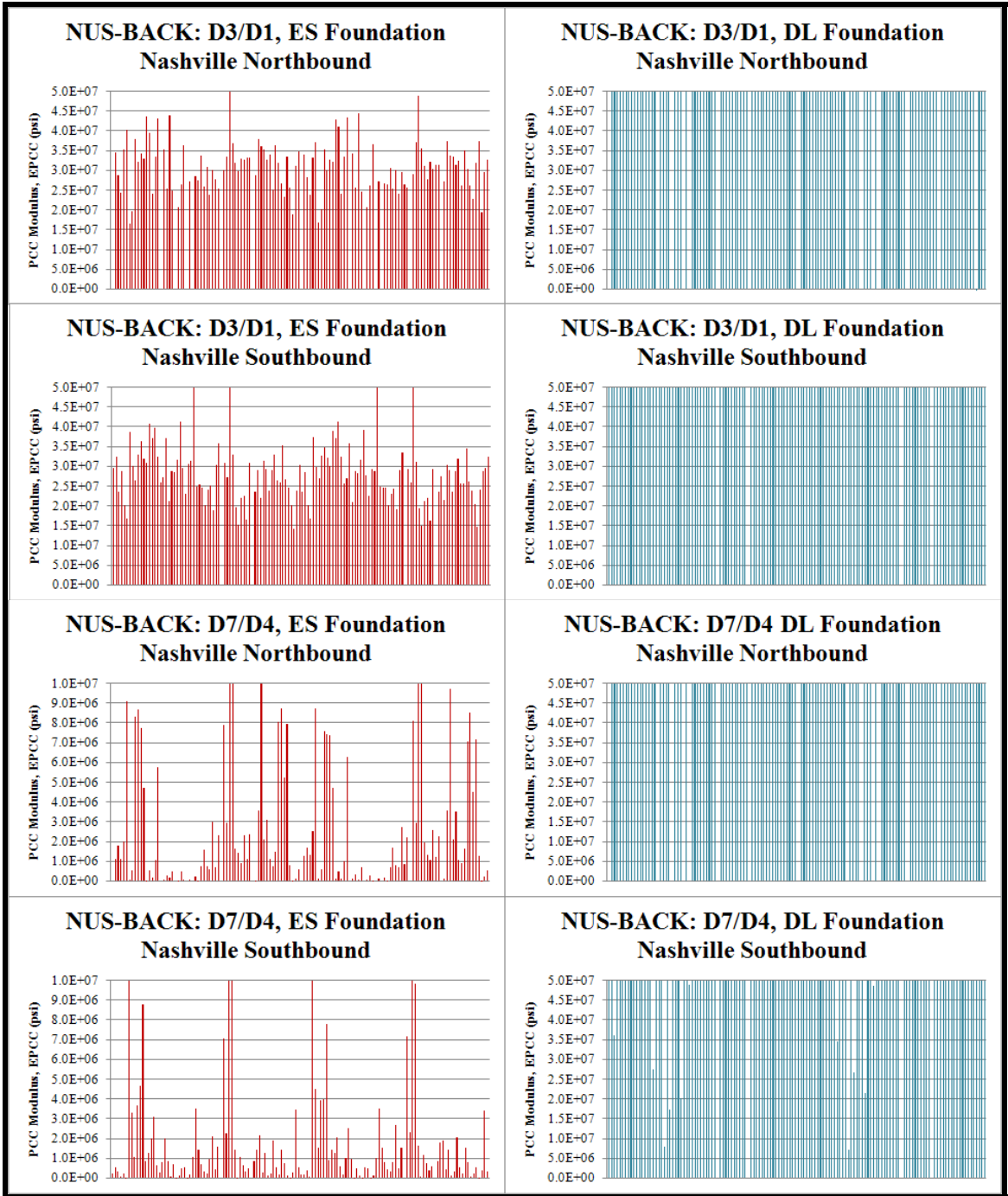


**FIGURE 34 Backcalculated  $E_{PCC}$  from NUS-BACK**

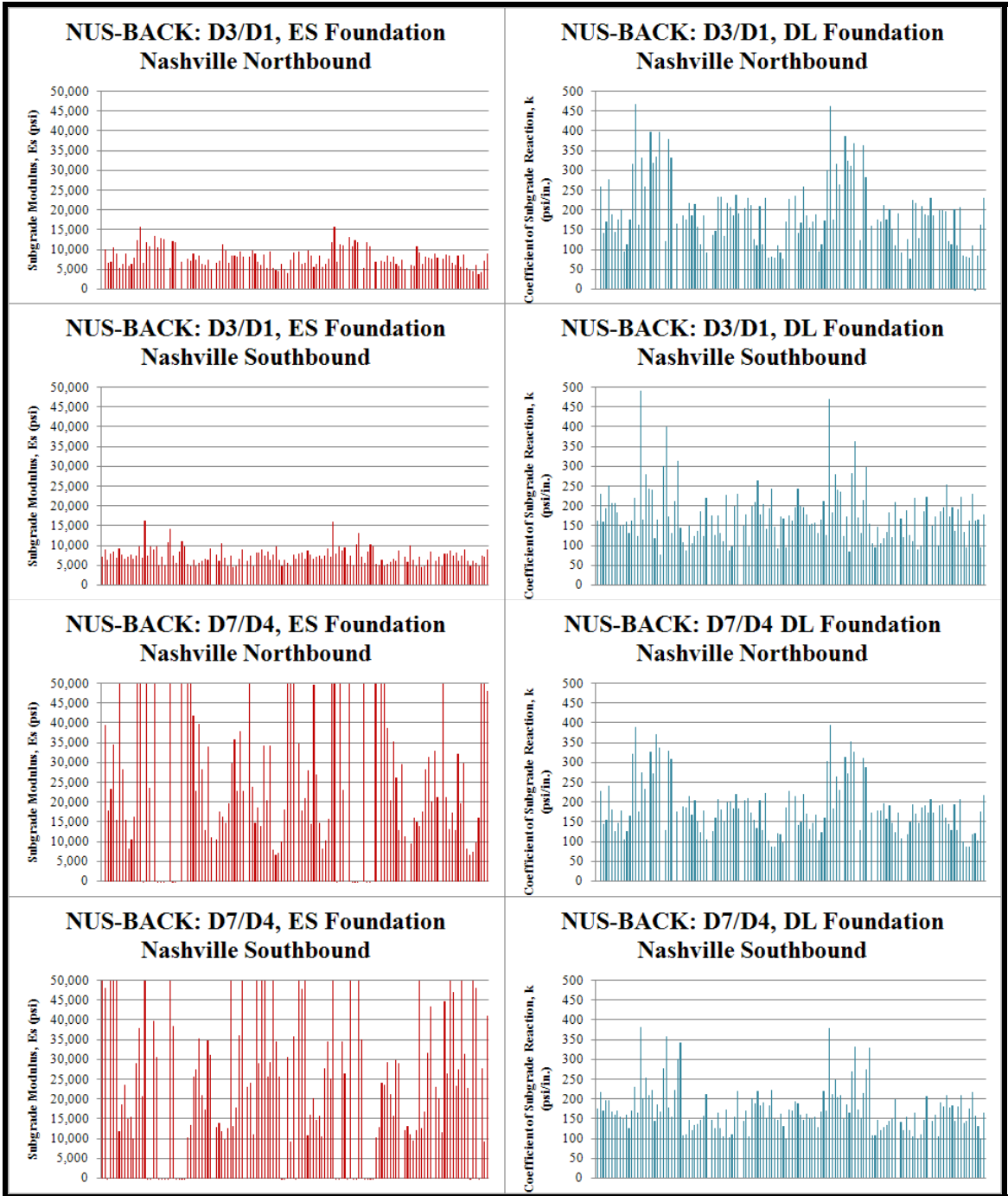


**FIGURE 35 Backcalculated Soil Stiffness from NUS-BACK**

### 4.3. AREA<sub>72</sub> Results

The AREA<sub>72</sub> backcalculation procedure was also used to estimate  $E_{PCC}$  and  $k$  for the Nashville pavement and subgrade. Figure 36 shows the estimates for  $E_{PCC}$ , and Figure 37 shows those for  $k$ .

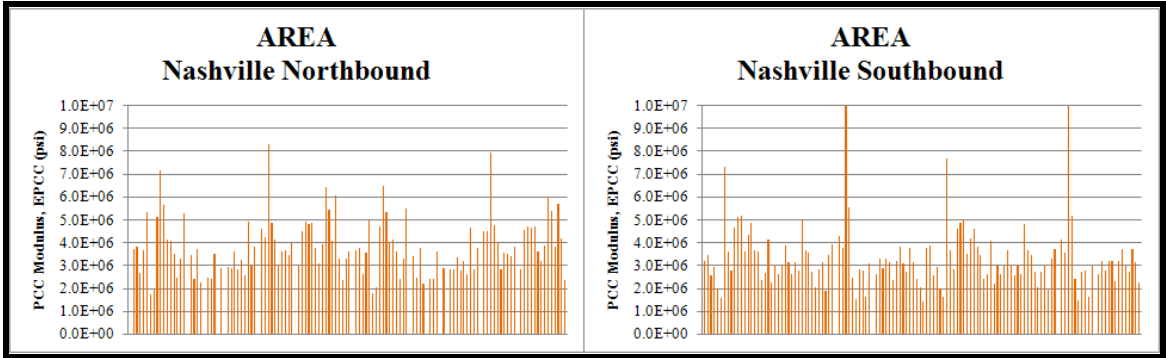


FIGURE 36 Backcalculated EPCC from AREA<sub>72</sub>

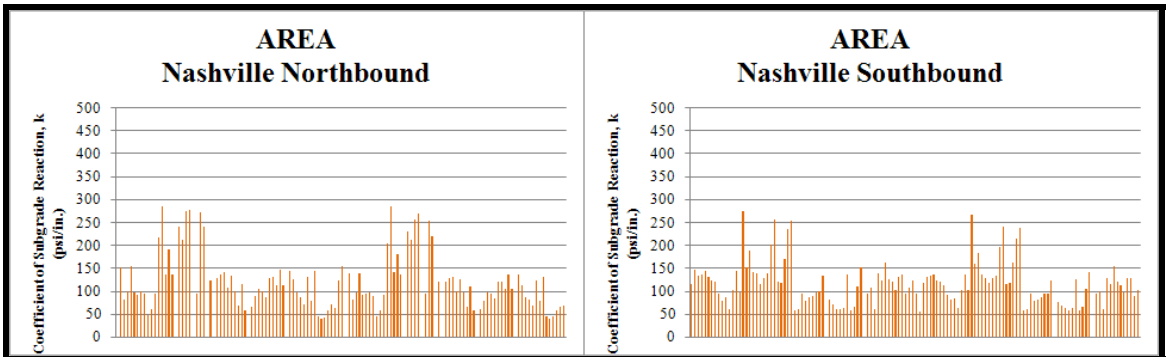


FIGURE 37 Backcalculated  $k$  from AREA<sub>72</sub>

#### 4.4. LTPP Forward Calculation Results

The LTPP forward calculation spreadsheet is capable of estimating the resilient modulus and composite pavement modulus for rigid pavements. Figure 38 shows the LTPP estimations for both.

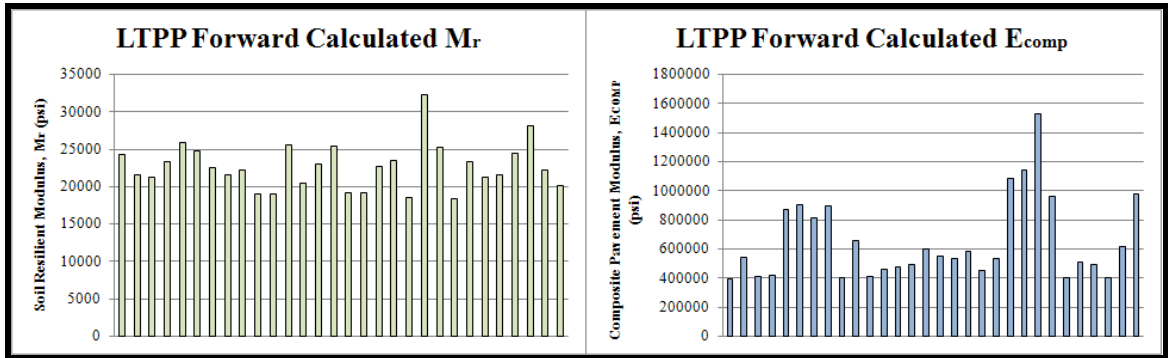


FIGURE 38  $M_r$  and  $E_{Comp}$  from LTPP Forward Calculation

#### 4.5. BAKFAA Results

Pavement and subgrade moduli were also estimated using BAKFAA, which requires seed moduli for the subgrade and the pavement. Two seed values were used for each input, and the results are given in Figure 39. Seed values for subgrade modulus were 15,000 psi and 20,000 psi. Those for pavement modulus were 4 million psi and 5 million psi.

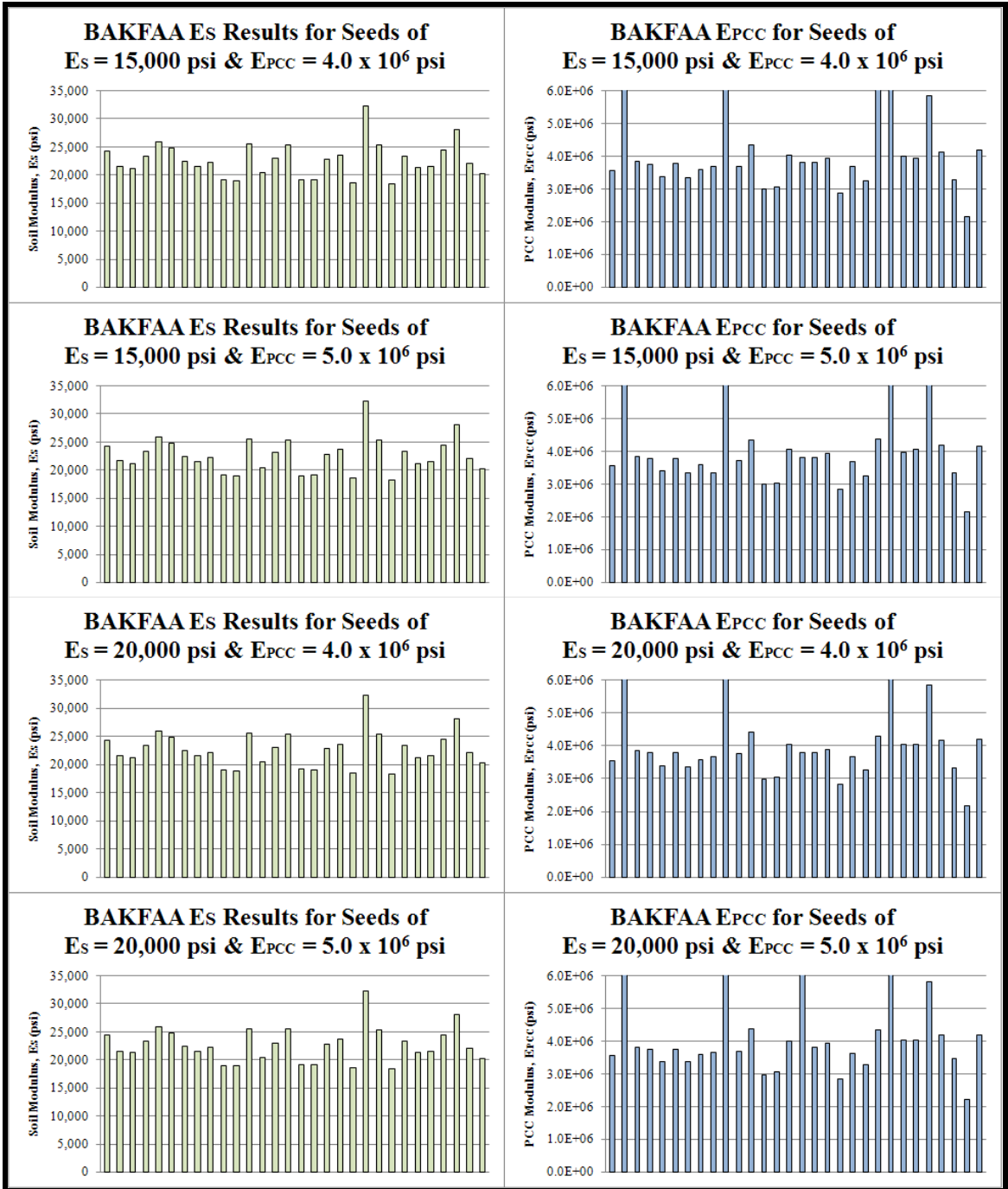


FIGURE 39  $E_s$  and  $E_{PCC}$  from BAKFAA

#### 4.6. ELMOD Results

ELMOD 5 backcalculation results are presented in Figure 40 using both the radius of curvature and the basin matching methods.

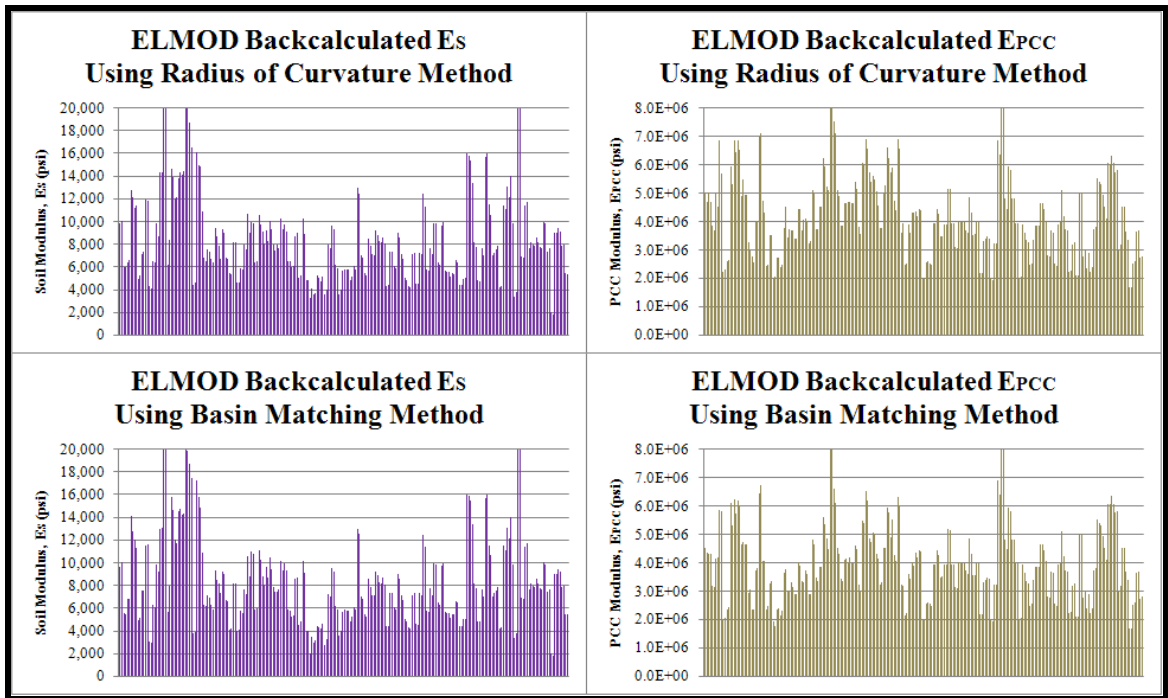
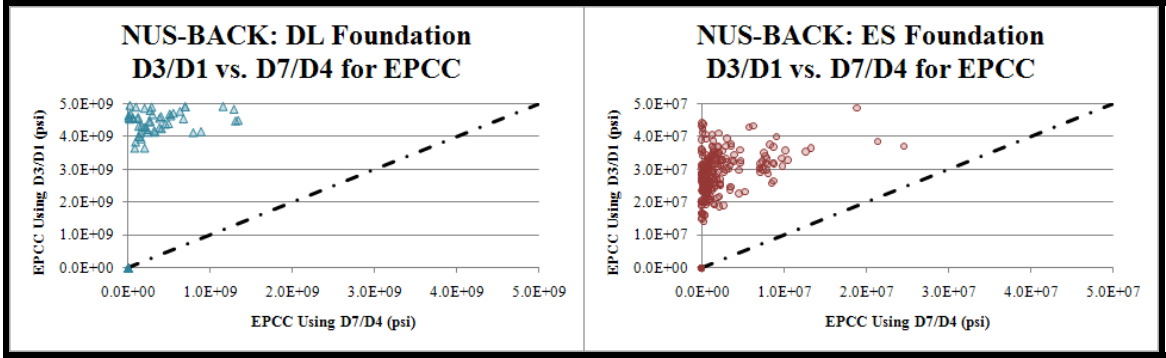


FIGURE 40  $E_s$  and  $E_{pcc}$  from ELMOD

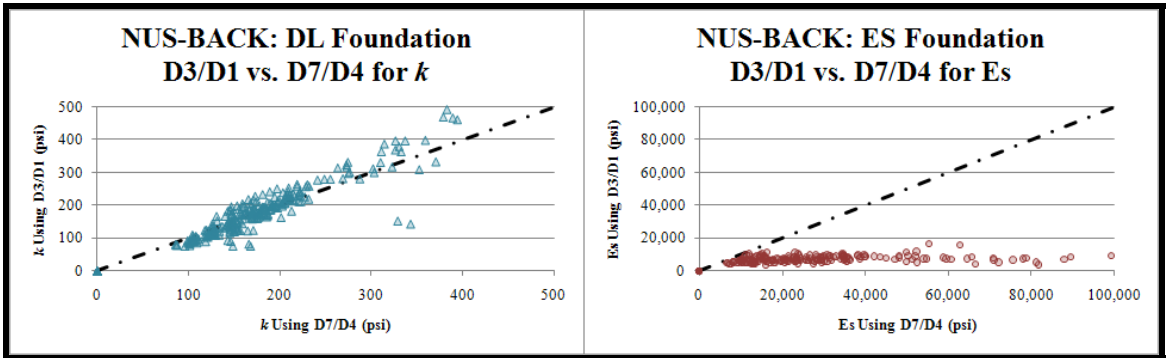
#### 4.7. Comparisons

Figure 41 compares the effectiveness of different sensor spacings for estimating  $E_{pcc}$  in NUS-BACK for both dense liquid and elastic solid foundations.



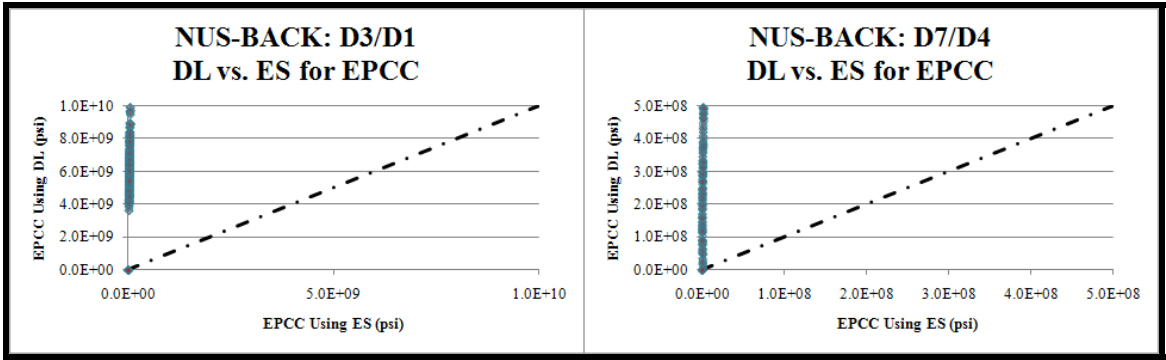
**FIGURE 41 NUS-BACK:  $D_3-D_1$  vs.  $D_7-D_4$  for  $E_{PCC}$**

Figure 42 compares the different sensor spacings for estimating  $k$  (for the dense liquid model) and  $E_s$  (for the elastic solid model).



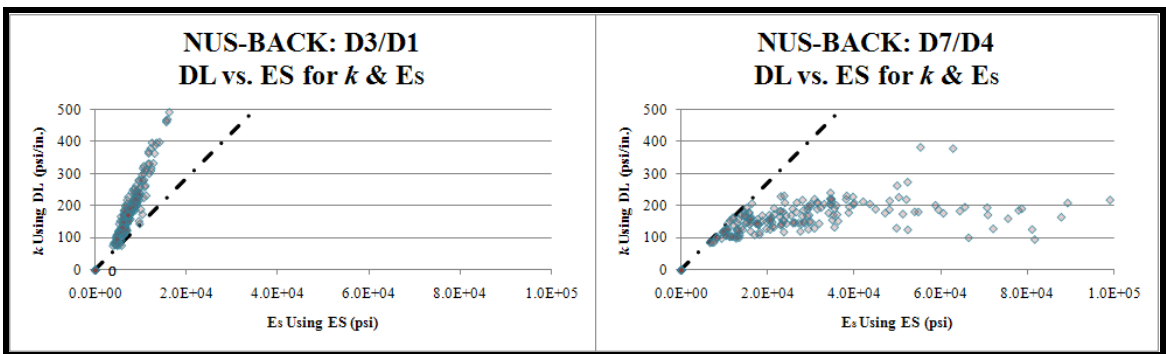
**FIGURE 42 NUS-BACK:  $D_3-D_1$  vs.  $D_7-D_4$  for  $k, E_s$**

Figure 43 illustrates the variability in the dense liquid and elastic solid models for estimating  $E_{PCC}$ .



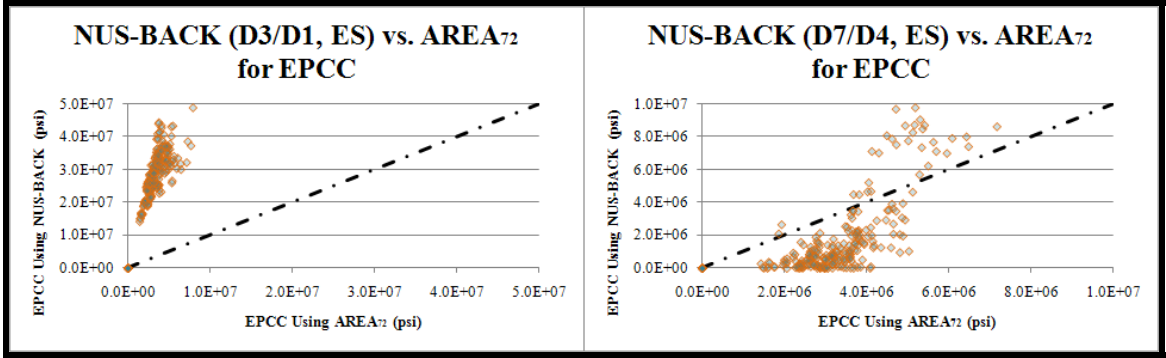
**FIGURE 43 NUS-BACK: Dense Liquid vs. Elastic Solid for  $E_{PCC}$**

Similarly, Figure 44 compares the ability of the two subgrade models to estimate subgrade stiffness. The line of equality is not 1:1 because the relationship between  $k$  and  $E_s$  is not 1:1. The reader is referred to section 5.6 for a more detailed explanation of this topic.



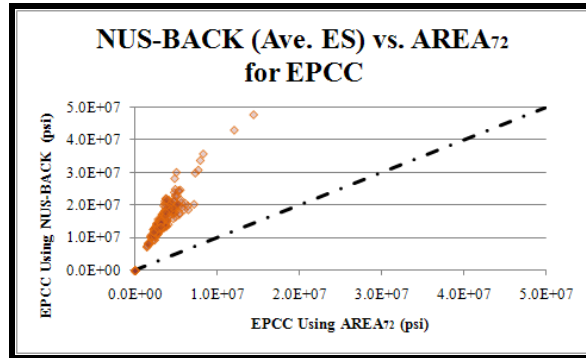
**FIGURE 44 NUS-BACK: Dense Liquid vs. Elastic Solid for  $k$  &  $E_s$**

The NUS-BACK elastic solid model for both sensor spacings is compared to the AREA<sub>72</sub> model for estimations of  $E_{PCC}$  in Figure 45.



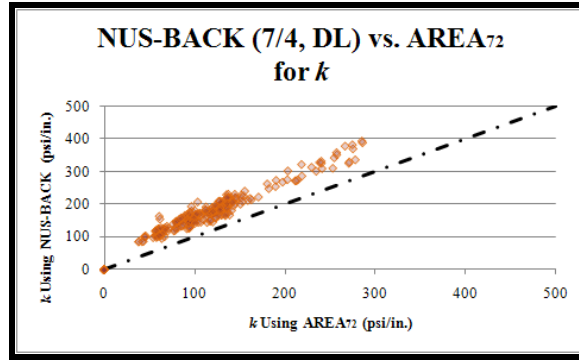
**FIGURE 45 NUS-BACK (Elastic Solid) vs. AREA<sub>72</sub> for E<sub>PCC</sub>**

For completeness, the average of the two NUS-BACK elastic solid models (both D<sub>3</sub>/D<sub>1</sub> and D<sub>7</sub>/D<sub>4</sub>) is compared to the AREA<sub>72</sub> model for estimating E<sub>PCC</sub> in Figure 46.



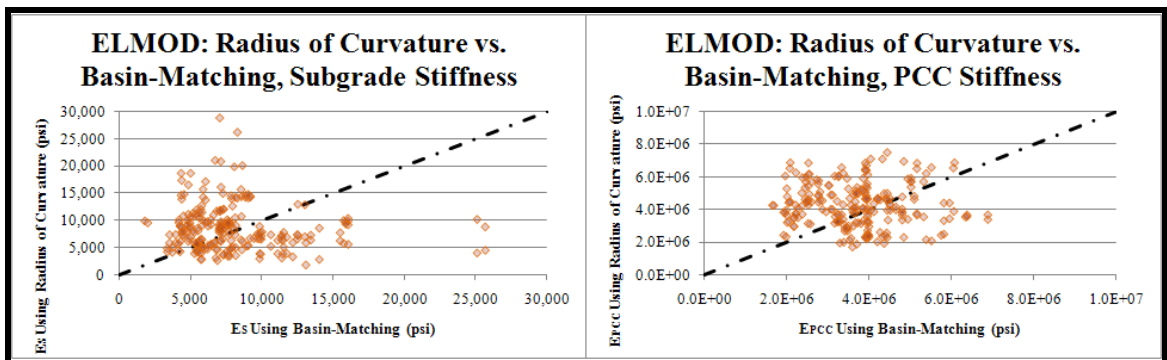
**FIGURE 46 NUS-BACK Average (Elastic Solid) vs. AREA<sub>72</sub> for E<sub>PCC</sub>**

Figure 47 compares the estimations of  $k$  from the NUS-BACK D<sub>7</sub>/D<sub>4</sub> dense liquid setup with those from the AREA<sub>72</sub> method.



**FIGURE 47 NUS-BACK D<sub>7</sub>-D<sub>4</sub> (Dense Liquid) vs. AREA<sub>72</sub> for *k***

Figure 48 compares the estimations of subgrade and pavement stiffness from ELMOD 5 according to which optimization procedure is used, basin-matching or radius of curvature.



**FIGURE 48 ELMOD: Radius of Curvature vs. Basin-Matching**

The NUS-BACK D<sub>7</sub>/D<sub>4</sub> dense liquid setup is compared to BAKFAA, LTPP, and ELMOD 5 for estimating subgrade stiffness in Figures 49, 50, and 51, respectively. Similarly, AREA<sub>72</sub> is compared to BAKFAA, LTPP, and ELMOD 5 in Figures 52, 53 and 54.

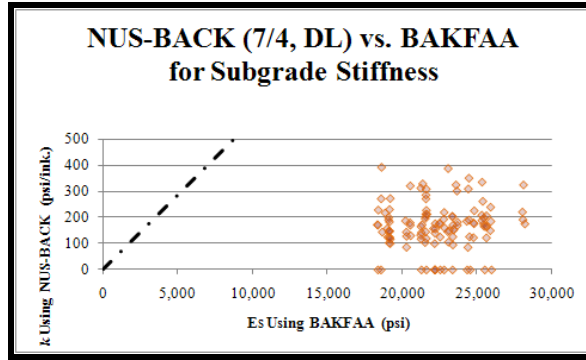


FIGURE 49 NUS-BACK D<sub>7</sub>-D<sub>4</sub> (DL) *k* vs. BAKFAA E<sub>S</sub>

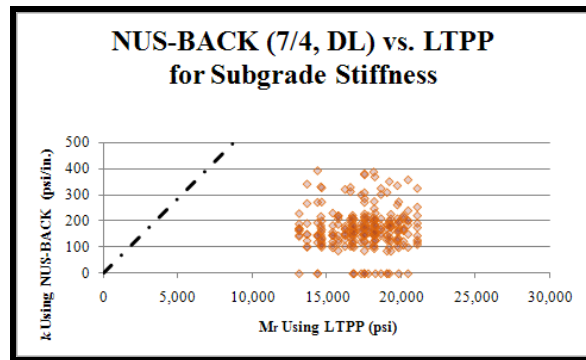


FIGURE 50 NUS-BACK D<sub>7</sub>-D<sub>4</sub> (DL) *k* vs. LTPP M<sub>r</sub>

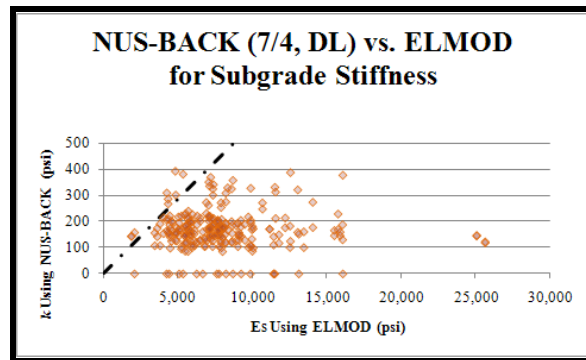
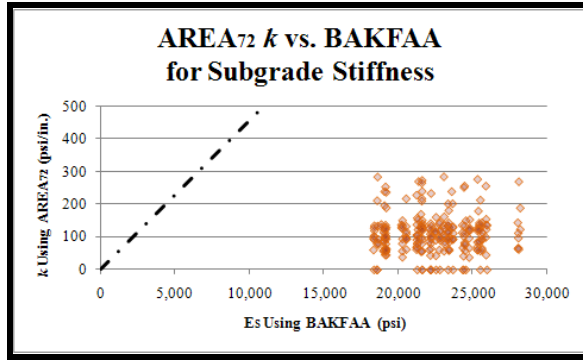
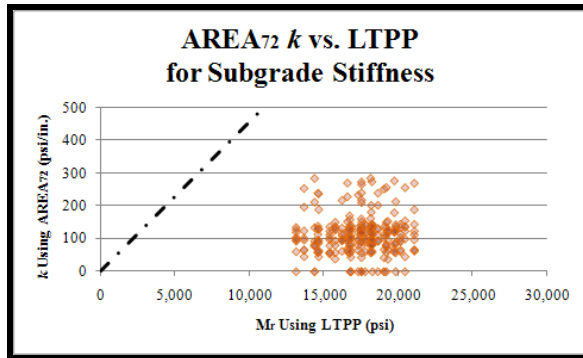


FIGURE 51 NUS-BACK D<sub>7</sub>-D<sub>4</sub> (DL) *k* vs. ELMOD E<sub>S</sub>



**FIGURE 52** AREA<sub>72</sub> *k* vs. BAKFAA  $E_s$



**FIGURE 53** AREA<sub>72</sub> *k* vs. LTPP  $M_r$

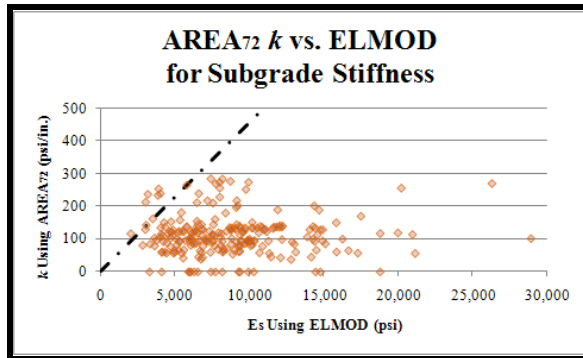


**FIGURE 54** AREA<sub>72</sub> *k* vs. ELMOD  $E_s$

The subgrade stiffness estimates from BAKFAA and LTPP are presented in Figure 55. Figure 56 shows the same for BAKFAA and ELMOD 5, and Figure 57 makes the comparison for LTPP and ELMOD 5.

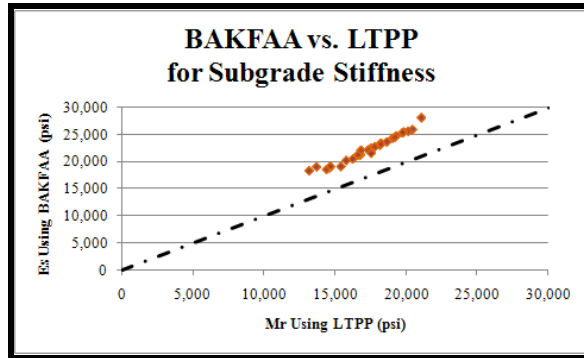


**FIGURE 55 BAKFAA  $E_S$  vs. LTPP  $M_r$**

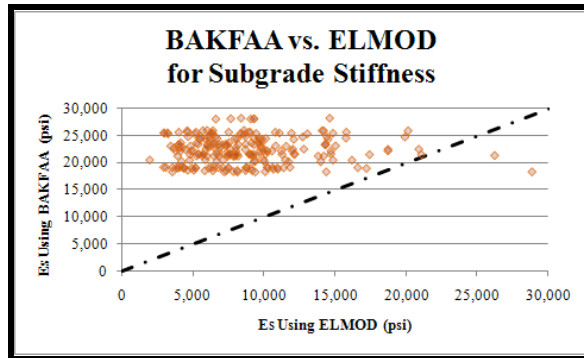


**FIGURE 56 BAKFAA  $E_S$  vs. ELMOD  $E_S$**

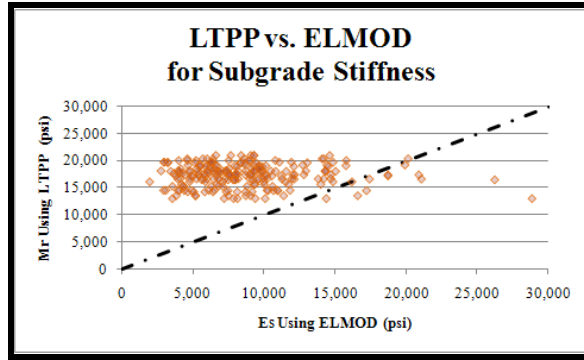


**FIGURE 57 LTPP  $M_r$  vs. ELMOD  $E_s$**

Estimations of the different procedures for  $E_{PCC}$  are presented in figures 58 – 63. The estimates of  $AREA_{72}$  are compared to those from BAKFAA, LTPP, and ELMOD 5 in Figures 58, 59, and 60, respectively. The BAKFAA estimates of  $E_{PCC}$  are plotted against those from LTPP and ELMOD 5 in Figures 61 and 62, respectively. Finally, a comparison between LTPP and ELMOD 5 for estimating  $E_{PCC}$  is given in Figure 63.

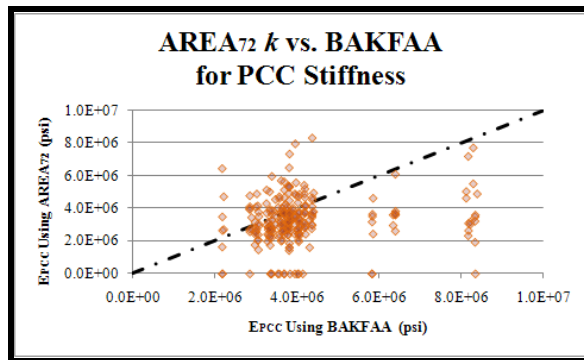


**FIGURE 58  $AREA_{72} E_{PCC}$  vs. BAKFAA  $E_{PCC}$**

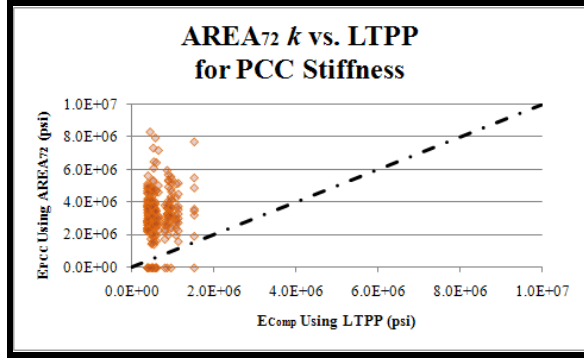


FIGURE 59 AREA<sub>72</sub> E<sub>PCC</sub> vs. LTPP E<sub>Comp</sub>

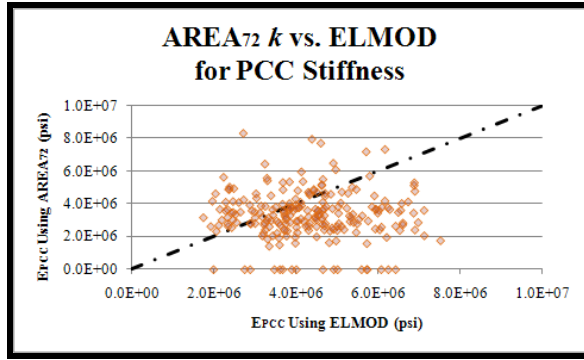


FIGURE 60 AREA<sub>72</sub> E<sub>PCC</sub> vs. ELMOD E<sub>PCC</sub>

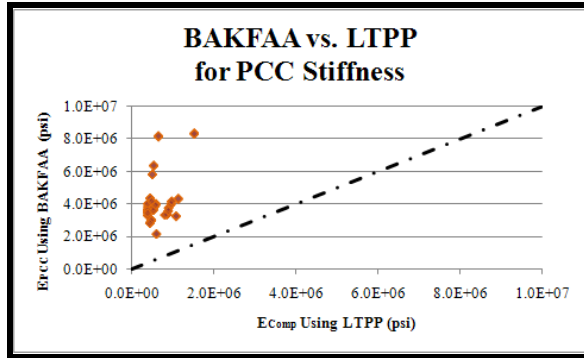
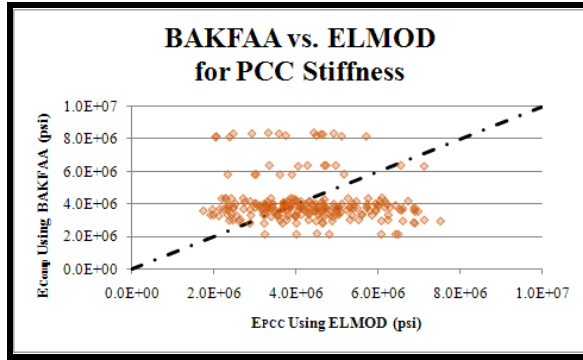
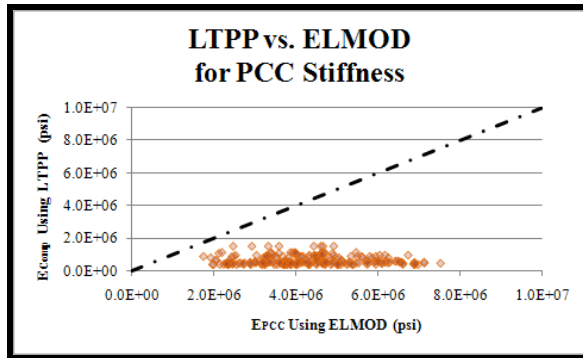


FIGURE 61 BAKFAA E<sub>PCC</sub> vs. LTPP E<sub>Comp</sub>



**FIGURE 62 BAKFAA  $E_{PCC}$  vs. ELMOD  $E_{PCC}$**



**FIGURE 63 LTPP  $E_{Comp}$  vs. ELMOD  $E_{PCC}$**

## **5. DISCUSSION**

### **5.1. SASW Results**

SASW results are presented in Table 12 of Section 4.1. The subgrade stiffness is consistently overestimated, and less than half of the estimates of  $E_{PCC}$  are reasonable. In fact, only one dispersion curve (Figure A2, Slab 17) is actually considered reasonable. It is not clear exactly why SASW performed so poorly at the Nashville site, but it is evident that SASW did not provide any valuable estimates for the Nashville site. This could have been due to human error, but the consistently unreasonable estimates suggest that SASW was not appropriate for the Nashville pavement. This could have been because of voids underneath the pavement that interfered with wave propagation, or simply because SASW is not an effective tool for analyzing rigid pavements.

### **5.2. NUS-BACK**

NUS-BACK is capable of modeling a foundation as dense liquid or elastic solid, and it can calculate layer moduli based on any two of seven measured deflections. The literature suggests that using the deflection measured directly under the load plate along with the third measured deflection ( $D_1$  and  $D_3$ , respectively) is best for estimating the pavement stiffness since those two deflections are due almost entirely to pavement response. Similarly,  $D_7$  and  $D_4$  are considered to work best for estimating subgrade moduli. Thus, NUS-BACK, on its own, provides many possible ways to backcalculate rigid pavement and subgrade stiffness.

Figures 34 and 35 in Section 4 show a graphical representation of the backcalculated values for pavement and subgrade stiffness, respectively, for different

combinations of the previously discussed methods. The  $E_{PCC}$  values were unreasonably large for the dense liquid model, and only moderately reasonable (between 2 and 3 million psi) for the  $D_3/D_1$  layout of the elastic solid model. The elastic solid  $D_3/D_1$  model consistently predicted values of  $E_{PCC}$  roughly 2 million psi lower than the laboratory estimated moduli.

The  $E_S$  values were more consistent throughout the different subgrade models and sensor spacings. The most consistent results, however, were observed when the dense liquid model was used. The dense liquid model gave  $k$  values mostly between 100 and 200 psi/in for both  $D_3/D_1$  spacing and  $D_7/D_4$  spacing. Unexpectedly, the  $D_3/D_1$  spacing estimated the most reasonable values for  $E_S$  with the elastic solid model, having a range of 5,000 to 10,000 psi. Further comparisons within the NUS-BACK results are discussed in section 5.6.

### **5.3. AREA<sub>72</sub>**

The AREA<sub>72</sub> method provides an estimation of the coefficient of subgrade reaction ( $k$ ) and the subgrade stiffness ( $E_{PCC}$ ). The estimate is made by taking the average of seven individual layer moduli estimations, one for each deflection measurement. Figures 36 and 37 in Section 4 show a graphical representation of the backcalculated moduli for the pavement and subgrade, respectively. The coefficients of subgrade reaction vary between about 75 and 125 psi/in., and the PCC moduli mostly fall between 2.5 and 4.5 million psi. The estimates of  $E_{PCC}$  were consistently 1 million psi below the laboratory estimate of  $E_{PCC}$ . Both of these ranges are within reason for the Nashville pavement system.

#### **5.4. LTPP Forward Calculation**

The LTPP forward calculation spreadsheet was used to estimate moduli for 30 selected deflection basins from the Nashville project. The NUS-BACK and  $AREA_{72}$  results were used to screen the database of Nashville data for basins that were most likely to yield reasonable estimates of layer moduli. Basins were chosen that corresponded to NUS-BACK and  $AREA_{72}$  estimates between 115 and 250 psi/in. for  $k$  and between 3 million and 6 million psi for  $E_{PCC}$ . The subgrade resilient modulus ( $M_r$ ) and composite pavement stiffness ( $E_{comp}$ ) that were estimated for those selected basins are illustrated graphically in Figure 38. The  $M_r$  estimates range between about 18,000 and 25,000 psi with good consistency. The composite pavement stiffness should be a close estimation of the PCC modulus since the Nashville pavement was only comprised of that single layer. The range of  $E_{comp}$  from forward calculation was about 400,000 to 600,000 psi with a few exceptions around 1 million psi. These estimates are unreasonably low for PCC stiffness.

#### **5.5. BAKFAA**

BAKFAA was used to analyze the same 30 deflection basins that were loaded into the LTPP forward calculation spreadsheets. BAKFAA is iteration-based software that relies on user-input values for seed moduli. Thus, unlike the previous closed-form methods, BAKFAA allows the user to alter the final estimate of moduli by using different seed values. Figure 39 shows the estimates that BAKFAA provides for various seed moduli. The  $E_{PCC}$   $E_S$  seeds were chosen based on the results of NUS-BACK and  $AREA_{72}$  backcalculations. Accordingly,  $E_S$  seeds of 15,000 and 20,000 psi were used,

and  $E_{PCC}$  seeds of 4 million and 5 million psi were used. The corresponding combinations and results are shown graphically in Figure 39.

At least for the variation in the seed values that were chosen, BAKFAA did not appear to be very sensitive to differences in seed values. For all 8 trial combinations the  $E_S$  estimate ranged between 19,000 and 24,000 psi fairly consistently. Similarly, the  $E_{PCC}$  estimates ranged between roughly 3 and 4 million psi. The  $E_{PCC}$  estimates are between 1 million and 2 million psi lower than the laboratory estimated moduli. The effect of averaging the basins from different load levels did not have any significant effect. The backcalculated moduli from the averaged basins are not noticeably different than those from the true basins.

## **5.6. ELMOD**

ELMOD 5.0 was used to backcalculate the layer moduli straight from the FWD output files. In practice, this feature makes ELMOD significantly more convenient than the other methods, because deflection basins are not entered manually by individual deflections and sensor spacings. The data is included in the .F25 file, and ELMOD provides the pertinent output as a Microsoft Access database file. As was mentioned in the literature review, ELMOD is capable of backcalculating moduli by matching either the radius of curvature of the basin or by matching the basin itself. Figure 40 summarizes the results from both techniques for  $E_S$  and  $E_{PCC}$ .

While there was significant scatter for the different basins, the overall results did not vary much based solely on the backcalculation technique. Furthermore, the scatter is likely due to inconsistent pavement distresses rather than errors in the backcalculation

program. The estimates for subgrade modulus were mostly between 5,000 and 10,000 psi. Those for PCC modulus were mostly between 2 million and 5 million psi. These ranges are both reasonable for the Nashville pavement and subgrade. However, the  $E_{PCC}$  estimates are consistently lower than the laboratory estimates.

### **5.7. NUS-BACK Variations**

Considering the different sensor arrangements and pavement modeling schemes that are possible with NUS-BACK, there are many different potential ways for NUS-BACK to backcalculate FWD data. If the NUS-BACK software were being used, it would be feasible to estimate moduli from 21 different 2-sensor arrangements, and each of those arrangements could be modeled as elastic solid or dense liquid. Since the graphical procedure was used for this study, the 2-sensor arrangements had to be limited for practicality. The two chosen sensor arrangements were  $D_3/D_1$  and  $D_7/D_4$ . The literature suggests that these two spacings give the best idea of pavement and subgrade stiffness, respectively. All 260 deflection basins from the Nashville project were analyzed in this manner.

Figure 41 in Section 4.7 compares the values that NUS-BACK estimated for  $E_{PCC}$  using  $D_3/D_1$  and  $D_7/D_4$ . Points lying on the dashed diagonal line represent deflection basins for which  $D_3/D_1$  and  $D_7/D_4$  both predict the same pavement stiffness. From the figure, it is clear that the  $D_3/D_1$  configuration estimates much higher PCC moduli than the  $D_7/D_4$  configuration for both dense liquid and elastic solid models. Figure 42 shows a similar comparison for subgrade stiffness instead of pavement stiffness. In this case, the sensor arrangement makes little difference for the dense liquid model, but for the elastic

solid model the D<sub>7</sub>/D<sub>4</sub> model is observed to estimate higher moduli than the D<sub>3</sub>/D<sub>1</sub> configuration.

Another important comparison to make for NUS-BACK procedures is the relative strength of the dense liquid and elastic solid models. Figure 43 compares the two models' estimates of pavement stiffness. The figure suggests that the dense liquid model predicts significantly larger  $E_{PCC}$  values than the elastic solid model. In addition, it can be seen that the values predicted by the dense liquid are unreasonably large.

For the comparison of  $k$  and  $E_S$ , two equality lines were initially drawn to represent Equations 4 and 73. It was quickly seen, however, that the difference in the two relationships was insignificant compared to the scatter of data and the two lines laid so close together that they could not be differentiated. Thus, for the remainder of this study, a single equality line was drawn for all comparisons between  $k$  and  $E_S$  that corresponds to  $E_S = 9.55k$ . Figure 44 shows the comparison between backcalculated  $E_S$  and  $k$  for the dense liquid and elastic solid models. Interestingly, the dense liquid model predicted higher values for the D<sub>3</sub>/D<sub>1</sub> spacing while the elastic solid model predicted higher values for the D<sub>7</sub>/D<sub>4</sub> spacing.

### **5.8. NUS-BACK vs. AREA<sub>72</sub>**

Comparisons were made between AREA<sub>72</sub> and several variations of NUS-BACK for estimating pavement and subgrade moduli. The comparison of Section 5.6 indicates that the dense liquid model is not appropriate for estimating the moduli of pavement layers in NUS-BACK. Therefore, only the elastic solid model was used within NUS-BACK for  $E_{PCC}$  backcalculation.

Figure 45 compares the both NUS-BACK arrangements to the AREA<sub>72</sub> model for estimating pavement stiffness. Figure 46 does the same, but takes the average of the D<sub>3</sub>/D<sub>1</sub> and D<sub>7</sub>/D<sub>4</sub> arrangements for NUS-BACK. The results show that the D<sub>7</sub>/D<sub>4</sub> arrangement causes NUS-BACK and AREA<sub>72</sub> to show the greatest agreement for E<sub>PCC</sub> backcalculation. The average NUS-BACK estimates also show fairly close agreement with AREA<sub>72</sub> estimates for PCC modulus. It is noted that the two comparisons including D<sub>3</sub>/D<sub>1</sub> show the least scatter and indicate an underprediction by AREA<sub>72</sub>, while the D<sub>7</sub>/D<sub>4</sub> NUS-BACK estimates seem to show an overprediction by AREA<sub>72</sub>. These results are not significant enough to indicate which method is best, but they do indicate that NUS-BACK and AREA<sub>72</sub> report E<sub>PCC</sub> values fairly close to one another.

In addition, NUS-BACK was compared to AREA<sub>72</sub> for the ability to estimate the subgrade stiffness. Figure 47 shows the dense liquid D<sub>7</sub>/D<sub>4</sub> NUS-BACK estimates plotted against the AREA<sub>72</sub> estimates. This relationship shows a high degree of continuity, with NUS-BACK consistently and slightly predicting higher soil moduli than AREA<sub>72</sub>. Again, this does not indicate whether one method is more accurate than the other, but it shows that the two methods estimate very similar ranges of moduli for the same deflection basins.

## **5.9. ELMOD Variations**

It was noted in Section 5.5 that the two backcalculation options with ELMOD do not have a significant impact on the final results. The two options are to simulate the radius of curvature of the deflection basin or to replicate the basin based on the individual deflections. Figure 48 shows the effect of these options for estimating both subgrade and

PCC stiffness. The figure shows a significant amount of scatter for both cases, but in both cases the scatter is centered on the line of equality.

### **5.10. Other Comparisons for Estimating Subgrade Stiffness**

NUS-BACK  $D_7/D_4$  (DL) and  $AREA_{72}$  were found to give consistent and reasonable results for the coefficient of subgrade reaction. The other backcalculation programs do not give  $k$  as a direct output, but the soil modulus ( $E_s$ ) was compared to  $k$  from NUS-BACK and  $AREA_{72}$  by the equation discussed in Section 5.6.

Figure 49 compares NUS-BACK with BAKFAA for estimating  $k$  and  $E_s$ , respectively. The figure shows that, according to the line of equality, BAKFAA predicts significantly higher soil moduli than NUS-BACK. Figure 50 compares NUS-BACK to the LTPP forward calculation spreadsheet for estimating  $k$  and  $M_r$ , respectively. In this case, the graph again suggests that NUS-BACK is estimating lower values than the compared technique. Figure 51 compares NUS-BACK to ELMOD for estimating soil stiffness. This case continues the trend of underestimation by NUS-BACK, but the agreement is much better than for the BAKFAA or LTPP methods. As expected, Figures 52 – 54 show very similar results for comparisons in which the NUS-BACK data was replaced by  $AREA_{72}$  data.

In order to further assess the various techniques for estimating subgrade stiffness, several additional comparisons were drawn. Figure 55 shows a direct comparison between the BAKFAA and LTPP methods for estimating  $E_s$  and  $M_r$ , respectively. The two methods show a consistent agreement with the LTPP method predicting slightly lower values than BAKFAA. Figure 56 then compares BAKFAA to ELMOD. In this

case, BAKFAA again predicts the higher values, but the agreement is less consistent and more scattered. Finally, LTPP and ELMOD are compared in Figure 57. The figure shows a mild agreement between the two methods, with ELMOD consistently predicting lower values than the LTPP spreadsheet. This shows that ELMOD predicted lower values than BAKFAA and the LTPP spreadsheet for soil stiffness.

### **5.11. Other Comparisons for Estimating PCC Stiffness**

AREA<sub>72</sub> was compared to the other studied methods for estimating PCC modulus. Figure 58 shows such a comparison between AREA<sub>72</sub> and BAKFAA with excellent agreement between the two data sets. Figure 59 compares AREA<sub>72</sub> to LTPP, but with less agreement in the data. The LTPP spreadsheet is observed to predict a lower value for  $E_{PCC}$  than AREA<sub>72</sub> in almost every case. Figure 60 shows close agreement between the estimated  $E_{PCC}$  values from AREA<sub>72</sub> and ELMOD. As with the other ELMOD plots, there is a good deal of scatter, but the scatter is centered on the line of equality.

To further investigate these techniques, BAKFAA was compared to the LTPP spreadsheet and ELMOD in Figures 61 and 62, respectively. Figure 61 shows little agreement between the LTPP and BAKFAA data, and it suggests that the LTPP spreadsheet estimated lower values than BAKFAA. Figure 62 shows a wide range of scatter for the BAKFAA and ELMOD estimates of  $E_{PCC}$ , but the data is centered on the line of equality. Finally, the LTPP and ELMOD estimates were compared in Figure 63. The figure shows relatively little agreement, and shows again that the LTPP spreadsheet tends to predict lower values than other similar procedures.

## 6. CLOSING

The purpose of this project was to analyze and compare backcalculation techniques for rigid and flexible pavements. Most of the techniques discussed have been in terms of the falling weight deflectometer (FWD), but the spectral analysis of surface waves (SASW) is also a viable approach. The literature review suggests that DIPLO-DEF is the most flexible program for analyzing FWD field data, and that automated procedures are being developed to ease the process of SASW inversion.

Field data for this project was limited to raw FWD and SASW data from a rigid pavement in Nashville, AR. The raw FWD data was used to perform backcalculations with five different procedures. DIPLO-DEF and MODULUS both seemed promising from the literature review, but the input/output process in a DOS-based environment proved too difficult to be practical for this project. The SASW field dispersion curves appeared to be flawed by some aspect of the field conditions. It is likely that air pockets existed between the concrete pavement and the subgrade which inhibited the regular propagation of Rayleigh waves. Nevertheless, the field dispersion curves were inverted by a simplified method.

Closed form solutions for rigid pavements were found to be very useful during this study because they facilitate the development of a user-friendly spreadsheet for backcalculation. ELMOD proved even more convenient by allowing the user to input a raw FWD file instead of entering individual basin dimensions. NUS-BACK and AREA<sub>72</sub> were analyzed via spreadsheet; LTPP forward calculations were performed using a publically available spreadsheet; BAKFAA was run by entering basin dimensions

through an easy-to-use graphical user interface; ELMOD was run by inputting raw FWD files.

The SASW results were not ideal, and a larger library of field data would likely give more reasonable and valuable results for comparison with FWD backcalculations. The simplified procedure that was used for this study is valuable for comparison with other testing methods, but an analysis using more advanced inversion procedures would also be practical to gauge the effect of automation on the final SASW-estimated layer moduli.

The discussion in Section 5 can be summarized by the following findings:

- The simplified SASW method was an ineffective and likely inappropriate tool for analyzing the rigid pavement in Nashville.
- The backcalculation procedures consistently estimated  $E_{PCC}$  values between 1 million and 2 million psi lower than the laboratory estimation. This could be due to flawed laboratory data.
- NUS-BACK  $D_7/D_4$  with dense liquid model and  $AREA_{72}$  are equally effective at estimating reasonable values for the coefficient of subgrade reaction,  $k$ , for rigid pavements. However, they both appear to predict much lower values than the other methods that were studied.
- The LTPP forward calculation spreadsheet for rigid pavements consistently underpredicts values of  $M_r$  and  $E_{Comp}$
- BAKFAA is an effective tool for estimating PCC moduli, but it seems to overpredict soil stiffness. This could be remedied by changing the values used for seed moduli.

- ELMOD reflects the scatter that is inherent in the field, but the overall quality of data is more consistent and reasonable than any of the other methods.

It is stressed that there is no “right” way to estimate in-situ pavement and soil properties. Every method is “wrong” to some extent, but the art of backcalculation requires the engineer to tweak whatever method(s) he or she is using to get the most reasonable results without resorting to destructive and expensive laboratory testing. The engineer’s knowledge of typical values, reasonable assumptions, and common sense is the most important element of backcalculation. That being said, FWD has shown a greater applicability to the type of pavement that was tested in this study, jointed reinforced concrete pavement (JRCP).

Since laboratory modulus tests were not available for the materials on which the FWD and SASW tests were run, the current study cannot assess the relative accuracy of the backcalculation procedures, but only their relative performance. Future studies would optimize their value by performing laboratory resilient modulus tests for a more valid comparison. In addition, the LTPP forward calculation, BAKFAA, ELMOD, and SASW could have been more adequately compared if raw data had been obtained for flexible or overlaid pavements. Nevertheless, the current study provides a detailed comparison of a simplified SASW inversion and several FWD backcalculation techniques for assessing the stiffness of rigid pavements and subgrade soils.

## REFERENCES

1. ASTM Designation: D 4694 – 96 (Reapproved 2003). Standard Test Method for Deflections with a Falling-Weight-Type Impulse Load Device.
2. Lytton, R.L, F.P. Germann, Y.J. Chou, and S.M. Stoffels. “Determining Asphaltic Concrete Pavement Structural Properties by Nondestructive Testing”, NCHRP Report 327, Transportation Research Board, Washington, D.C., 1990.
3. Selvadurai, A.P.S. “Elastic Analysis of Soil-Foundation Interaction”, Developments In Geotechnical Engineering, vol 17, Elsevier Scientific Publishing Company, 1979.
4. Jumikis, A.R. “Theoretical Soil Mechanics”, American Book Company, 1969.
5. Winkler, E. *Theory of Elasticity and Strength*. Prague: H. Dominicus, 1867 (in German).
6. Westergaard, H.M. “Stresses in Concrete Pavements Computed by Theoretical Analysis,” *Public Roads*, 7, No. 2, 23-35 (1926).
7. Scott, R.F. “Foundation Analysis”, Prentice-Hall, Inc., Englewood Cliffs, NJ, 1981.
8. Boussinesq, J. Application des Potentiels a l’Etude de l’ Equilibre et du Mouvement des Solides Elastique. Gauthier-Villars, Paris, 1885.
9. Panc, V., *Theories of Elastic Plates*, Noordhoff International Publishing, Leyden, Czechoslovakia, 1975.
10. Losberg, A. “Structurally Reinforced Concrete Pavement”, Doktorsavhandlingar Vid Chalmers Tekniska Hogskola, Goteborg, Sweden, 1960.
11. Hall, K.T., C.E. Correa, S.H. Carpenter, and R.P. Elliott. Rehabilitation Strategies for Highway Pavements. National Cooperative Highway Research Program, Web Document 35 (Project C1-38), May 2001.
12. National Highway Institute. Portland Cement Concrete Pavement Evaluation and Rehabilitation. FHWA-NHI-131062. CD-ROM. NHI, Virginia, 2001.
13. Strategic Highway Research Program: SHRP’s Layer Moduli Backcalculation Procedure, Strategic Highway Research Program, December 1993.
14. Stubstad, R.N., Jiang, Y.J., and E.O. Lukanen. “Guidelines for Review and Evaluation of Backcalculation Results”, Long-Term Pavement Performance Program, FHWA-HRT-05-152, 2006.

15. Khazanovich, L., McPeak, T.J., and S.D. Tayabji. "LTPP Rigid Pavement FWD Deflection Analysis and Backcalculation Procedure", *Nondestructive Testing of Pavements and Backcalculation of Moduli: Third Volume, ASTM STP 1375*, S.D. Tayabji and E.O. Lukanen, Eds., American Society for Testing and Materials, West Conshohocken, PA, 2000.
16. "AASHTO Guide for Design of Pavement Structures", American Association of State Highway and Transportation Officials, Washington, D.C., 1993.
17. Hall, K.T., Darter, M.I., and C.M. Kuo. "Improved Methods for Selection of  $k$  Value for Concrete Pavement Design", *Transportation Research Record* 1505, pp. 128-136, Washington, D.C., 1995.
18. Netemeyer, R. and S. Munsell. "Layer By Layer Evaluation of a PCC Pavement As It Was Constructed. Comparison of Backcalculated Material Values to Lab Material Values", RDT-99-002, Missouri Department of Transportation, Material and Research Division, 1995.
19. Huang, Y.H. *Pavement Analysis and Design*, Prentice Hall, pp. 316-317, 1993.
20. Ioannides, A.M. *ILLI-BACK: Experimental Version 3.3 User's Manual*, 1990.
21. Fwa, T.F., Tan, K.H., and S. Li. "Closed-Form and Semi-Closed-Form Algorithms for Backcalculation of Concrete Pavement Parameters" *Nondestructive Testing of Pavements and Backcalculation of Moduli: Third Volume, ASTM STP 1375*, S.D. Tayabji and E.O. Lukanen, Eds., American Society for Testing and Materials, West Conshohocken, PA, 2000.
22. Fwa, T.F. and B.H. Setiadji. "Evaluation of Backcalculation Methods for Nondestructive Determination of Concrete Pavement Properties", *Transportation Research Record: Journal of the Transportation Research Board*, No. 1949, Transportation Research Board of the national Academies, Washington, D.C., 2006, pp. 83-97.
23. Burmister, D.M. "The General Theory of Stresses and Displacements in Layered System", *Journal of Applied Physics*, Vol. 16, pp. 89-94 and 126-127, 1945.
24. Khazanovich, L. "Dynamic Analysis of FWD Test Results for Rigid Pavements", *Nondestructive Testing of Pavements and Backcalculation of Moduli: Third Volume, ASTM STP 1375*, S.D. Tayabji and E.O. Lukanen, Eds., American Society for Testing and Materials, West Conshohocken, PA, 2000.
25. McPeak, T.J and L. Khazanovich. "Backcalculation of Asphalt-Overlaid Concrete Pavements", *Proceedings, Aircraft/Pavement Technology: In the Midst of Change*, Seattle, Washington, American Society of Civil Engineers, 1997.

26. Hogg, A.H.A. "Equilibrium of a Thin Plate on an Elastic Foundation of Finite Depth", *Philosophical Magazine*, Vol. 35 (243), pp. 265-276, 1944.
27. Wiseman, G. and J. Greenstein. "Comparison of Methods of Determining Pavement Parameters from Deflection Bowl Measurements", *Proceedings of the 7<sup>th</sup> Asian Regional Conference on Soil Mechanics and Foundation Engineering*, pp. 158-165, 1983.
28. ELMOD<sup>®</sup> 5. Dynatest International.  
<http://www.dynatest.com/downloads/2007jan/Elmod5%2025102006.pdf>. Accessed March 19, 2008.
29. Appeah, A.K. and L. Al-Qadi. "Assessment of Falling Weight Deflectometer Data for Stabilized Flexible Pavements", *Transportation Research Record* 1709, pp. 19-25, Washington, D.C., 2000.
30. Federal Aviation Administration. "R&D Review", TC07-0045, Issue 2, pp. 13-14, 2007.
31. Gopalakrishnan, K. and M.R. Thompson. "Comparative effect of B777 and B747 Trafficking On Elastic Layer Moduli of NAPTF Flexible Pavements", 2004 FAA Worldwide Airport Technology Transfer Conference, Atlantic City, New Jersey, April 2004.
32. Hayhoe, G.F. "LEAF – A New Layered Elastic Computational Program for FAA Pavement Design and Evaluation Procedures", 2002 Federal Aviation Administration Technology Transfer Conference, 2002.
33. Kothandram, S. and A.M. Ioannides. "DIPLODEF: A Unified Backcalculation System for Asphalt and Concrete Pavements", *Transportation Research Record* 1764, pp. 20-29, Washington, D.C., 2001.
34. Khazanovich, L. and A.M. Ioannides. "DIPLOMAT: Analysis Program for Bituminous and Concrete Pavements", *Transportation Research Record* 1482, pp. 52-60, Washington, D.C., 1995.
35. Nazarian, S. and K. H. Stokoe II. "Use of Surface Waves in Pavement Evaluation" In *Transportation Research Record* 1070, pp. 132-144, Washington, D.C., 1986.
36. Rosenblad, B., E. M. Rathje, and I. I. Stokoe. "Shear Wave Velocity Profiling by the SASW Method at Selected Strong-Motion Stations in Turkey", 99?
37. HP 35670A Product Overview.  
[http://www.mae.wmich.edu/Labs/Noise\\_and\\_Vibration/HP\\_analyzer.pdf](http://www.mae.wmich.edu/Labs/Noise_and_Vibration/HP_analyzer.pdf). Accessed February 19, 2008.

38. Gucunksi, N., and R. D. Woods. "Instrumentation for SASW Testing", *Geotechnical Special Publication*, n 29, Recent Advances In Instrumentation, Data Acquisition and Testing In Soil Dynamics, October 21, 1991, pp. 1-16.
39. Rix, G. J. and E. A. Leipski. "Accuracy and Resolution of Surface Wave Inversion", *Geotechnical Special Publication*, n 29, Recent Advances In Instrumentation, Data Acquisition and Testing In Soil Dynamics, October 21, 1991, pp. 17-32.
40. Goel, A. and A. Das. "A Brief Review on Different Surface Wave Methods and Their Applicability for Non-Destructive Evaluation of Pavements", *Nondestructive Testing and Evaluation*, January 2008, pp. 337-350.
41. Ryden, N., Ulriksen, P., Park, C.B., Miller, R.D., Xia, J., and J. Ivanov. "High Frequency MASW for Non-Destructive Testing of Pavements – Accelerometer Approach", *Proceedings of the SAGEEP*, Denver, Colorado, RBA-5, 2001.
42. Kausel, E. and J.M. Roesset. "Stiffness Matrices for Layered Soils", *Bulletin of the Seismological Society of America*, Vol. 71, No. 6, p. 1743-1761, 1981.
43. Barfield, O.E. "Mechanistic Procedure for Prediction of the In-situ Resilient Modulus of Unbound Aggregate Base from Seismic Testing", Thesis for Masters of Science in Engineering, The University of Texas at Austin, 2006.
44. Darendeli, M.B., Stokoe, K.H., II, and R. Gilbert. "Development of a New Family of Normalized Modulus Reduction and Material Damping Curves", Ph.D., University of Texas at Austin, 2001.
45. Meshkani, A., Abdallah, I., and S. Nazarian. "Determination of Nonlinear Parameters of Flexible Pavement Layers from Nondestructive Testing", Conducted for TXDOT, Research Report TX 1780-3, 2004.
46. Ishibashi, I. and X. Zhang. "Unified Dynamic Shear Moduli and Damping Ratios of Sand and Clay", *Soils and Foundations*, Vol. 33, No. 1, pp. 182-191, 1993.
47. Zhou, H. "Comparison of Backcalculated and Laboratory Measured Moduli on AC and Granular Base Layer Materials", *Nondestructive Testing of Pavements and Backcalculation of Moduli: Third Volume, ASTM STP 1375*, S.D. Tayabji and E.O. Lukanen, Eds., American Society for Testing and Materials, West Conshohocken, PA, 2000.
48. Web Soil Survey. Natural Resources Conservation. United States Department of Agriculture. <http://websoilsurvey.nrcs.usda.gov/app/>. Accessed March 22, 2008.
49. ASTM Designation: D 6758-02. Test Method for Measuring Stiffness and Apparent Modulus of Soil and Soil-Aggregate In-Place By an Electro-Mechanical Method.

**APPENDIX A      RAW DATA FROM SASW TESTING**

**FIGURE A1 Nashville, AR – AR4/US278/Main St – Slab 3**

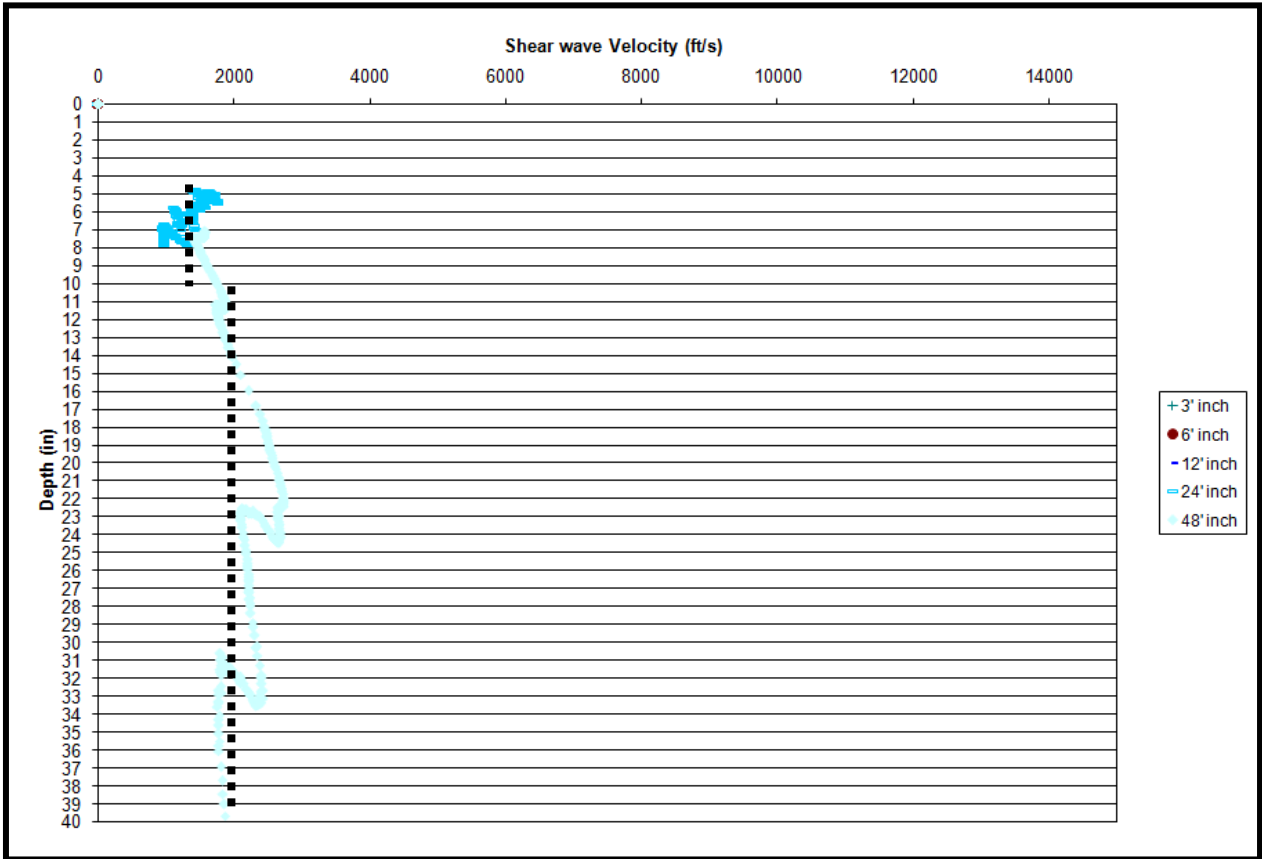


**TABLE A1 Analysis of Slab 3**

Depth (in.)	Measured $V_s$ (ft/s)	Assumed $\nu$	Assumed $\gamma$ (pcf)	$G_{seis}$ (psi)	$G$ (psi)	$E$ (psi)
0 – 6	-	-	-	-	-	-
6 – 11	1,500	0.40	115	55,000	24,200	67,760
11 – 40	2,100	0.40	115	109,000	47,960	134,288

**FIGURE A2 Nashville, AR – AR4/US278/Main St – Slab 17**

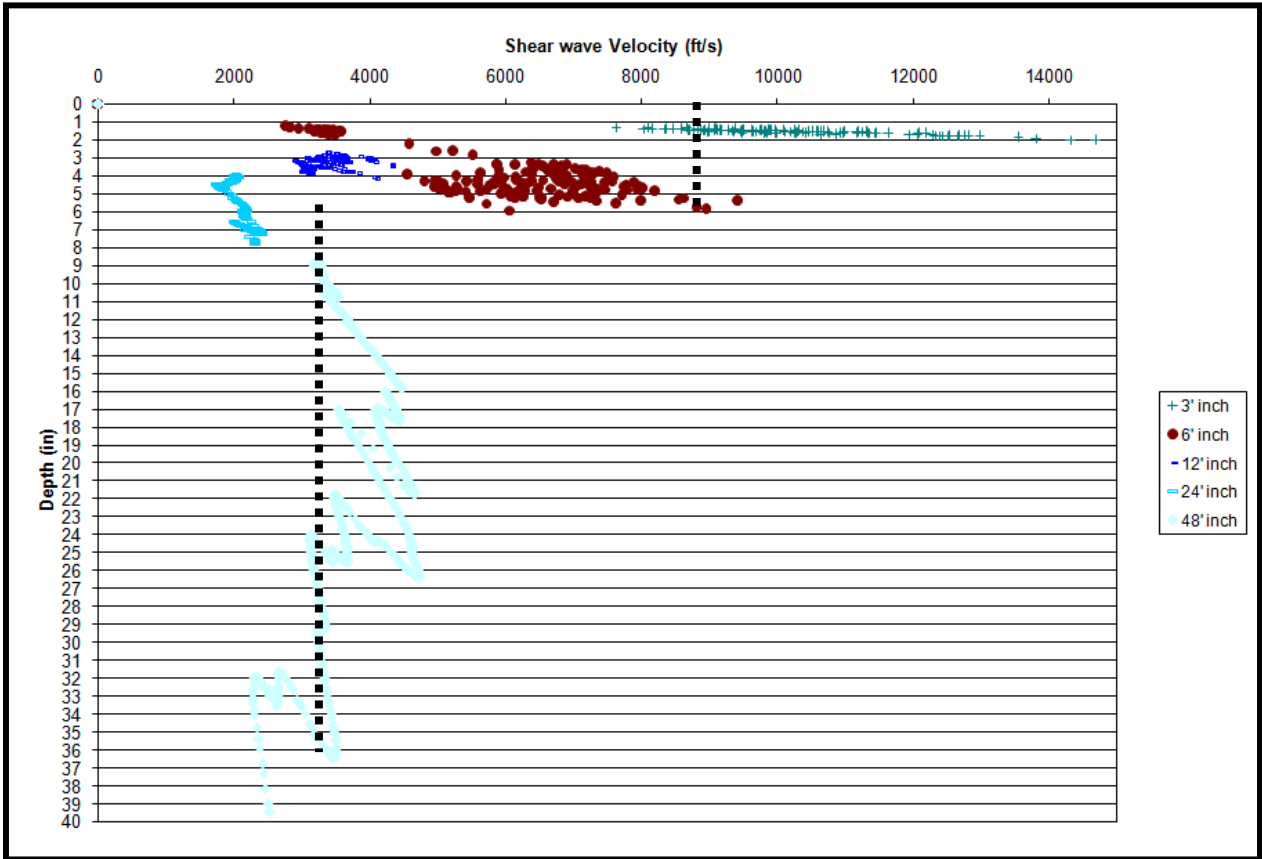


**TABLE A2 Analysis of Slab 17**

Depth (in.)	Measured $V_s$ (ft/s)	Assumed $\nu$	Assumed $\gamma$ (pcf)	$G_{seis}$ (psi)	$G$ (psi)	$E$ (psi)
0 – 6	8,700	0.15	150	2,448,000	1,077,000	2,478,000
6 – 36	3,600	0.40	115	321,000	141,240	395,472

**FIGURE A3 Nashville, AR – AR4/US278/Main St – Slab 25**

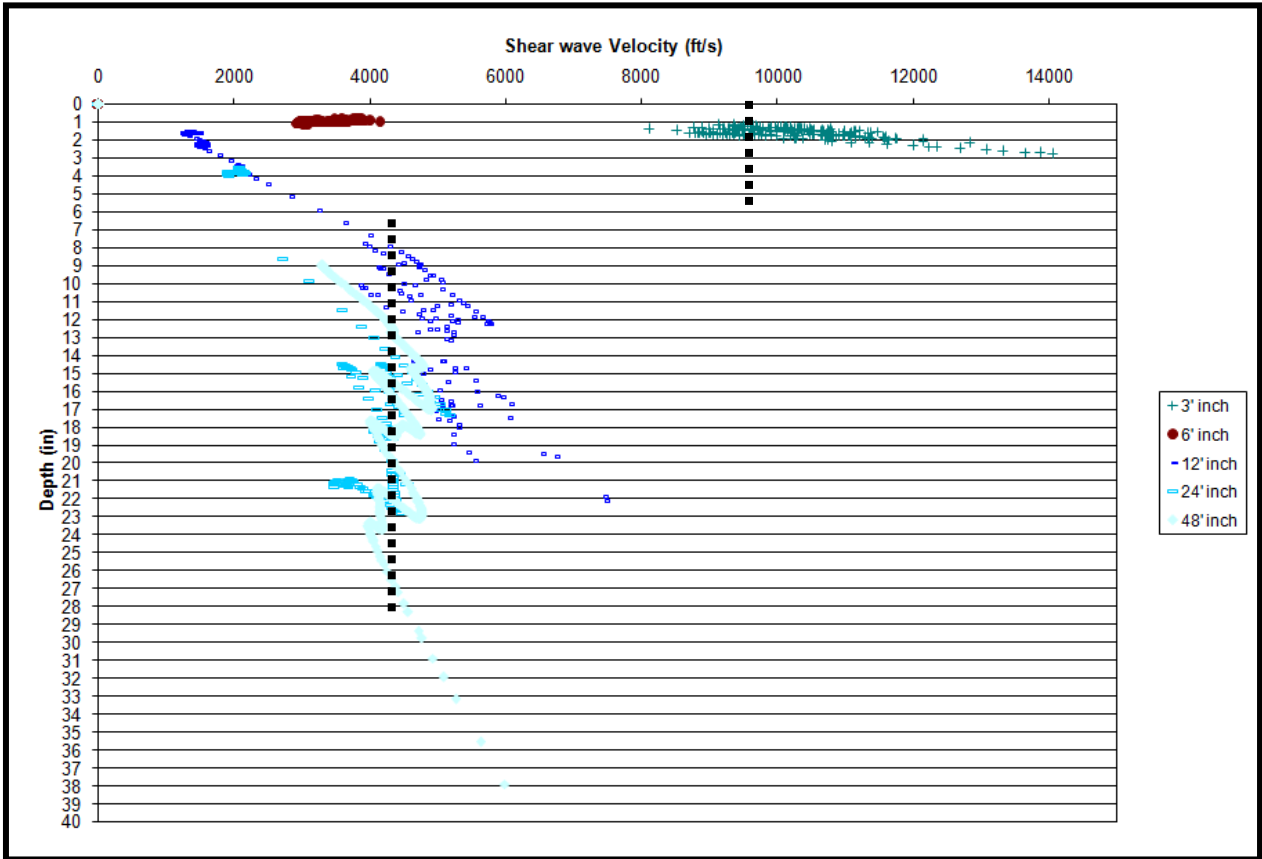


**TABLE A3 Analysis of Slab 25**

Depth (in.)	Measured $V_s$ (ft/s)	Assumed $\nu$	Assumed $\gamma$ (pcf)	$G_{seis}$ (psi)	$G$ (psi)	$E$ (psi)
0 – 6	9,700	0.15	150	3,043,000	3,043,000	6,999,000
6 – 28	4,300	0.40	115	458,000	201,520	564,256

**FIGURE A4 Nashville, AR – AR4/US278/Main St – Slab 34**

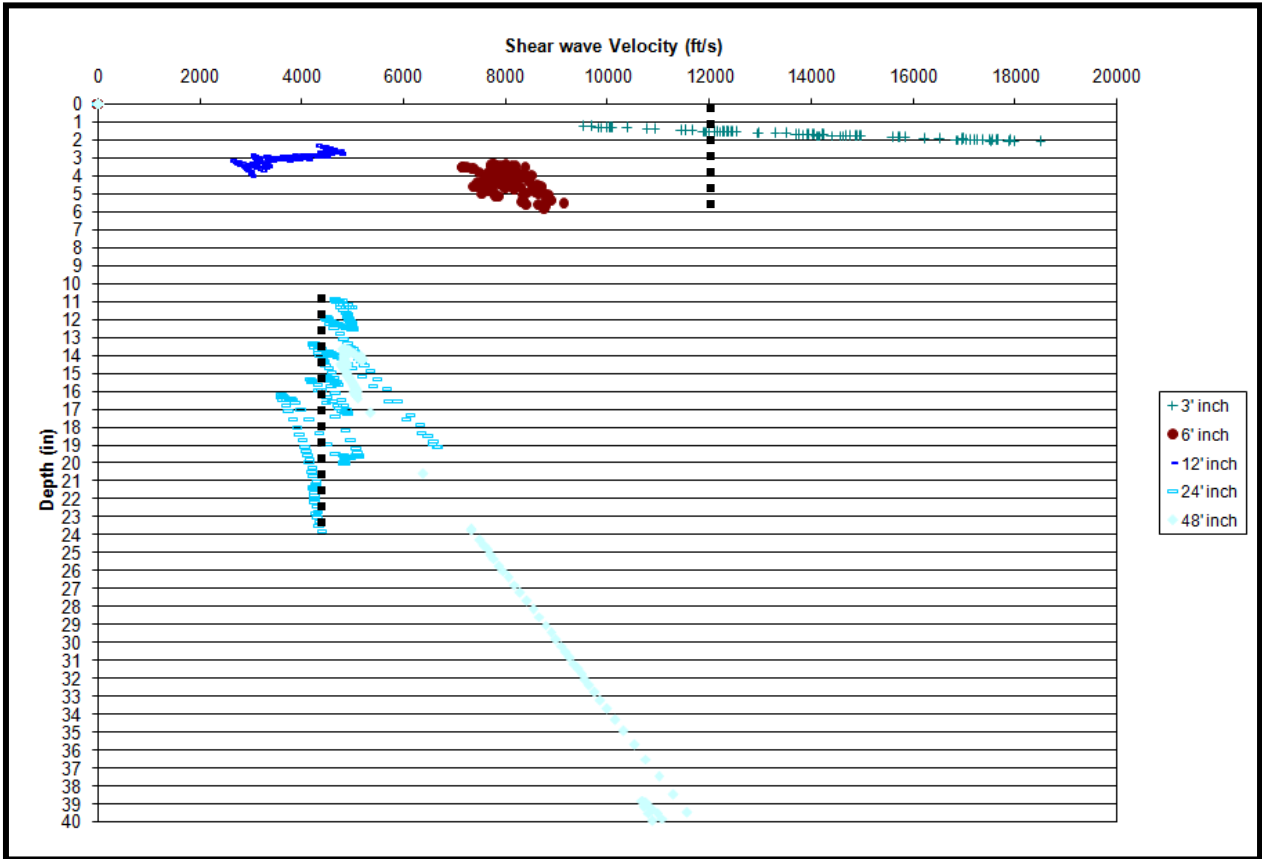


**TABLE A4 Analysis of Slab 34**

Depth (in.)	Measured $V_s$ (ft/s)	Assumed $\nu$	Assumed $\gamma$ (pcf)	$G_{seis}$ (psi)	$G$ (psi)	$E$ (psi)
0 – 6	12,500	0.15	150	5,054,000	5,054,000	11,624,000
6 – 10	-	-	-	-	-	-
10 – 23	4,500	0.40	115	502,000	220,880	618,464

**FIGURE A5 Nashville, AR – AR4/US278/Main St – Slab 42**

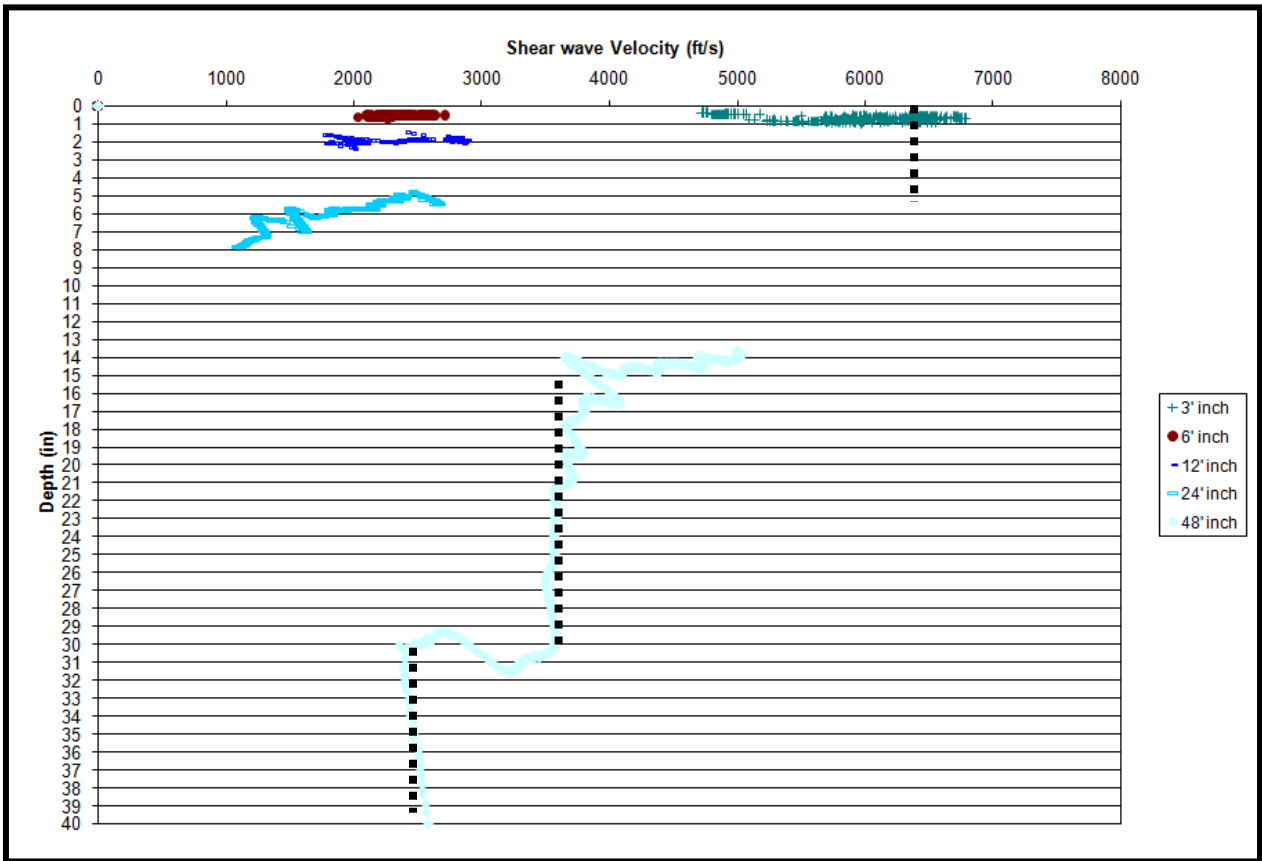


**TABLE A5 Analysis of Slab 42**

Depth (in.)	Measured $V_s$ (ft/s)	Assumed $\nu$	Assumed $\gamma$ (pcf)	$G_{seis}$ (psi)	$G$ (psi)	$E$ (psi)
0 – 6	6,500	0.15	150	1,366,000	1,366,000	3,142,000
6 – 15	-	-	-	-	-	-
15 – 30	3,600	0.40	115	321,000	141,240	395,472
30 – 40	2,400	0.40	115	142,000	62,480	174,944

**FIGURE A6 Nashville, AR – AR4/US278/Main St – Slab 52**

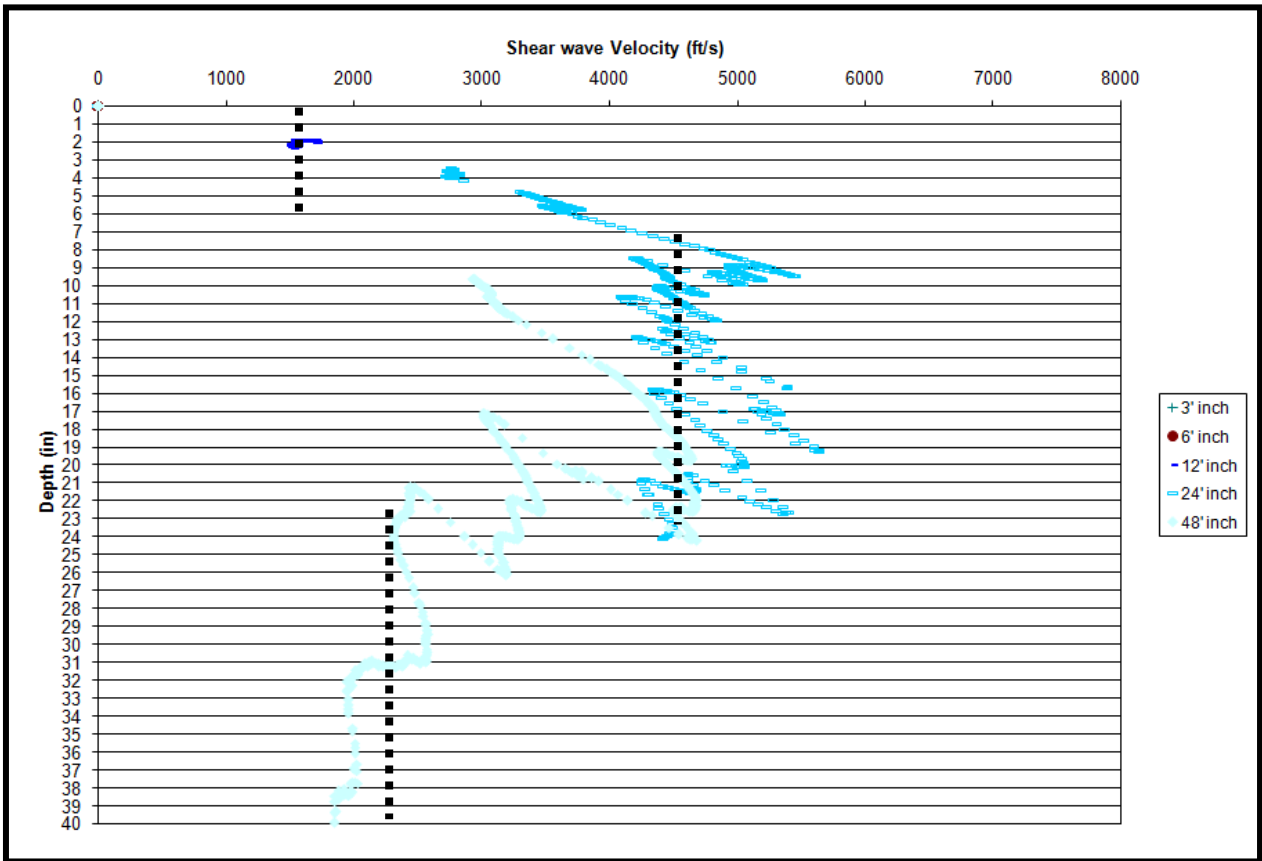


**TABLE A6 Analysis of Slab 52**

Depth (in.)	Measured $V_s$ (ft/s)	Assumed $\nu$	Assumed $\gamma$ (pcf)	$G_{seis}$ (psi)	G (psi)	E (psi)
0 – 6	1,600	0.15	150	82,000	82,000	189,000
6 – 23	4,600	0.40	115	524,000	230,560	645,568
23 – 40	2,300	0.40	115	131,000	57,640	161,392

**FIGURE A7 Nashville, AR – AR4/US278/Main St – Slab 66**

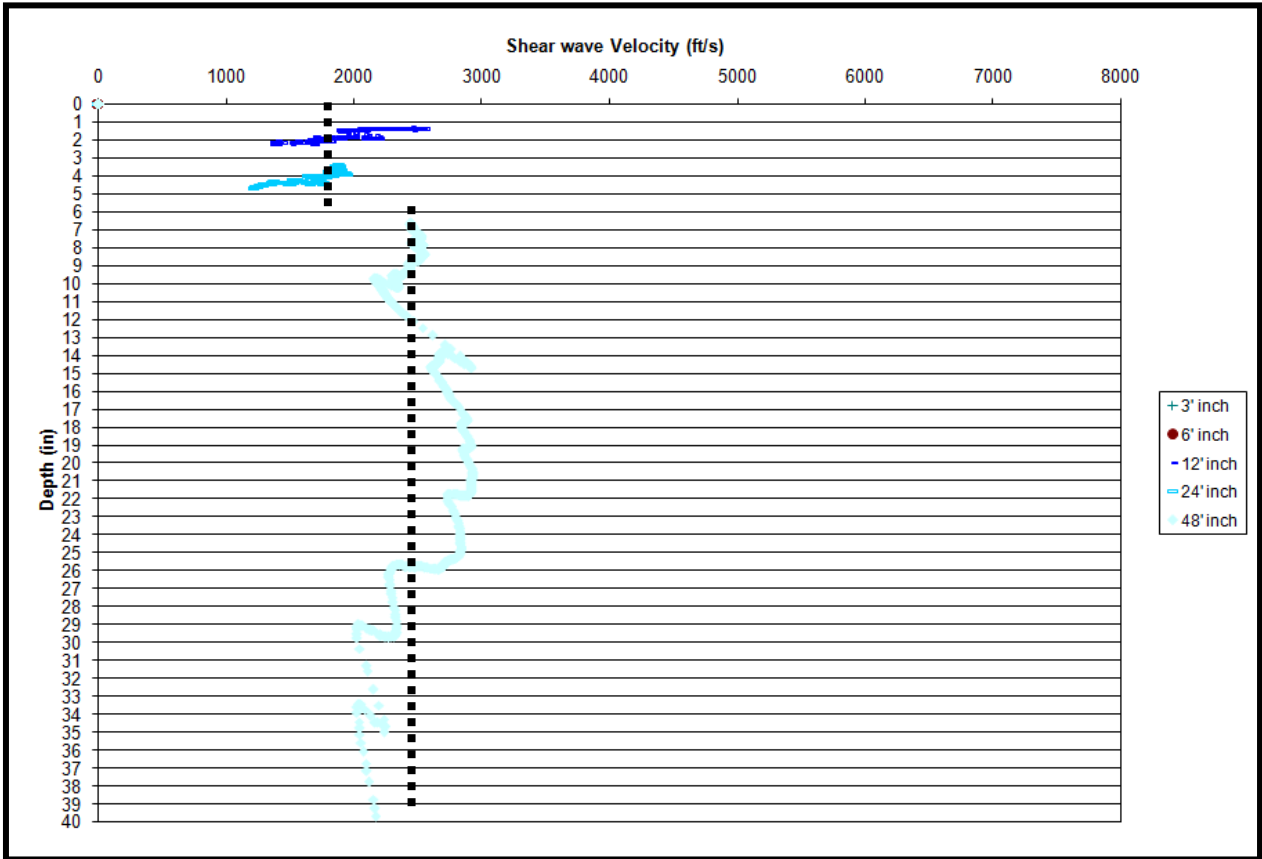


**TABLE A7 Analysis of Slab 66**

Depth (in.)	Measured $V_s$ (ft/s)	Assumed $\nu$	Assumed $\gamma$ (pcf)	$G_{seis}$ (psi)	$G$ (psi)	$E$ (psi)
0 – 6	1,700	0.15	150	93,000	93,000	214,000
6 – 28	2,500	0.40	115	155,000	68,200	190,960

**FIGURE A8 Nashville, AR – AR4/US278/Main St – Slab 76**

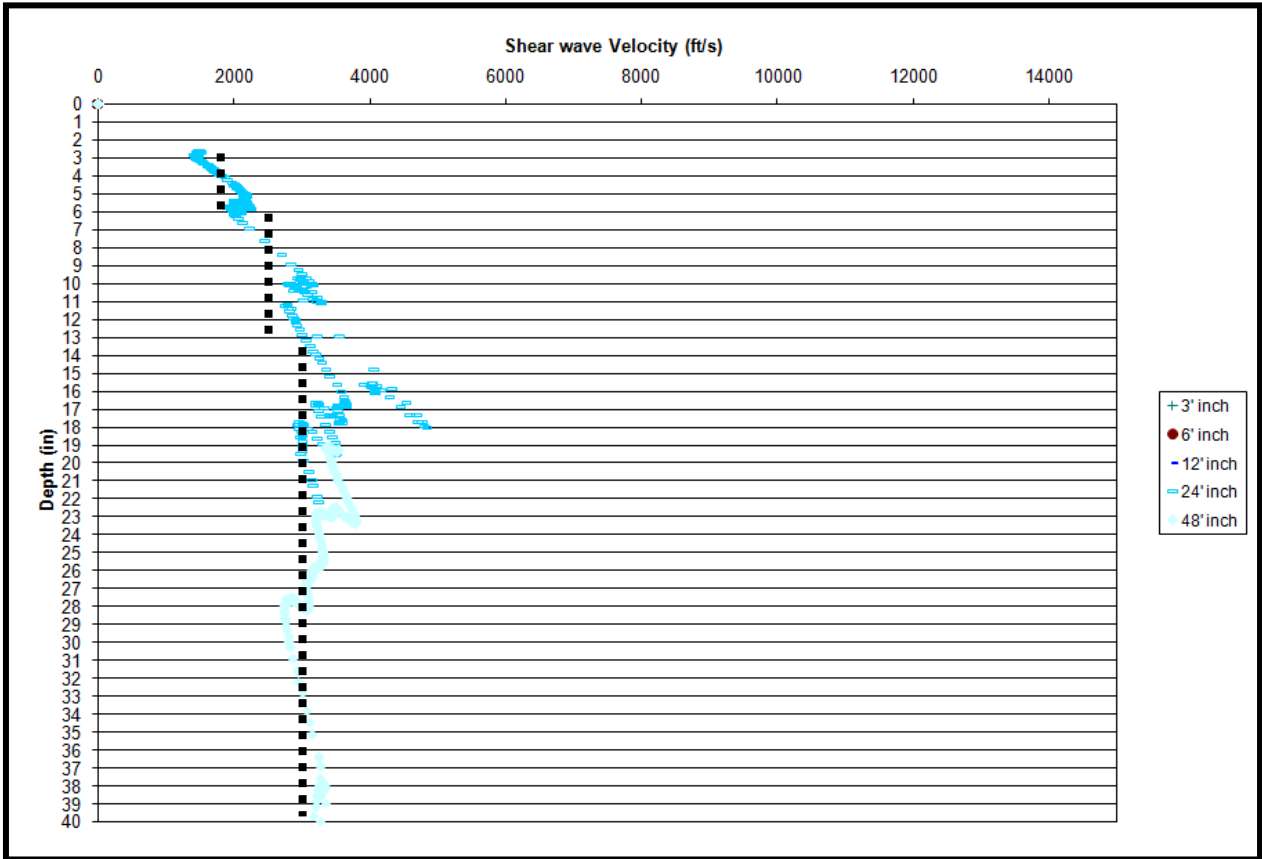


**TABLE A8 Analysis of Slab 76**

Depth (in.)	Measured $V_s$ (ft/s)	Assumed $\nu$	Assumed $\gamma$ (pcf)	$G_{seis}$ (psi)	G (psi)	E (psi)
0 – 6	2,000	0.15	150	129,000	129,000	297,000
6 – 13	2,700	0.40	115	180,000	79,200	221,760
13 – 40	3,300	0.40	115	270,000	118,800	332,640

**APPENDIX B      RAW DATA FROM FWD TESTING**

Table B1

Raw FWD Data from Nashville, Northbound Lane

#	AC Temp		Surf Temp	Air Temp	NASHVILLE - NORTHBOUND																			
	-C	-F			Load 1	Deflection @ Radius (mils @ in.)					Load 2	Deflection @ Radius (mils @ in.)												
					(lb)	0.000	7.990	12.005	24.010	35.975	47.980	59.985	71.989	83.994	(lb)	0.000	7.990	12.005	24.010	35.975	47.980	59.985	71.989	83.994
1	28.6	32.7	21.4	9438	10.272	9.098	8.772	6.772	4.720	2.850	1.512	0.701	0.598	12748	13.799	12.209	11.752	9.071	6.370	3.882	2.150	0.988	0.882	0.882
2	28.6	32.3	21.6	9390	8.370	7.539	7.161	5.390	3.799	2.441	1.591	0.961	0.669	12843	11.449	10.240	9.760	7.382	5.228	3.390	2.252	1.370	0.961	0.961
3	28.6	32.3	21.2	9215	9.402	7.858	7.299	5.228	3.610	2.370	1.610	1.091	0.780	12430	12.870	10.772	10.051	7.260	5.071	3.370	2.319	1.571	1.130	1.130
4	28.6	31.9	21.1	9438	11.669	9.728	9.079	6.461	4.118	2.642	1.831	1.189	0.799	12636	15.799	13.220	12.382	8.870	5.811	3.752	2.642	1.669	1.150	1.150
5	28.6	32.4	20.9	9517	6.772	6.161	5.980	4.909	4.020	3.189	2.720	2.059	1.551	12780	9.441	8.591	8.350	6.902	5.669	4.571	3.980	2.799	0.689	0.689
6	28.6	32.5	21.3	9517	8.350	7.571	7.252	5.598	4.150	2.969	2.260	0.870	0.740	12907	11.512	10.409	10.020	7.780	5.819	4.240	3.311	1.280	1.071	1.071
7	28.6	32.7	20.9	9310	9.500	8.669	8.331	6.409	4.579	3.150	2.280	1.740	1.331	12700	12.780	11.630	11.209	8.661	6.209	4.331	3.220	2.449	1.890	1.890
8	28.6	33.1	21.2	9342	8.130	7.469	7.319	6.201	4.772	3.480	2.591	1.839	1.331	12732	11.091	10.150	9.961	8.409	6.500	4.752	3.551	2.531	1.811	1.811
9	28.6	32.9	21.2	10759	8.591	7.980	7.772	6.559	5.051	3.681	2.811	2.000	1.461	14228	11.791	10.961	10.650	8.980	6.961	5.000	3.772	2.689	1.961	1.961
10	28.6	32.9	21.3	9374	8.642	8.039	7.882	6.689	5.421	4.201	3.299	2.441	1.902	12748	11.709	10.890	10.689	9.000	7.240	5.591	4.331	3.260	2.520	2.520
11	28.6	33.4	21.3	9422	8.409	7.689	7.441	5.961	4.441	3.031	2.059	1.358	1.059	12748	11.500	10.441	10.118	8.091	6.039	4.142	2.819	1.929	1.520	1.520
12	28.6	32.9	21.1	9565	6.429	5.858	5.669	4.409	3.169	2.118	1.539	1.059	0.799	12748	8.941	8.118	7.870	6.130	4.441	3.000	2.169	1.539	1.189	1.189
13	28.6	33.0	20.9	9183	7.650	7.209	7.150	5.740	4.382	3.071	2.181	1.311	0.831	12573	10.461	9.831	9.760	7.760	5.740	3.988	2.791	1.752	1.051	1.051
14	28.6	32.9	20.8	9724	5.059	4.260	3.929	2.669	1.811	1.299	0.969	0.669	0.579	13018	6.720	5.689	5.299	3.669	2.512	1.752	1.280	0.949	0.740	0.740
15	28.6	33.0	20.9	9342	8.039	7.402	7.150	5.752	4.610	3.480	2.610	1.889	0.870	12748	10.630	9.689	9.311	7.382	5.791	4.249	3.150	1.169	0.909	0.909
16	28.6	32.6	21.3	9469	7.969	6.811	6.331	4.461	2.969	1.752	1.059	0.839	0.650	12748	10.760	9.260	8.539	6.110	4.150	2.429	1.500	1.181	0.929	0.929
17	28.6	32.6	21.2	9533	8.161	7.071	6.689	4.929	3.441	2.291	1.661	1.189	0.909	12891	11.209	9.720	9.189	6.791	4.791	3.189	2.350	1.728	1.339	1.339
18	28.6	32.4	21.2	9597	6.701	6.012	5.760	4.520	3.319	2.311	1.661	1.150	0.831	12430	8.969	8.059	7.701	6.091	4.539	3.201	2.311	1.598	1.169	1.169
19	28.6	32.3	20.8	9485	12.209	11.069	10.720	8.319	5.720	3.110	1.480	0.969	0.681	12939	16.469	14.850	14.350	11.118	7.591	4.098	1.929	1.299	0.941	0.941
20	28.6	31.9	21.2	9485	8.882	8.012	7.760	6.012	4.189	2.500	1.559	1.051	0.689	12509	11.551	10.421	10.051	7.799	5.429	3.272	2.150	1.390	0.949	0.949
21	28.6	31.9	21.2	9422	10.689	10.071	10.201	7.020	4.421	2.449	1.382	0.681	0.520	12923	14.591	13.689	13.799	9.591	6.110	3.449	2.039	1.098	0.661	0.661
22	28.6	31.8	21.8	9453	6.819	5.882	5.531	4.000	2.740	1.720	1.059	0.650	0.551	12700	9.382	8.091	7.689	5.579	3.831	2.382	1.421	0.858	0.760	0.760
23	28.6	31.4	21.1	9422	5.161	4.469	4.181	2.980	2.039	1.311	0.870	0.559	0.500	12446	7.299	6.331	5.949	4.289	2.921	1.831	1.209	0.791	0.650	0.650
24	28.6	31.4	23.4	9342	8.469	7.642	7.390	5.689	4.031	2.689	1.870	1.169	0.740	12398	11.780	10.512	10.201	7.858	5.539	3.709	2.610	1.630	1.000	1.000
25	28.6	35.4	24.4	9008	10.559	9.579	9.260	7.260	5.118	3.071	1.488	0.850	0.559	12430	14.831	13.319	12.969	10.091	7.142	4.260	2.098	1.098	0.831	0.831
26	28.6	35.5	24.3	9485	7.850	7.031	6.689	4.969	3.390	2.118	1.319	0.720	0.402	12748	10.890	9.669	9.201	6.909	4.760	3.000	1.858	1.000	0.591	0.591
27	28.6	34.4	23.9	10440	7.461	6.421	6.012	4.110	2.642	1.571	1.020	0.642	0.539	13416	10.339	8.902	8.272	5.772	3.752	2.299	1.461	0.720	0.689	0.689
28	28.6	37.3	24.6	9597	5.339	5.421	5.142	3.461	2.181	1.291	0.720	0.488	0.319	12859	7.449	7.500	7.091	4.831	3.150	1.858	1.012	0.720	0.469	0.469
29	28.6	37.2	23.8	9342	10.961	10.150	9.949	8.339	6.630	4.868	3.630	2.461	1.660	12748	14.941	13.839	13.579	11.350	9.020	6.610	4.941	3.331	2.240	2.240
30	28.6	37.1	24.3	9247	11.181	10.531	10.409	8.689	6.669	4.618	3.331	2.142	1.339	12636	15.461	14.480	14.228	11.909	9.189	6.370	4.610	2.980	1.882	1.882
31	28.6	36.7	23.8	9263	9.980	8.969	8.669	6.791	4.902	3.280	2.331	1.488	1.020	12668	13.650	12.260	11.882	9.311	6.728	4.531	3.240	2.130	1.441	1.441
32	28.6	36.8	24.0	9199	12.610	12.189	11.189	8.319	5.941	3.988	2.709	1.752	1.189	12493	17.150	16.650	15.201	11.370	8.142	5.461	3.799	2.429	1.661	1.661

**Table B2 Raw FWD Data from Nashville, Northbound Lane (Continued)**

#	AC Temp		Surf Temp	Air Temp	NASHVILLE - NORTHBOUND																			
	°C	°F			Load 1	Deflection @ Radius (mils @ in.)			Load 2			Deflection @ Radius (mils @ in.)												
	°C	°F	°C		(lb)	0.000	7.990	12.005	24.010	35.975	47.980	59.985	71.989	83.994	(lb)	0.000	7.990	12.005	24.010	35.975	47.980	59.985	71.989	83.994
33	28.6	36.4	23.8		9263	10.740	9.811	9.551	7.650	5.598	3.709	2.429	1.539	0.980	12207	14.728	13.441	13.091	10.469	7.720	5.098	3.402	2.110	1.402
34	28.6	36.3	23.7		9597	10.461	9.500	9.209	7.421	5.618	3.902	2.642	1.480	0.909	12557	14.079	12.780	12.390	9.969	7.520	5.209	3.512	2.039	1.280
35	28.6	35.8	24		9358	11.181	9.740	9.020	6.512	4.728	3.339	2.531	1.890	1.441	12525	14.882	13.020	12.071	8.799	6.441	4.610	3.539	2.669	2.059
36	28.6	35.6	23.9		10520	10.220	9.480	9.331	7.350	5.280	3.520	2.402	1.488	0.941	13798	13.921	12.921	12.689	9.980	7.189	4.839	3.331	2.091	1.331
37	0	0	0		9676	7.142	6.429	6.189	4.839	3.559	2.429	1.740	1.118	0.890	12605	9.850	8.811	8.520	6.681	4.929	3.390	2.409	1.618	1.260
38	28.6	35.8	23.8		0	0.000	0.000	0.000	0.000	0.000	0.000	0.000	0.000	0.000	0	0.000	0.000	0.000	0.000	0.000	0.000	0.000	0.000	0.000
39	28.6	35.6	23.8		9772	8.551	7.720	7.480	6.161	4.921	3.720	2.850	2.059	1.512	12732	11.661	10.531	10.220	8.402	6.760	5.091	3.929	2.850	2.039
40	28.6	36.2	23.7		9740	10.250	9.429	9.240	7.760	5.929	4.260	3.098	2.091	1.409	12605	13.909	12.709	12.488	10.488	8.020	5.799	4.228	2.870	1.961
41	28.6	35.2	23.8		9867	5.370	5.098	5.071	4.512	3.929	3.252	2.760	2.260	1.850	12652	7.461	6.941	6.890	6.130	5.339	4.409	3.740	3.000	2.449
42	28.6	35.2	23.3		10297	9.240	8.669	8.461	7.181	5.890	4.598	3.650	2.740	2.020	13305	12.610	11.839	11.531	9.760	8.000	6.220	4.949	3.701	2.752
43	28.6	35.3	24.1		9390	12.961	11.799	11.402	9.150	7.031	5.012	3.531	2.299	1.520	12461	17.350	15.720	15.181	12.150	9.382	6.661	4.760	3.118	2.059
44	28.6	35.3	23.6		9633	11.949	9.781	8.980	6.311	4.240	2.689	1.799	1.110	0.760	12477	16.059	13.150	12.130	8.539	5.791	3.728	2.520	1.618	1.130
45	28.6	35.7	24.1		9247	12.551	11.728	11.500	9.461	7.071	4.858	3.539	2.350	1.520	12302	17.059	15.921	15.531	12.791	9.591	6.598	4.839	3.189	2.059
46	28.6	35.7	23.5		9406	12.189	11.291	11.039	9.020	6.791	4.661	3.161	2.091	1.520	12541	16.339	15.091	14.720	12.059	9.079	6.240	4.291	2.909	1.980
47	28.6	35.8	23.7		9660	12.872	10.220	9.559	6.929	4.909	3.280	2.240	1.480	1.000	12430	16.331	13.701	12.839	9.331	6.630	4.429	3.059	2.000	1.370
48	0	0	0		9788	7.870	6.988	6.630	4.882	3.461	2.319	1.579	1.039	0.630	12605	10.642	9.429	8.941	6.669	4.760	3.189	2.201	1.390	0.858
49	28.6	35.4	23.5		0	0.000	0.000	0.000	0.000	0.000	0.000	0.000	0.000	0.000	0	0.000	0.000	0.000	0.000	0.000	0.000	0.000	0.000	0.000
50	28.6	35.3	23.4		9469	10.480	9.390	9.051	7.000	5.118	3.520	2.461	1.559	1.000	12605	14.000	12.559	12.079	9.339	6.850	4.689	3.280	2.098	1.319
51	28.6	35.8	23.7		10472	9.500	8.539	8.240	6.480	4.780	3.311	2.358	1.591	1.039	13464	12.811	11.461	11.071	8.780	6.480	4.559	3.311	2.150	1.469
52	28.6	35.9	23.9		9406	12.390	11.610	11.189	9.000	7.000	5.039	3.669	2.402	1.500	12668	16.811	15.728	15.118	12.130	9.370	6.720	4.858	3.181	2.000
53	28.6	35.4	23.4		9485	7.909	7.071	6.819	5.201	3.669	2.429	1.630	1.012	0.642	12461	10.831	9.861	9.382	7.209	5.098	3.402	2.331	1.409	0.941
54	28.6	35.9	24.1		9485	8.181	7.252	6.941	5.311	3.902	2.669	1.890	1.228	0.799	12621	11.150	9.909	9.531	7.339	5.402	3.752	2.650	1.752	1.161
55	28.6	36.3	23.8		9485	8.551	7.228	6.772	4.890	3.382	2.189	1.461	0.902	0.630	12636	11.728	9.949	9.319	6.791	4.701	3.071	2.039	1.260	0.909
56	28.6	36.2	23.9		9597	8.720	7.858	7.571	5.858	4.189	2.752	1.831	1.079	0.661	12748	11.720	10.579	10.189	7.909	5.689	3.740	2.512	1.500	0.941
57	28.6	36.7	23.8		9740	7.760	6.941	6.720	5.299	3.929	2.760	1.969	1.280	0.858	12748	10.571	9.449	9.161	7.240	5.461	3.831	2.728	1.811	1.189
58	28.6	36.3	23.6		9422	9.831	8.949	8.689	6.780	4.909	3.339	2.272	1.311	0.669	12461	13.409	12.189	11.858	9.291	6.760	4.598	3.130	1.839	0.961
59	28.6	36.4	23.8		9358	8.949	7.909	7.531	5.681	4.051	2.661	1.740	0.980	0.642	12621	12.150	10.752	10.240	7.728	5.539	3.650	2.409	1.319	0.941
60	28.6	36.3	24.2		9629	6.941	6.181	5.921	4.598	3.390	2.319	1.630	1.228	0.961	12605	9.512	8.480	8.189	6.339	4.689	3.240	2.272	1.752	1.339
61	28.6	36	24.2		9740	9.951	9.012	8.772	6.988	5.181	3.531	2.409	1.488	0.929	12466	13.311	12.118	11.831	9.500	7.039	4.811	3.319	2.031	1.299
62	28.6	35.9	24.4		9501	11.661	10.929	10.760	7.740	5.319	3.220	2.109	1.441	0.831	12605	15.772	14.728	14.441	10.421	7.209	4.390	2.650	1.500	1.220
63	28.6	35.3	24.5		9613	11.311	9.839	9.331	6.929	4.740	3.020	1.868	0.969	0.669	12461	14.780	13.000	12.350	9.240	6.429	4.110	2.539	1.402	0.941
64	28.6	36.3	24.4		9485	14.031	11.961	11.000	7.969	5.650	3.760	2.579	1.591	1.118	12509	18.291	16.701	14.449	10.520	7.429	5.000	3.461	2.169	1.598
65	28.6	36.2	24.6		9390	11.720	10.902	10.752	9.079	7.169	5.390	4.000	2.571	1.402	12557	15.591	14.500	14.311	12.091	9.610	7.181	5.299	3.339	1.799

Table B3

Raw FWD Data from Nashville, Southbound Lane

#	NASHVILLE - SOUTHBOUND																								
	AC Temp		Surf Temp		Air Temp		Load 1		Load 2		Deflection @ Radius (mils @ in.)		Deflection @ Radius (mils @ in.)		Deflection @ Radius (mils @ in.)										
	°C	°C	°C	°C	°C	(lb)	0.000	7.990	12.005	24.010	35.975	47.980	59.985	71.989	83.994	0.000	7.990	12.005	24.010	35.975	47.980	59.985	71.989	83.994	
1	28.6	33.3	22.6	0	0.000	0.000	0.000	0.000	0.000	0.000	0.000	0.000	0.000	0.000	0.000	14132	10.591	9.402	7.012	5.118	3.402	2.461	1.669	1.189	
2	28.6	33.1	22.2	11125	7.988	7.031	6.728	5.220	3.791	2.469	1.799	1.189	0.799	0.461	0.260	12700	12.630	11.539	11.252	9.260	7.252	5.130	3.520	2.382	1.579
3	28.6	33.4	22.8	9601	9.311	8.512	8.319	6.831	5.331	3.791	2.610	1.772	1.150	0.680	0.380	12662	13.461	11.890	11.441	8.850	6.551	4.551	3.240	2.081	1.390
4	28.6	33.7	22.8	9501	9.890	8.760	8.409	6.480	4.760	3.311	2.319	1.559	0.980	0.560	0.300	12891	9.520	8.350	7.969	6.079	4.469	3.150	2.299	1.630	1.209
5	28.6	33.1	22.5	10042	6.941	6.071	5.799	4.370	3.169	2.189	1.591	1.169	0.839	0.500	0.280	12557	9.480	8.630	8.441	6.850	5.358	3.980	3.209	2.441	1.858
6	28.6	34.5	22.7	9565	6.780	6.240	6.091	4.909	3.839	2.831	2.291	1.760	1.331	0.880	0.480	12636	17.500	15.020	14.280	10.799	7.701	5.020	3.280	1.961	1.181
7	28.6	34.6	22.9	9231	13.220	11.429	10.858	8.240	5.858	3.831	2.480	1.449	0.850	0.480	0.260	12700	14.988	12.980	12.402	9.331	6.701	4.551	3.169	2.169	1.591
8	28.6	34.2	22.8	9390	11.220	9.681	9.201	6.941	4.941	3.358	2.331	1.559	1.150	0.680	0.380	12748	9.921	9.071	8.752	7.150	5.610	4.260	3.280	2.488	2.020
9	28.6	34.2	23.1	9915	7.209	6.579	6.370	5.209	4.110	3.118	2.402	1.780	1.459	1.061	0.680	12509	13.031	12.272	12.240	10.980	9.220	7.150	5.461	3.669	2.260
10	28.6	33.5	22.9	9533	9.441	8.941	8.941	8.012	6.760	5.272	4.071	2.689	1.661	1.061	0.680	12764	12.020	11.228	11.189	9.500	7.591	5.831	4.571	3.409	2.409
11	28.6	34.7	23.1	9597	8.720	8.161	8.160	6.909	5.539	4.260	3.331	2.512	1.760	1.260	0.760	12446	10.630	9.650	9.382	7.520	5.772	4.272	3.220	2.409	1.720
12	28.6	34.3	23.1	9326	7.780	7.130	6.870	5.520	4.228	3.091	2.358	1.661	1.260	0.760	0.460	12605	7.449	6.689	6.331	4.709	3.280	2.098	1.390	0.980	0.701
13	28.6	35.2	23.4	9681	5.500	4.890	4.650	3.409	2.358	1.500	0.961	0.720	0.571	0.380	0.220	12859	6.728	5.752	5.311	3.630	2.382	1.551	1.130	0.890	0.701
14	28.6	35.4	23.6	9501	5.071	4.311	3.969	2.709	1.772	1.130	0.850	0.669	0.500	0.380	0.220	12430	12.882	11.350	10.882	8.110	5.402	3.280	2.000	1.161	0.681
15	28.6	35.1	23.5	9342	9.929	8.850	8.500	6.370	4.280	2.559	1.539	0.839	0.512	0.300	0.160	12636	8.650	7.429	7.031	5.189	3.630	2.461	1.752	1.220	0.909
16	28.6	36.4	24.1	9565	6.409	5.461	5.169	3.772	2.630	1.780	1.272	0.890	0.650	0.460	0.260	12875	7.850	7.020	6.811	5.469	4.260	3.130	2.319	1.500	1.098
17	0	0	0	9517	5.858	5.240	5.091	4.039	3.110	2.291	1.689	1.118	0.811	0.560	0.340	0	0.000	0.000	0.000	0.000	0.000	0.000	0.000	0.000	0.000
18	28.6	36.7	23.3	0	0.000	0.000	0.000	0.000	0.000	0.000	0.000	0.000	0.000	0.000	0.000	14085	8.799	7.350	6.941	5.071	3.500	2.252	1.500	1.000	0.689
19	28.6	36	23.6	10822	6.571	5.512	5.189	3.780	2.591	1.650	1.091	0.689	0.539	0.380	0.220	12668	10.150	8.390	7.850	5.691	3.669	2.228	1.319	0.902	0.720
20	28.6	36.6	24.1	9533	7.740	6.409	6.000	4.189	2.772	1.681	1.000	0.650	0.531	0.380	0.220	13050	7.449	6.819	6.339	4.350	2.799	1.709	1.130	0.799	0.618
21	28.6	36.7	23.2	9740	5.461	4.941	4.591	3.118	1.969	1.209	0.780	0.571	0.429	0.300	0.160	13194	10.252	8.799	7.701	4.941	3.012	1.760	1.091	0.740	0.598
22	0	0	0	10074	7.531	6.240	5.598	3.610	2.228	1.280	0.839	0.579	0.488	0.340	0.180	0	0.000	0.000	0.000	0.000	0.000	0.000	0.000	0.000	0.000
23	28.6	37.7	23.7	0	0.000	0.000	0.000	0.000	0.000	0.000	0.000	0.000	0.000	0.000	0.000	13066	16.839	15.110	14.650	11.461	8.240	5.319	3.370	1.791	0.890
24	28.6	38.2	23.6	9660	12.559	11.280	10.949	8.642	6.201	3.988	2.520	1.291	0.669	0.429	0.260	12668	9.571	7.909	7.280	4.870	3.098	1.870	1.161	0.709	0.579
25	28.6	38.7	24.1	9597	7.079	5.791	5.358	3.512	2.220	1.311	0.811	0.500	0.429	0.300	0.160	14005	9.409	7.858	7.890	5.689	3.902	2.429	1.512	0.882	0.512
26	0	0	0	10759	6.870	5.811	5.610	4.059	2.709	1.630	1.071	0.618	0.402	0.260	0.140	0	0.000	0.000	0.000	0.000	0.000	0.000	0.000	0.000	0.000
27	28.6	39.4	24.1	0	0.000	0.000	0.000	0.000	0.000	0.000	0.000	0.000	0.000	0.000	0.000	12907	12.701	11.500	11.059	8.429	5.980	3.858	2.539	1.449	0.961
28	0	0	0	9555	9.299	8.382	8.071	6.150	4.331	2.799	1.799	1.039	0.669	0.460	0.260	0	0.000	0.000	0.000	0.000	0.000	0.000	0.000	0.000	0.000
29	28.6	39.9	24	0	0.000	0.000	0.000	0.000	0.000	0.000	0.000	0.000	0.000	0.000	0.000	12557	12.118	10.870	10.402	7.909	5.661	3.709	2.429	1.512	1.020
30	28.6	40	24.6	9708	8.819	7.902	7.571	5.740	4.059	2.669	1.780	1.039	0.760	0.500	0.300	12700	12.500	11.201	10.760	8.169	5.752	3.669	2.319	1.252	0.819
31	28.6	40	24.3	9517	9.039	8.098	7.799	5.868	4.079	2.598	1.642	0.870	0.571	0.380	0.220	12557	10.421	9.260	8.890	6.902	5.012	3.370	2.311	1.469	1.000
32	28.6	39.7	24.3	9660	7.441	6.630	6.402	4.902	3.551	2.402	1.642	1.031	0.701	0.460	0.260	12590	5.123.405	4.271.7	4.130.8	3.117.1	2.110.2	1.469.1	1.000.0	0.701.0	

Table B4 Raw FWD Data from Nashville, Southbound Lane (Continued)

#	AC Temp		Surf Temp		Air Temp		NASHVILLE - SOUTHBOUND																						
	°C	°F	°C	°F	°C	°F	0.000	7.990	12.005	24.010	35.975	47.980	59.985	71.989	83.994	95.999	107.999	119.999	131.999	143.999	155.999	167.999	179.999	191.999	203.999	215.999	227.999	239.999	251.999
33	28.6	39.5	24.3	9629	9.331	8.240	7.909	6.039	4.461	3.118	2.228	1.480	1.012	12636	12.720	11.311	10.839	8.319	6.189	4.350	3.118	2.110	1.358						
34	28.6	39.8	24.3	9613	7.890	7.031	6.720	5.091	3.689	2.480	1.709	1.110	0.799	12636	10.831	9.709	9.272	7.091	5.150	3.500	2.409	1.598	1.110						
35	28.6	39.5	24.5	9310	10.079	9.031	8.650	6.661	4.760	3.260	2.252	1.421	0.941	12360	13.421	12.098	11.598	8.988	6.480	4.441	3.079	1.961	1.311						
36	28.6	39	24.6	9517	9.539	8.850	8.799	7.571	6.071	4.441	3.150	1.850	1.209	12477	12.780	11.882	11.780	10.039	8.020	5.858	4.130	2.512	1.642						
37	28.6	38.6	24.8	10058	9.319	8.299	7.980	6.110	4.480	3.020	2.059	1.402	0.961	13066	12.461	11.012	10.551	8.161	5.988	4.071	2.819	1.890	1.370						
38	0	0	0	9278	11.150	10.449	10.331	8.728	6.850	4.929	3.591	2.331	1.531	12525	14.921	14.031	13.811	11.669	9.150	6.500	4.760	3.110	2.059						
39	28.6	37.6	24.7	0	0.000	0.000	0.000	0.000	0.000	0.000	0.000	0.000	0.000	0	0.000	0.000	0.000	0.000	0.000	0.000	0.000	0.000	0.000						
40	28.6	38	24.3	9597	9.161	8.441	8.252	6.882	5.559	4.272	3.331	2.402	1.598	12493	12.571	11.591	11.402	9.480	7.669	5.921	4.661	3.311	2.240						
41	28.6	37.4	23.6	10743	9.339	8.512	8.461	6.799	5.252	3.780	2.728	1.870	1.358	13761	12.571	11.579	12.272	9.252	7.118	5.142	3.752	2.591	1.870						
42	28.6	37.1	24.3	9629	5.299	4.850	4.791	4.000	3.260	2.531	2.071	1.571	1.201	12605	7.370	6.740	6.630	5.571	4.559	3.579	2.909	2.220	1.610						
43	28.6	37.5	24.2	10615	7.539	6.728	6.500	5.209	4.130	3.201	2.591	2.020	1.531	13766	10.228	9.181	8.870	7.150	5.650	4.370	3.559	2.760	2.142						
44	28.6	37.1	24.5	9517	8.760	8.098	7.969	6.520	4.980	3.520	2.449	1.661	1.079	12573	11.929	11.059	10.870	8.850	6.811	4.791	3.409	2.252	1.539						
45	28.6	37	24.4	10552	8.839	7.819	7.469	5.610	4.039	2.780	2.012	1.390	1.012	13448	12.012	10.579	10.091	7.630	5.480	3.791	2.728	1.909	1.382						
46	28.6	36.5	24.1	9708	7.740	6.941	6.689	5.169	3.791	2.579	1.772	1.142	0.799	12557	10.429	9.409	9.098	7.051	5.220	3.559	2.461	1.630	1.079						
47	28.6	36.9	24	10663	8.780	7.929	7.689	5.949	4.421	3.110	2.272	1.571	1.110	13687	11.909	10.669	10.339	8.098	6.071	4.299	3.161	2.220	1.559						
48	28.6	37.4	24.4	10201	7.720	6.839	6.539	4.949	3.579	2.441	1.709	1.130	0.760	13146	10.469	9.272	8.850	6.791	4.941	3.362	2.390	1.559	1.039						
49	0	0	0	9708	7.839	7.071	6.850	5.429	4.118	2.921	2.079	1.358	0.890	12525	10.642	9.618	9.280	7.402	5.598	3.961	2.839	1.870	1.220						
50	28.6	37.6	24.1	0	0.000	0.000	0.000	0.000	0.000	0.000	0.000	0.000	0.000	0	0.000	0.000	0.000	0.000	0.000	0.000	0.000	0.000	0.000						
51	28.6	37.6	23.8	9772	8.559	7.591	7.260	5.488	3.858	2.469	1.579	0.941	0.591	12477	11.441	10.150	9.681	7.331	5.142	3.331	2.209	1.311	0.850						
52	28.6	37.3	23.7	10552	7.370	6.630	6.402	5.071	3.850	2.740	2.012	1.339	0.949	13735	10.142	9.299	8.961	7.150	5.449	3.921	2.870	1.961	1.382						
53	28.6	37.8	24	9804	7.272	6.571	6.339	5.142	4.071	3.110	2.461	1.811	1.311	12716	10.110	9.201	8.819	7.260	5.760	4.390	3.500	2.591	1.870						
54	28.6	38.2	24.2	9915	8.571	8.059	7.941	6.591	4.988	3.539	2.539	1.701	1.079	12668	11.488	10.839	10.630	8.902	6.728	4.811	3.461	2.260	1.500						
55	28.6	37.7	24	9613	9.098	8.531	8.480	7.118	5.650	4.051	2.949	2.000	1.358	12605	12.209	11.402	11.311	9.520	7.571	5.449	4.031	2.720	1.882						
56	28.6	38.2	24	9708	7.520	6.780	6.520	5.059	3.720	2.620	1.760	1.130	0.740	12605	10.228	9.209	8.850	6.909	5.071	3.480	2.409	1.569	1.071						
57	28.6	38	23.9	9326	10.740	9.902	9.701	7.799	5.811	3.969	2.740	1.661	1.020	12493	14.031	12.980	12.760	10.220	7.579	5.280	3.650	2.299	1.409						
58	28.6	38.6	23.9	9740	7.000	6.291	6.039	4.642	3.382	2.311	1.650	1.031	0.701	12525	9.539	8.598	8.311	6.402	4.720	3.291	2.319	1.520	1.000						
59	28.6	39.7	24.6	9517	9.839	9.461	9.461	8.272	6.811	5.331	4.169	2.858	1.941	12477	13.209	12.701	12.559	11.091	8.980	6.988	5.469	3.689	2.531						
60	28.6	40	24.6	9555	11.350	10.760	10.709	9.362	7.819	6.161	4.929	3.409	2.339	12382	14.921	14.150	14.020	12.358	10.280	8.142	6.480	4.618	2.988						
61	28.6	40.1	25.1	10583	14.031	13.079	13.071	11.118	9.161	7.031	5.360	3.669	2.339	13496	18.110	16.929	16.839	14.260	11.642	8.831	6.681	4.531	2.969						
62	28.6	40.6	24.4	9772	9.059	8.531	8.480	7.291	6.020	4.630	3.569	2.441	1.610	12716	12.209	11.429	11.350	9.772	8.059	6.169	4.701	3.252	2.142						
63	28.6	40.7	25.8	10408	12.370	11.480	11.480	9.280	7.000	4.799	3.311	2.079	1.291	13766	15.882	14.740	14.709	11.799	8.909	6.311	4.409	2.760	1.780						
64	28.6	40.2	26.4	9326	14.591	13.551	13.331	11.098	7.969	4.941	3.189	1.941	1.091	12589	18.969	17.689	17.161	14.118	10.118	6.390	4.110	2.559	1.500						
65	28.6	40.6	26.3	9692	8.520	7.709	7.500	5.850	4.098	2.681	1.760	1.118	0.780	12525	11.539	10.441	10.161	7.949	5.618	3.689	2.488	1.591	1.100						



The purpose of this appendix is to provide a transparent documentation of the method by which moduli were obtained from SASW tests. As was described in the literature review, SASW field tests involve measuring the phase velocity of Rayleigh waves for various seismic disturbances at several different sensor spacings. Wider sensor spacings (i.e. 24-in. instead of 6-in.) are used to measure relatively low-frequency waves that correspond to deeper sampling depths. Figure C1 shows an idealized field dispersion curve for a pavement structure.

Note that the data points from smaller sensor spacings correspond to shallower depths than the data points from larger sensor spacings. Also notice that the field dispersion curve exhibits a decrease in shear wave velocity with increasing depth. This is because, for a pavement system, the stiffest layers are at the top. If a similar test were run on bare soil for the design of a new roadway, the field dispersion curve would have a different shape. There would not be a stiff layer on top, and the soil stiffness would likely increase with depth due to increased confining pressure. The range of shear wave velocities for this scenario would be lower than what is measured for pavement layers, and the general shape would be close to a lateral reflection of the curve in Figure C1.

The process now described may be thought of as a simplified inversion process, as mentioned in the literature review. In this process, the first step is to identify depths at which the dominant shear wave velocity exhibits an abrupt change. Such changes are indicative of a change in the material through which the shear wave is traveling. If the depth of the pavement layer(s) is already known, this information should be used to aid in the interpretation of the field dispersion curve. Especially if the shear wave velocity changes uniformly, minimally, haphazardly, or in any fashion that hinders inversion,

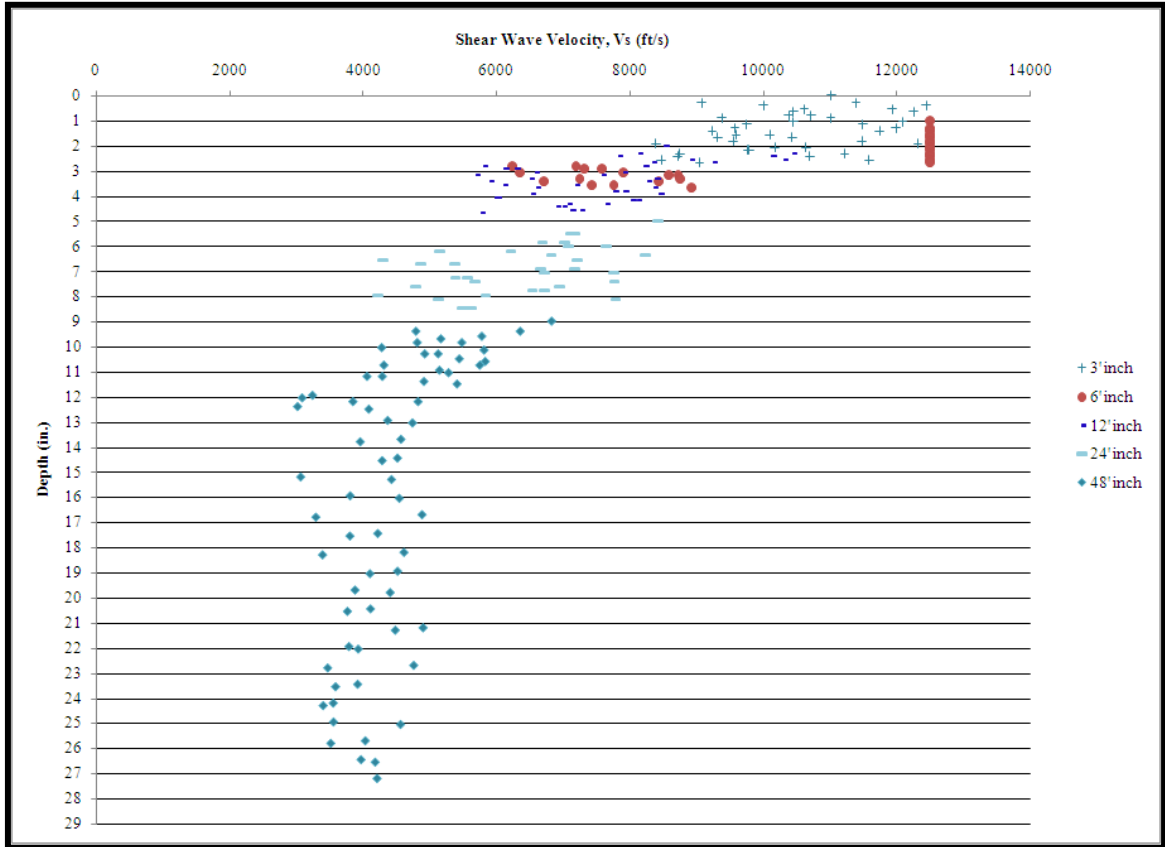


**Figure C1 Idealized Field Dispersion Curve**

the known layer thicknesses should be used to aid in interpretation.

After the field dispersion curve has been discretized into sections of semi-uniform shear wave velocity a representative shear wave velocity is estimated for each discretized layer. More complex inversion methods utilize stiffness matrices and the analytic minimization of corresponding error functions for this step. Such methods are convenient for automation, but unless they enhance the resolution of the field dispersion curve, they will not ultimately enhance the accuracy of the estimated layer moduli. In the present study layer moduli were estimated by “eyeballing” the field dispersion curve and

drawing in sections of vertical lines (representing constant shear wave velocity through a depth) that best and most realistically represent the field data.

Table C1 summarizes the data that can be taken from the hypothetical field dispersion curve in Figure C2. The next step for data reduction is to either measure, estimate or assume the quantities that are needed to relate shear wave velocity to Young's Modulus. These quantities include unit weight and Poisson's ratio. If the unit weight of the material in any given layer is unknown, the probable constituent of that layer should be guessed and its unit weight assumed. Poisson's Ratio is not usually measured, and it may be estimated using sources such as Table 2 in the literature review or estimated using engineering judgment.

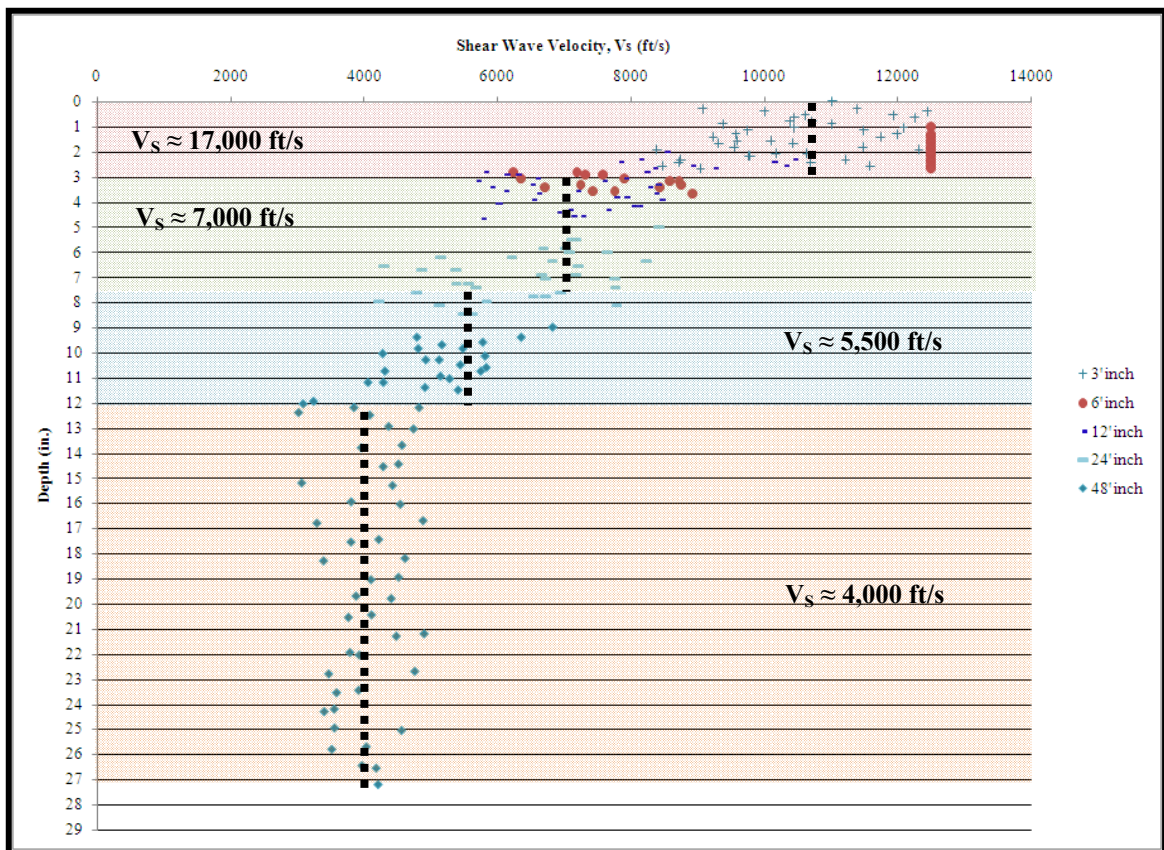


**Figure C2 Discretized Field Dispersion Curve**

After measuring, estimating or assuming the necessary material characteristics, the shear wave velocity is converted into a value for seismic shear modulus (G) using Equation 60 from the literature review, shown below. The mass density may be calculated by dividing the material's unit weight by gravity. Then, Young's modulus is estimated from the assumed value for Poisson's ratio using Equation 61 from the literature review, also shown below. As discussed in the literature review, seismic values for Young's modulus may be taken as equal to resilient modulus ( $M_r$ ).

$$G = V_s^2 \cdot \rho \dots\dots\dots \text{Eq. 60}$$

$$E = 2G(1 + \nu) \dots\dots\dots \text{Eq. 61}$$

Lastly,  $M_r$  is adjusted to account for the stress-sensitive behavior of soil moduli. For this study,  $M_r$  was adjusted using Darendeli's model for fine-grained soils (44). This relationship is defined in the literature review by Equations 62 and 64, and is repeated below. This model (as would similar models) is used to generate a curve for  $G/G_{\max}$  versus strain.

$$\frac{G}{G_{\max}} = \frac{1}{1 + \left(\frac{\gamma}{\gamma_r}\right)^a} \dots\dots\dots \text{Eq. 62}$$

$$\gamma_r = \left(0.0352 + 0.0010 \times PI \times OCR^{0.3246}\right) \cdot \sigma_0'^{0.3483}; a = 0.9190 \dots\dots \text{Eq. 64}$$

This model requires several additional assumptions. First, the overconsolidation ratio is assumed equal to one. This is reasonable since the soils in Nashville, AR have not supported glaciers or other tremendous weights in their geologic past. Secondly, the effective confining stress was taken equal to 0.5 atmospheres. The literature suggests

that values in this region are common and appropriate (44). These two assumptions facilitate the development of the graph in Figure C3, which was used to reduce all of the moduli estimates from the Nashville site.

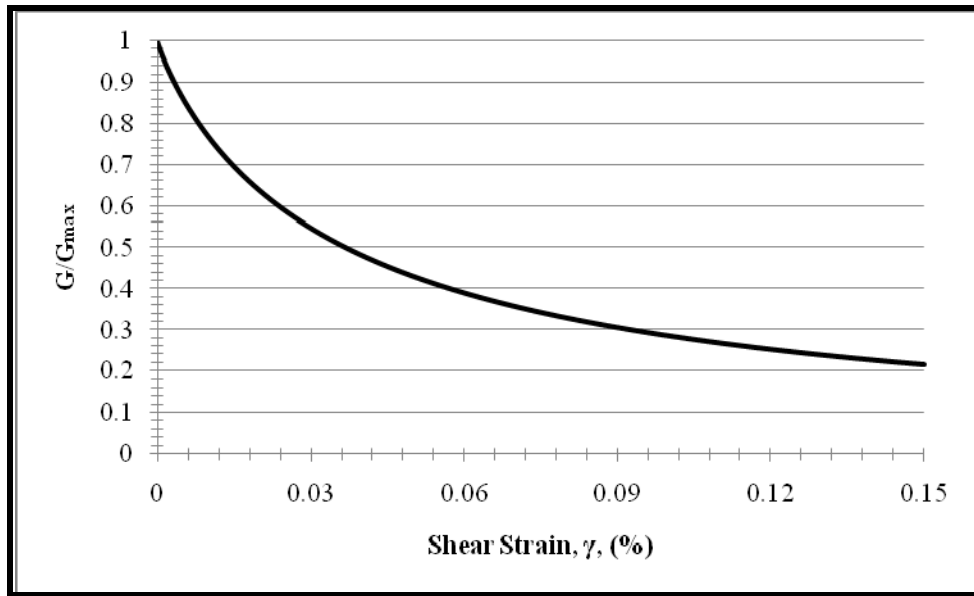


**Figure C3 Darendeli's Modulus Reduction Curve for Fine-Grained Soils**

Next, the estimated layer modulus for each of the discretized layers is adjusted to a FWD/Truck-loading strain using Figure C3. This may be accomplished on an analytical basis. The first step in this process is to identify a shear strain that is representative of FWD/Truck loading. The FWD can be used to identify such a strain. Using a representative deflection basin, first calculate the horizontal distance from the load plate at which deflections are due entirely to subgrade deformation. This distance is called  $a_e$  and is found using Equations 1-4. The normal strain at this point ( $\epsilon_{FWD}$ ) is calculated as the vertical deflection divided by the subgrade sampling depth. The

subgrade sampling depth is taken as 1.5 times the radius of the FWD load plate minus the depth of pavement layer(s).

$\epsilon_{FWD}$  may then be converted to a shearing strain ( $\gamma_{FWD}$ ) using the principles of Equation 61 and Mohr's Circle. The first step is to replace the Young's Modulus and Shear Modulus terms in Equation 61 with their component quantities, as shown below in Equation 61.B. Rearranging this relationship to the form of Equation 61.C gives a solvable expression for shear strain ( $\gamma$ ). The normal stress ( $\sigma$ ) and strain ( $\epsilon$ ) are available from FWD data, Poisson's Ratio ( $\nu$ ) is assumed, and the shear stress ( $\tau$ ) may be found using Mohr's circle.

$$\frac{\sigma}{\epsilon} = 2 \frac{\tau}{\gamma} (1 + \nu) \dots \dots \dots \text{Eq. 61.B}$$

$$\gamma = \frac{2\tau(1 + \nu)}{E} \dots \dots \dots \text{Eq. 61.C}$$

The current analysis used a simplified procedure for determining  $\gamma_{FWD}$ . Instead of an analytical estimation, a general rule of thumb was employed. That is, the FWD load was assumed to impart a shear strain of 0.05%. This undoubtedly introduces some error into the problem, but the assumption is that this error will not significantly affect the final estimation.

Using  $\gamma_{FWD}$  as an input, Figure C3 is used to find a single reduction factor for all of the seismically determined modulus. Figure C4 illustrates this procedure. Finally, each of the seismically measured moduli is multiplied by the reduction percentage. These final values are representative of the soil moduli at an appropriate load level for highway design.

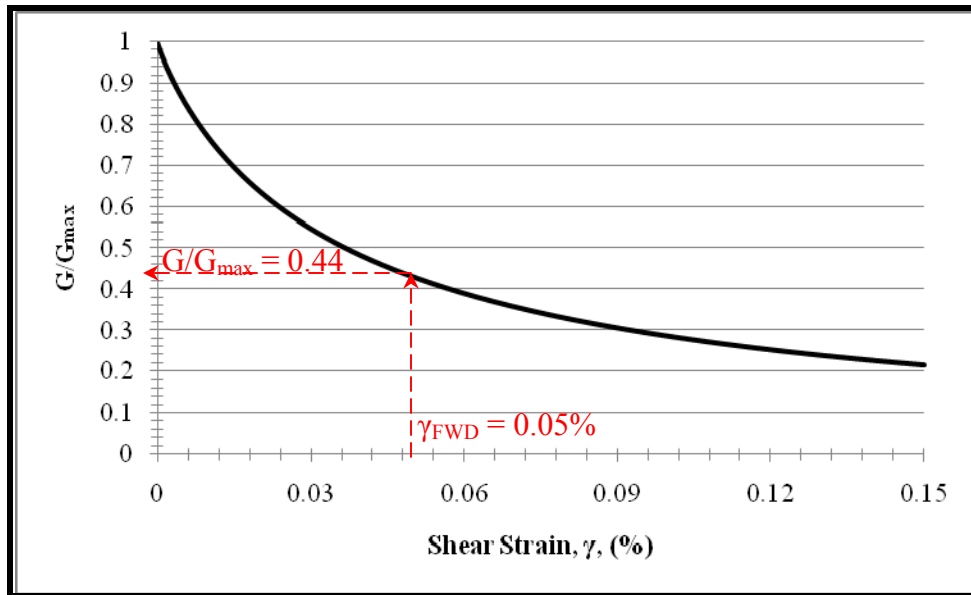


**Figure C4 Simplified Determination of  $\gamma_{FWD}$**

